NASA-CR-191671

INVESTIGATIONS OF DETAIL DESIGN ISSUES FOR THE HIGH SPEED ACOUSTIC WIND TUNNEL USING A 60th SCALE MODEL TUNNEL

by

P. S. Barna

Final Report

Contract # 17-GFY900125

* * * * *

Part I

Tests with Open Circuits

Revised March 1991

ACKNOWLEDGEMENT

Most of the test data presented in this report were obtained by co-op students Mr. Glen Ostrowski and Miss Susan Rickard under the supervision of Mr. Earl Booth. Design of the model tunnel was performed by P. S. Barna & Associates, Ltd.

Investigations of Detail Design Issues for the High Speed Acoustic Wind Tunnel Using a 60th Scale Model Tunnel

by

P. S. Barna

Part I. Tests with Open Circuit

Contract # 17-GFY900125

January, 1991

SUMMARY

This report summarizes the tests on the 1:60 scale model of the High Speed Acoustic Wind Tunnel (HSAWT) performed during the period of November 1989 to December 1990.

Throughout the testing the tunnel was operated in the "open circuit mode," that is when the airflow was induced by a powerful exhaust fan located outside the tunnel circuit.

The tests were first performed with the closed test section and were subsequently repeated with the open test section. While operating with the open test section, a novel device, called the "nozzle-diffuser," was also tested in order to establish its usefulness of increasing pressure recovery in the first diffuser.

The tests established the viability of the tunnel design. The flow distribution in each tunnel component was found acceptable and pressure recovery in the diffusers were found satisfactory. The diffusers appeared to operate without flow separation.

All tests were performed at NASA Langley Research Center.

TABLE OF CONTENTS

INTRODUCTION

It is a well known practice to test out any major windtunnel design on a scale model tunnel as a precaution. The scale of such tunnels is a matter of choice. Some tunnels, such as the 22ft-by-14ft low speed tunnel (V/STOL) was first tested on a 24th scale model tunnel, while the DNW was tested on a 10th scale model. It is rather unusual to find tests performed on a 60th scale model, which may be considered truly a pilot-scale device.

Justification for such a a small scale model was borne out from results experienced with a model of the 22ft-by-14ft low speed tunnel which was built to a 60th scale and was subsequently extensively tested over a period of some two years. Major results obtained on this pilot-scale tunnel were indeed found compatible with results found earlier on the full scale prototype [1]. Moreover, the tests furnished additional and extremely useful information pertaining to certain design features clearly undesirable for future tunnel designs.

When compared with a large model, the pilot scale model has the following advantages:

1. It is much more economical to construct and demands much less space;
2. It is less time consuming to manipulate experiments;
3. It is more flexible and results may be produced faster than with a large scale tunnel;
4. If handled properly, results can agree well with prototype results.

The conclusions reached above do not suggest exclusion of the construction of a model tunnel on a larger scale should this be desired. If anything, prior testing of a pilot tunnel will enhance success of a larger model by eliminating possible errors ahead of time.

BRIEF DESCRIPTION OF THE MODEL TUNNEL

The pilot-scale model tunnel under consideration was designed to have a 9:1 contraction ratio and to embody three diffusers, which combined, provided the desired area increase. Located downstream from the Test Section the first diffuser has a modest 2:1 area increase while the second diffuser, downstream from the fan section, has a 2.5:1 area increase. Both diffuser have low side angles, about 2 degrees. The third diffuser is located upstream of the contraction and is a wide angle diffuser with side angle about 15 degrees and with an area increase of 1.8:1.

A special design feature of this tunnel is the absence of any area change between the first and second diffuser. In other words, the cross sectional area of the ducts between the exit of the first diffuser and the inlet to the second diffuser remains the same including the annular passage of the fan section. Similarly, there is no area change between the exit from the second diffuser and the inlet to the third diffuser. This design philosophy was adopted from studies of the DNW Tunnel located in Holland [2].

The basic floor plan (Master Plan) for the closed return circuit model tunnel is shown in figure 1, where the various components are provided with numbers from one to fifteen and they are recognized as follows:

1. Closed test section; 2. First diffuser; 3. First corner; 4. First cross-leg; 5. Second corner; 6. Fan section; 7. Second diffuser; 8 and 9. Third and fourth corners; 10. Wide angle diffuser; 11. Calming chamber; 12. Contraction; 13. Fan nacelle; 14. Spool insert (removable); 15. Open test chamber. The pilot-scale model tunnel could be operated both with closed and open test sections, and are shown at the same location.

For all flow studies discussed in this report, the closed return-circuit of the tunnel was changed into an open-circuit and the flow was induced by a powerful centrifugal fan as shown in figure 2. The changeover was attained by turning the corners No. 8 and 9 outwardly. While the fan was inducing airflow by suction through 8, the air entered 9 through a well rounded bell-mouth. A wire screen was stretched across the tunnel entry to prevent foreign objects from entering the tunnel circuit. To reduce turbulence a wire screen was also provided at entry to the calming section, while a honeycomb was placed inside it.

Access to velocity traverses and also static pressure ports were provided at relevant points along the circuit at 14 locations, as shown in figure 2, with letters T and P.

The tunnel was fabricated, mostly using transparent plastic material, except for the corners which were made of aluminum. Figure 3 shows a photograph of the tunnel.

INSTRUMENTATION AND METHOD OF TESTING

A single electronic pressure gage was used for taking both velocity traverses and measuring pressures. A manually operated scanning valve was employed to monitor the pressures at various locations. Various Pitot tubes were used for measuring total pressure and these were inserted into the stream through small openings. All measurements were taken under steady flow conditions, while running the fan with constant speed. All of the velocity traverses were obtained in the horizontal plane at locations 1 to 13, while in the vertical plane, traverses were taken at location 4, 6 and 9 as well. It is noted that at locations 4 and 6 the traverses were made with a Pitot cylinder, consisting of a long 1/8 inch diameter tube provided with a small port facing the stream. During the traversing, the tube remained extended

across the section being at least twice as long as the section width. This was done in order to avoid skewing the profiles which is generally experienced during the gradual withdrawal of a standard Pitot tube while traversing.

Prior to the tests the electronic pressure gage was calibrated.

RESULTS WITH THE CLOSED TEST SECTION

Horizontal traverses

Traverses taken in the horizontal plane are presented in figure 4, where the normalized velocity $U = u/U_{max}$ is plotted against normalized traverse distance $Y = y/w$. (Note: zero is at inboard).

Figure 4a shows the traverse taken at entry (#1) just downstream from the corner and the "humps and hollows" signify the effects of the turning vanes on the flow. Each vane produces a defect in its wake and these effects may be anticipated.

Figure 4b shows the traverse taken at entry (#2) to the contraction which is located downstream from the wide angle diffuser. The continuous downward trend of the flow distribution with increasing distance from the inner wall at location #2 needs consideration. It could be either due to the turning of the flow upstream or due to some flow distortion in the wide angle diffuser. However, turning was already completed by the vanes upstream at location #1, where the downward trend in figure 4a is clearly missing. Therefore turning may not be the cause, unless there remains some "flow history effect"having effects downstream. On the other hand, if there was a flow separation in the wide angle diffuser, the downward trend would appear different from that shown in figure 4b. Both effects are open for speculation and the real answer may need further studies.

Figure 4c taken at entry to the closed test section (#3) appears to be perfectly uniform and seems to be free of the irregularities experienced upstream. Apparently, the contraction is a satisfactory design.

Figure 4d taken at exit from the closed test section (#4) shows signs of a small boundary layer build-up, while the "core-flow" remains uniform.

Figure 4e taken midway along the first diffuser (#5) shows further signs of boundary layer build-up, the thickness being estimated as about 15 percent, while figure 4f, taken at exit from the first diffuser, shows an approximate build-up of about 23 percent. The remaining core-flow appears uniform.

Figure 4g shows the traverse taken just downstream from the first corner following the first diffuser (#7). Large velocity defects appear in the wakes of the turning vanes, and these persist further downstream from the second corner, as shown in figure 4h (#8). One may notice, however, that there is some improvement in the distribution at location #8 because the flow near the inner and outer walls seemed to have increased speed.

The flow distribution in the annulus of the fan section (#9) is shown in figures 4i and 4j, where 4i is the distribution inboard and 4j is the outboard distribution. In figure 4i, velocity rises rapidly near the nacelle to a maximum, then decreases almost linearly attaining the lowest value at the outer casing. Similar fall-off has been experienced with other wind tunnels also, and it may be regarded as common occurrence. The outboard distribution, however, differs inasmuch as the velocity distribution remains uniform over a considerable--say 70 percent part--of the annulus.

The difference in the in- and outboard flow distribution is really problematic. When the corner was removed from the second open circuit and there was straight

inflow allowed to enter the fan section the difference vanishes as shown in figure 46(a). Here all distributions appear about the same, i. e. uniform over 80 percent of the traverse and falling off over the remaining 20 percent. It appears from figure 41, that in the second open circuit (W series) the inboard distribution downstream from the corner is similar to that shown in figure 4i. This appears as a typical flow-history effect.

The flow distribution in the second diffuser is markedly influenced by the wake downstream from the nacelle as shown by the four traverses taken along the diffuser. The large dip near the center region, shown by figures 4k and 4m (#10 and #11) is due to the presence of the nacelle and the effects remain strong even further downstream, as shown by figures 4n and 4o (#12 and #13). At the same time, some skewness of the distribution becomes noticeable.

Near the walls the velocity gradient appears to be reasonable and there seems to be no signs of separation.

This result is due to adjustment of the turning vanes in corners 1 and 2. Initially, separation was noted on the inboard side of the second diffuser. Adjusting the turning vane FLAPS of the turning vanes cured this problem.

Vertical traverses

Vertical traverses taken at locations 4 and 6 are shown in figures 5a and 5b. It appears that at entry to the first diffuser the boundary layer is slightly thicker in the vertical than in the horizontal plane. This may be due to the difference between the height and the width. Probably the actual boundary layer thickness is the same all the way around the perimeter. Since, however, the results are presented normalized (and the height is less than the width) it seems as if the boundary layer was thicker. The

same explanation may apply to figure 5b as well. Thus one may conclude, that the velocity profiles are compatible in both the horizontal and the vertical planes.

It is a simple matter to check this effect in profile at #4, since the aspect ratio of that section is known. At location #6, however, the height and width are identical, since the section is circular, therefore this explanation is not sufficient. A more likely explanation is, that since there is more expansion in the vertical direction, the boundary layer is thicker. Possibly, the diffuser design could be modified to reduce this effect.

At location #9, the velocity distribution shown in figure 5c appears in good agreement with that shown in figure 4i obtained over the inboard section of the fan annulus.

Velocity traverses along the closed test section

Velocity traverses were also established along the 16 inch long closed test section at fifteen consecutive cross sections located about 1 inch apart. Velocity distribution was found uniform all the way albeit the natural growth of the boundary layer along the test section walls. The boundary layer thickness, delta δ, was found about 2.2 percent at inlet and about 9 percent at exit from the test section based on a 4.4 inch width of the section. When compared with a boundary layer developed over an infinitely wide flat plate, assuming turbulent boundary layer, one can calculate the thickness as being approximately the same value (Appendix 1).

Pressure distribution

The static pressure distribution around the tunnel circuit is shown in figure 6 where subatmospheric pressure (psf) is plotted against the various locations marked 1 to 14.

More particularly: stretch 1-2 is located between the inlets to the third diffuser and contraction, respectively, as shown in figure 2, and no significant change in pressure appears. The large drop between 2-3 is due to acceleration in the contraction. A small rise in pressure between 3-4 in the closed test section was observed which is rather unusual, because normally some loss in static pressure is expected*. Pressure recovery in the first diffuser occurs between locations 4-6 and the break in the line at 5 is due to a rate of change in the area increase of the first diffuser. The losses in the first and second turning vanes including the small cross-leg as well, are shown by the lines 6-7 and 7-8. The pressure drop between 7-8 is markedly larger than between 6-7. Insignificant losses occur over the fan section 8-9 and 9-10. While the pressure rise in the second diffuser is shown between locations 10-13, the small loss of pressure between 13-14 is due to the exit turning vanes.

Pressure recovery in the first diffuser was found to be about 59.5 percent and in the second diffuser, about 75.5 percent. When comparing these values with those published in the "Diffuser Data Book" [3], one finds fair agreement with the book value concerning the first diffuser, because recovery is based on the dynamic head measured along the centerline. The unusually high recovery in the second diffuser is due to two caused: for one, it has a larger area ratio and larger length-to-throat ratio; second, recovery was based on mass-averaged dynamic head rather than centerline dynamic head owing to the large velocity defect downstream from the nacelle. Details of diffuser recovery calculations are presented in Appendix II.

Static pressure distribution around the tunnel circuit shows the pressure changes across the first and second set of turning vanes (#6-#7 and #7-#8). One can

* Experiments with the closed test section show a slight decrease in dynamic pressure, being 58 psf at inlet and 57.3 psf at outlet. Static pressure at inlet was - 66.1 psf and 64.6 psf at outlet. Substituting these figures in Bernoulli's equation one finds that the losses are negative, which, to make sense, needs to be positive.

notice a change in the gradient thus observing that the changes are unequal. Referring to data obtained while operating with the closed test section, one finds a drop of 2.52 psf across the first and 6.73 psf across the second corner. The higher resistance observed across the second set of turning vanes may be caused by a number of factors and will be later again discussed.

The turning vanes under consideration were the Dimmock vanes which were designed according to established specifications [4]. Calculations show that friction along the first cross leg located between the first and second corner amounted to be only about 0.42 psf, therefore friction could not be the cause for the large drop across the second set of turning vanes.

The Dimmock vanes were subsequently replaced with another type of turning vanes, called the Salter vanes [5], which are known to have less resistance to flow. The same peculiarity was again experienced. This problem will be again addressed under the section "Efficiency of the turning vanes."

Static pressure changes across the fan section and across the third corner were found negligible while the pressure rise along the second diffuser was found satisfactory.

THE OPEN TEST SECTION

Description of the open test section

The open test section essentially consists of a rectangular box constructed of 1/2 inch thick plexiglass. It is about 20 inches long, 13 inches high and also about 13-7/8 inches wide. The sides of this box are held together with 1-inch aluminum equal angles fastened with screws. A removable lid permits access to its interior. Flow enters the box at one end and leaves at the opposite (exit) end. Hence the open test

section joins the exit end of the contraction (where the flow enters) and exits on the opposite end to which the first diffuser is attached, as shown schematically in figure 7a. It is of interest to note, that the upstream end-wall was made movable so that the distance between inlet and outlet walls is adjustable. Details of the traverse locations are shown in figure 7b.

The essential difference between a test section closed and open is the arrangement of the walls surrounding the flow. With the closed test section (CTS) the tunnel walls remain adjacent to the flow, while with the open test section the walls are at some distance away from the flow which, upon entering the open test section, becomes a jet.

The open test section of the model tunnel under consideration contains two elements essential to efficient operation:

1. The Collector
2. The Nozzle Diffuser

The collector is located at the far end of the open test section and the jet, after having traversed the entire length of the open test section, flows into it before moving into the first diffuser. The collector separates the entrained fluid from the recirculating flow moving around the tunnel circuit.

The nozzle diffuser is located at the near end of the open test section where the flow enters. It is a novel device which slightly widens the jet, thus giving the flow a better chance of energy recovery as it moves along in the first diffuser.

Figure 8 shows the general arrangement of the model tunnel circuit with the open test section. Figure 9 shows a side view of the open test section while figure 10 shows the interior from above with the lid removed. The flow is from the left to the right.

Details of the collector

Studies on collectors were already performed some time ago in the open test section of the 24th scale tunnel modelled after the 22 ft-by-14.5 ft low speed tunnel (also known as the V/STOL tunnel) and the results of these test were reported [6]. More experiments on collectors were performed recently on the 1:60 scale model of the same tunnel which indicates that the most satisfactory results are roughly identical with those obtained earlier. Accordingly, the collector adopted for the present tunnel is a short converging duct with a 15 degree side angle, 10 degree top and bottom angle and a depth of 3.0 inches. It has fixed walls and was made of 1/4 inch thick plexiglass and was provided with corner fillets for smooth transition of the flow into the first diffuser, as shown in figure 11. The design allows for an adjustable air gap from 1/8 to 7/8 of an inch width.

Details of the nozzle-diffuser*

The nozzle-diffuser (ND) is a short diverging duct fitted to the exit of the tunnel contraction and is located at the inlet end of the open test section. The general purpose of the nozzle-diffuser is:

a. to increase pressure recovery in the first diffuser
b. to enhance flow distribution
c. to reduce demand for fan power

Tests performed earlier on the 1:60 scale of the Low Speed model tunnel already showed results of flow improvement [7]. Since it was anticipated that optimum performance may be obtained with small wall angles, the nozzle-diffuser was designed to allow for infinitely variable side angle, from zero to 12 degrees, while the top/bottom could only be varied stepwise from zero to 2, 3 and 4 degrees, respectively.

* Patent application for the nozzle-diffuser has been prepared and will be filed shortly.

The side angles could be adjusted from the outside of the test chamber by employing a simple mechanism. Variation of the top/bottom angle was attained by using interchangeable sides, each side having a different top/bottom angle as shown in figure 12. The nozzle-diffuser was also fabricated from 1/4 inch-thick plexiglass.

Test set-up of the open test section

Unlike the tests performed with the CTS, where the geometry of the test section was limited to one configuration, tests with the open test section could be varied owing to the flexibility in the use of its components. Accordingly, tests could be performed with or without the collector or the nozzle-diffuser for that matter. Furthermore, the length of the jet could be varied by moving the end-wall adjacent to the contraction. In addition, one set of tests was performed with a square edge leading to the first diffuser, while another set was done with the edge rounded off.

The most relevant tests were performed with the free jet being fixed to a 10 inch length (corresponding to 50 ft. in prototype). With this set distance of the free jet, the optimum gap width and the best configuration of the nozzle-diffuser was established.

INSTRUMENTATION AND METHOD OF TESTING

Testing substantially followed the methods employed earlier with the closed test section, mainly attending to flow velocity traverses and pressure measurements around the tunnel circuit shown in figure 13. With the variation of the test set-up, many of these tests were repeated.

Both, for taking velocity traverses and measuring pressures, a single electronic pressure gage was used. A manually operated scanning valve was employed to monitor the pressures at various locations around the tunnel circuit shown on figure 13 from 1 to 14. Pitot tubes of various length were used to measure total pressure and

these were inserted into the stream through small openings located near the static pressure ports. Velocity traverses were also obtained right across the open test section at locations 1-inch apart. Velocity traverses were made in the horizontal plane at locations 1 to 13, while in the vertical plane traverses were limited to locations 4,6 and 9.

All measurements were taken under steady flow conditions while running the fan with constant speed.

RESULTS WITH THE OPEN TEST SECTION

a) Results with Collector

Velocity traverses around the tunnel circuit

Traverses taken at locations 4, 6, 9 and 13 are presented in figures 14, 15, 16 and 17. At locations 4 and 6, traverses in both the horizontal and the vertical planes appear to be substantially the same, as shown in figures 8 and 9, respectively. It is noted, that at 4, that is at the entry to the first diffuser, uniform distribution is limited to the central region extending between Y=0.32 to 0.725, figure 14; the outer regions show marked velocity defects which, ultimately, lead to high blockage. At location 6, at exit from the first diffuser, a marked change from the entry conditions is experienced, as shown in figure 15. Owing to a heavy build-up of the boundary layer uniform flow can no longer be observed. Further downstream, at the fan section, location 9, the outer horizontal velocity distribution is almost uniform across the annulus, while both the inner horizontal and the vertical distributions show some similarity by first increasing to Y=0.15, then slightly decreasing with increasing radial distance, as shown in figure 16. A marked fall-off between Y=0.8 and 1 is also observed. At location 13, at exit from the second diffuser the defect in the center region, shown in figure 17, is again due to the presence of the nacelle, as found with the closed TS.

Pressure Distribution

Pressure distribution around the tunnel circuit is shown in figure 18 where static pressure is plotted for locations 1 to 14. The static pressure drop between locations 2 and 3 was found to be 49.1 psf and the emerging jet velocity at 3 was calculated as 201.5 ft/s. Recovery in the first diffuser was found 31.4 psf and in the second diffuser 9 psf. Losses in the second corner were found again higher than in the first corner. It is noted that substantial loss, amounting to 11 psf was experienced inside the open test section (between locations 3 and 4) owing to jet mixing effects.

(b) Results with collector and with nozzle diffuser

Calibration of the collector involved tests for establishing the gap width for optimum pressure recovery in the first diffuser. With the test section length set at about 11 inches, the gap width was stepwise varied from 1/8 to 7/8 inch with 1/8 inch increments and for each setting the pressure rise in the first diffuser was noted. A set of typical results are plotted in figure 19, where the optimum pressure recovery may be observed with a 1/4 inch gap setting without using the nozzle-diffuser. Tests performed with the use of the nozzle-diffuser show optimum with a 3/8 inch gap. This small difference may be considered as negligible.

Calibration of the nozzle-diffuser involved tests for establishing the combination of wall angles which yield optimum recovery in the first diffuser while keeping the collector gap width 1/4 inch and the test section length 10 inches.

Results of tests show that optimum recovery was observed with the following combination of angles:

Side angle, alpha, deg.	Top/bottom angle, beta, deg
4	4
6	2

At these angles pressure recovery was about 37 psf, as shown in figure 20. When using the collector alone without the nozzle-diffuser recovery was only about 31.4 psf. Thus, the introduction of the nozzle-diffuser represents approximately 17.5 percent increase in recovery.

TEST RESULTS WITH COLLECTOR AND NOZZLE-DIFFUSER AT OPTIMUM SETTING

Velocity traverses around the tunnel circuit

Traverses taken at locations 4, 6, 9, and 13 are presented in figures 21, 22, 23, and 24. At location 4 there appears a difference between the horizontal and vertical traverse, as shown in figure 21. In the horizontal plane, uniform flow extended over about 60 percent of the traverse distance, while in the vertical plane uniform flow was limited to only about 14 percent of the vertical traverse distance. The nozzle-diffuser seems to produce more uniform flow distribution in the horizontal than in the vertical plane. This may either be due to the aspect ratio of the sides or due to the collector geometry; perhaps even both have some effects. Maximum velocity was V_{max}=231.8 ft/s, which is about 8 ft/s higher than in the test performed with the collector only. At location 6 uniform flow was observed over 30 percent of the horizontal distance, hence it was limited to the central region, while in the vertical plane uniform flow was absent, as shown in figure 22. At location 9 both the horizontal inner and outer traverses appear to be about the same, while the vertical distribution falls off with increasing

annular distance, as shown in figure 23. At location 13 the traverse exhibits a distribution similar to that experienced earlier with the collector only, see figure 24.

Pressure distribution

Static pressure distribution around the tunnel both with the nozzle-diffuser and the collector at optimum setting is shown in figure 25, where static pressure is plotted for locations 1 to 14. The static pressure drop between location 2 and 3 was found to be 54.45 psf and the average air velocity at the exit from the contraction at 3 was calculated V_{ave}=212.4 ft/s, about 5 percent higher than was experienced without the nozzle-diffuser. Recovery in the first diffuser was found 37.1 psf and in the second diffuser 10.15 psf. Thus, with the application of the nozzle-diffuser there appeared an improvement in recovery amounting in the first diffuser to 5.7 psf and in the second diffuser 1.15 psf. Losses in the second corner were again found higher than in the first corner. Pressure loss inside the open test section was found 10.7 psf, just slightly less than 11 psf found earlier.

Velocity distributions inside the open test section

Velocity distributions inside the open test section are shown in figures 26 and 27 where dynamic pressure is plotted against distance from the inner wall. Each curve represents a distribution at successive locations these being 1 inch apart. It is known that jet core contracts with increasing distance owing to mixing effects with its surroundings. This effect may be observed in figure 26 where the uniform distribution in the jet decreases with increasing distance measured from the jet entrance into the open space. As the jet moves downstream, it entrains more and more fluid and rounded shoulders appear at the end of the uniform center region. Results shown on figure 26 were obtained without the nozzle-diffuser. Introduction of the nozzle-diffuser results in an improvement of the velocity distribution by widening the uniform center

region and by keeping the width of the uniform distribution almost constant as shown in figure 27. Figure 28 resulted from a superposition of the two flowfields in plane view: one with the nozzle-diffuser side angles set to zero and one with 6 degree side angles. Only traverses at 3-3, 3-5, 3-7, 3-9 and 3-11 are shown. The solid lines are the results with the zero side angle while the dashed lines are taken with the 6 degree angle. The improvement in velocity distribution is clearly visible. The slight skewing of the flow fields is frequently due to probe effects. As the Pitot probe is gradually withdrawn from the stream the flow picks up some speed because of the reduced resistance caused by the stem.

The static pressure along the centerline between the exit from the nozzle-diffuser and the inlet to the collector was found practically constant although the static pressures at various locations inside the open test "chamber" varied. For this reason the static pressure port was located near the exit plane of the nozzle-diffuser.

Velocity "contour plots" are presented in figure 29. The shaded pictures visually introduce the three distinct flowfields which may readily be recognized as: a) the wide, fast moving central core region; b) the adjacent and relatively thin shear layer; c) the outer, slow moving region which contains mostly the recirculating flow.

EFFICIENCY OF THE TURNING VANES

The efficiency of turning vanes relates to the pressure loss of the airflow around the bends in which the vanes are located. In general, vane efficiency increases with decreasing losses. In particular, discussion in this report concerns the first and second corners rather than the third and fourth, because the flow is much faster in the first and second corner, where the losses are expected to be high.

Two sets of turning vanes were tested and each set was designed on already established principles. The results of tests showed that in each set of vanes the losses were found somewhat higher than anticipated in the first corner and substantially higher in the second corner.

Design details of the turning vanes

The design of turning vanes in windtunnels generally falls into two major categories: vanes of constant wall thickness and vanes with varied wall thickness. Experience teaches that vanes consisting of constant thickness are, in general, an economically sound and sufficiently satisfactory proposition. Two types appear in the literature:

Vanes of constant thickness and constant spacing (pitch or gap), were developed and tested by C. Salter around 1946 [5]. Vanes of constant thickness but with varied spacing were developed and tested by N. A. Dimmock around 1950 [4], with a view to be employed in corners of circular cross section. The spacing adopted by Dimmock has a well defined arithmetic progression expressed by simple parameters based on the pipe diameter. Both designs propose the use of sheet metal for the vane material bent around a circular arc.

Vanes with varied thickness resemble airfoils bent on a radius, and their use for pilot scale model tunnels may be considered uneconomical and impractical (1) because they are expensive, and (2) because very low Reynold's numbers.

Design details of the turning vanes in the pilot scale model are shown figures 30, 31, and 32. Figure 30 shows the first two corner sections fitted with Dimmock vanes, where the proper location of each vane across the diagonal and the spacing between the vanes is shown. The diagonal section of the corner is an ellipse with

major axis 4.42 inches and minor axis 3.125 inches. On the same drawing a set of the Salter type vanes are also shown and the details appear on figure 31. Although these vanes were not fabricated at the time when the Dimmock vanes were made, it is noted that both the Dimmock and the Salter vanes were originally designed with sharpened trailing edges. However, some time later, Salter vanes were eventually fabricated using a simpler way of construction, as shown in figure 32. Also note that while the Dimmock design has 7 active, the Salter design has 16 active vanes.

Method of testing turning vanes

Static ports located on the interior side of the tunnel ducting, shown earlier in figure 2 served the purpose to measure the static pressure changes across each set of vanes, while changes in dynamic pressure were established by taking traverses up- and downstream from each set of vanes. This practice allowed the calculation of losses from the total pressure changes across the corner, in accordance with the routine testing procedures outlined in various papers.

As before, all tests were performed under steady flow conditions with the fan rotating at one constant speed. For measuring static pressure an electronic pressure gage was employed. It is noted that both the Salter and the Dimmock vanes were provided with a sharp trailing edge which could be adjusted for symmetric flow distribution further downstream in the form of aluminum trailing edge flaps that were tuned to provide best performance.

Test results on turning vanes

Details of test results are presented in APPENDIX III(a) where results obtained with both the Dimmock and the Salter vanes are shown. The following is considered as a representative set of results obtained with a closed test section operation:

DIMMOCK VANES: First corner total pressure loss was 6.25 psf and 9.49 psf, for the second corner.

SALTER VANES: First corner total pressure loss was 3.86 psf and 6.99 psf for the second corner.

It was also observed that the flowrate around the tunnel circuit was higher during the tests with the Salter vanes. The flowrate was 24.8 cuft/sec in tests with the Dimmock vanes as against 27.3 cuft/sec with the Salter vanes.

Velocity traverses (expressed in dynamic pressure) obtained at locations 6, and 8 are shown in figures 33, and 34. It appears that the flow downstream from the Salter vanes was more uniform, which could be expected, considering the number of vanes in the Salter corner being double those of the Dimmock corner.

SOME ADDITIONAL EXPERIMENTS

a) Experiments with the second open circuit

Tests were performed with the second open circuit set-up in order to study certain effects of the flow which could not be established while experimenting with the first open circuit.

The schematic plan view of the second open circuit is shown in figure 35. In this scheme the third and fourth corners were joined together (at T-14), while the first and second corners were disconnected and were turned outwardly around 180 degrees. Air entered the circuit through a well rounded intake followed by a short duct fitted to the second corner. The air exited through the first corner which was followed by a suitable diffuser leading to the inlet of the exhaust fan.

The first and second corners were still equipped with the Salter type vanes, the third and fourth with Dimmock vanes.

Effects of interest were:

a) the flow distribution downstream from the third and fourth corners;
b) the flow distribution at entry to and exit from the contraction;
c) the losses associated with all the four corners;
d) the flow distribution in the open test section;
e) the velocity distribution at inlet and exit from the first and second diffuser.

Method of testing

The first set of test results available for this report were obtained with the open test section. As before, traverses were obtained at locations 1 to 13 and an extra traverse was added, 14, located between the third and fourth corners. It is noted that the location numbers remained the same as with the first open circuit.

During the tests both the nozzle-diffuser and the collector were fixed at optimum setting (alpha=6, beta=2 degrees for the nozzle-diffuser, and 0.25 inches gap for the collector). The tests were performed with a constant fan speed.

Test results

Comparisons between traverses taken with the first and second open circuit will be limited in this report to relevant locations. For the sake of ready comparison, each figure pertains to two graphs: on the left is one presenting test results obtained with the first open circuit, while on the right are results obtained with the second open circuit.

Pressure distribution

When comparing the two pressure distributions, shown in figure 36, the first difference occurs in the static pressure change P2-P3 along the contraction, which also means a difference in the flow rates. With the first open circuit P2-P3=55.2-3.1= 51.3 psf, resulting in a dynamic head at contraction exit as q=49.45 psf, (using 0.964 contraction coefficient) hence the velocity V=206 ft/sec. With contraction exit area 0.11 sq ft the flow rate Q=22.66 cft/sec. With the second open circuit, similar calculations lead to P2-P3=41.8 psf, q=40.29 psf, V=186 ft/sec and Q=20.46 cft/sec.

Thus the flow rate in the second open circuit is about 10 percent less than in the first. The reason for this is twofold: a) In the second open circuit, the flow entered through a 6.25 inch diameter pipe in which a screen is located, whereas in the first circuit, it entered through a 10 inch diameter pipe, where the screen offered less resistance owing to a much lower dynamic head. b) The air leaving the second circuit had a larger dynamic head than in the first circuit, hence the losses incurred in the second circuit diffuser, leading to the exhaust fan, were also higher.

Test results show, that the static pressure at the end of the first circuit (location 14) was -32.5 psf where the weighted average dynamic head calculated from the flow rate was q=2.02. Hence the total pressure at the first circuit exit was about -32.5 + 2.02 = 30.48 psf. At the exit end, location 6, of the second circuit test results show a static pressure of -38.1 with a much larger dynamic head of 10.8 psf; hence the total pressure at the second circuit exit was -38.1 + 10.8 = -27.3 psf. From this the losses in the exit diffuser, amounting to about 35 percent of the dynamic head, need to be deducted. Therefore, at entry to the exhaust fan the total pressure was -31.08 psf. This is close to the figure, 30.48, obtained with the first circuit. (It would be even closer

if the small losses in the short exit diffuser in the first circuit were also taken into consideration).

Pressure recovery, Pr, in the first and second diffuser is as follows:

First open circuit: first diffuser Pr=34; second Pr=9.4 psf

Second open circuit: first diffuser Pr=27.8; second Pr=7.2.

When corrected for the average dynamic head, results of the first diffuser agree well; however, the second diffuser is less efficient when operating in the second open circuit.

Flow traverses

Location 4. At the entrance to the first diffuser the horizontal traverses for both the first and second circuit appear to be similar and satisfactory, with the uniform flow extending over about 60 percent of the duct width. The vertical traverses, however, differ a great deal from the horizontal, as shown in figure 37. When comparing results of the first with second open circuit, the flow distributions at location 4 are similar. It would be of considerable interest to further explore the difference existing in flow distribution between the horizontal and the vertical planes.

Location 6. At the exit of the first diffuser, when comparing results of the first with the second open circuit, one finds the flow distributions again similar, as shown in figure 38.

Downstream from location 6, the flow turns outward in the second open circuit and comparison between flow distributions is no longer required. Suffice to say, that velocity distributions at #4 and #6 are similar, hence effects of the second open circuit on the flow distribution in the first diffuser is only minimal.

Location 7. While in the first open circuit, location 7 is situated between the first and second corners, in the second open circuit it is located downstream from the screen through which the flow enters the circuit. Thus in the first circuit the distribution is markedly influenced by the history of the flow, while in the second circuit, the flow has just started moving around the circuit and is therefore almost perfectly uniform, as shown in figure 39.

Location 8. It is a surprise to observe the similarity of the flow distribution downstream from the second corner, when considering the marked difference in the upstream flow distribution. Both distributions demonstrate a marked fall-off in the outer 25-30 percent width of the traverse, as shown in figure 40. It may be readily understood in the case of the first circuit that this fall-off is due to the already existing decline upstream of the corner. In the case of the second circuit, however, there appears uniform flow upstream of the corner, yet a similar decline is experienced downstream, thus suggesting an unsatisfactory corner vane performance, needing attention.

Location 9. A similarity may be observed in the velocity distribution across the fan annulus where the velocity steadily decreased in going from the fan nacelle to the tip. There the similarity ends and some of the roles become reversed, as shown in figure 41. In the first circuit the inside horizontal traverse appears markedly higher than the outside and the vertical, which almost run together. Not so in the second open circuit, where the flow velocities are highest at the outside and lowest on the inside.

Location 10. The reverse distribution role experienced at location 9 persists at location 10 also: in the first circuit velocity peaks around Y=0.2, while in the second circuit it peaks around Y=0.8. The central velocity defect, caused by the nacelle,

remains more or less unaffected, as shown in figure 42. The shifting of the velocity peaks from the inner to the outer flow region strongly suggests the distribution's dependence on flow history. This, of course, differs in the second circuit from the first circuit, and its effects are specially noticeable in the return leg of the tunnel.

Location 13. The same considerations apply to the exit end of the large (second) diffuser where the velocity peak in the first circuit appears at around Y=0.3 and in the second circuit at around Y=0.7, as shown in figure 43. The velocity defect, however, has for some reason disappeared. Effects of flow history are probably responsible for the disappearance of the flow defect which persisted in the tests with the first open circuit.

Perhaps the most important results in this series of tests concerns the flow distribution in the return leg (location 14) and also downstream from the fourth corner (location 1) in the second open circuit. The results presented here lead to the understanding of the flow pattern upstream of the contraction with a different history from that experienced with the first open circuit.

Location 14 and 1. While the results are presented side by side, they do apply only to the second open circuit. It is of interest to note that at location 14, since the velocity defect at the center region had disappeared, a single velocity peak occurred around Y=0.4 where it shifted from Y=0.7 at location 13. In fact, a considerable rearrangement of flow must have occurred between locations 13 and 14 for the better rather than the worse, as shown in figure 44. Further downstream, after turning the fourth corner, at location 1, the velocity distribution became quite acceptable over an 80 percent of the traverse width. The slow velocity "pick-up" in the inner region up to Y=0.2 can be corrected by the screens.

b) Experiments concerning the flow distribution at the fan section with a modified second open circuit.

These experiments were performed with the second open circuit modified to allow straight inflow to the fan section. Accordingly the second corner was removed from the circuit, while both the rounded air intake and the short parallel duct attached to the air intake were directly joined to the fan section as shown in figure 45. This arrangement allowed the flow to enter the fan section with a uniform upstream velocity distribution, thus eliminating the effects of the corner vanes on the downstream flow.

The test results show that at location #9 the in-and out-board as well as the vertical distribution became identical for practical purposes. However, while uniform velocity distribution was observed over 80 percent of the fan annulus (except near the hub), over the remaining 20 percent a sharp decrease occurred, as shown in figure 46(a), where the normalized V/V_{ave} is plotted against distance x/w. (Plotting V/V_{ave} allows direct comparison because V_{ave} is related to flow rate Q).

With the corner vanes installed in their proper location, the velocity distribution becomes markedly different. It appears from figure 46(b), that while the outer horizontal and the vertical distribution are close to each other, the inner horizontal is well above the other two. Thus the presence of the corner vanes adversely affects the flow distributions, which ultimately leads to a problem in the fan performance and in the fan design.

DISCUSSION OF THE RESULTS

Closed test section

The velocity distribution at inlet to the closed test section shows perfect uniformity which implies a sound contraction design. The small growth of the

boundary layer over the length of the test section, is about the same as the predicted 9 percent thickness developing over a flat plate assuming the 1/7 power distribution law. Thus the blockage to the first diffuser is low, resulting in a pressure recovery of about 59.5 percent which is considered satisfactory and compares favorably with values for an equivalent conical diffuser published in the "Diffuser Data" book [3].

Velocity defects, resembling to "humps and hollows," found downstream from the turning vanes, are natural wake effects which can be tempered with certain design modifications to be discussed in the section under "efficiency of turning vanes." Suffice to say that the larger the vanes, the less their numbers, the larger the defects will be.

The three velocity distributions, observed at the fan section, (two in the horizontal and one in the vertical plane) differ somewhat and this concerns the fan design. The largest difference was observed between the in-and out-board distributions, while in-board and the vertical closely agree. These differences are not large and the problem in this instance may not be severe. Since, however, the problem is associated with the turning vanes, it may need some further investigation.

The velocity distribution downstream from the fan shows the wake effect of the nacelle but the large defect in the center region does not appear to harm the performance of the second diffuser which shows no sign of separation. Pressure recovery in the second diffuser, based on the average flow velocity, was found 75.8 percent and this too is considered satisfactory.

At the inlet to the third diffuser (wide angle, location #1) the flow uniformity appears to be slightly disturbed by the presence of the turning vanes. This could be improved by application of additional screens. At the entrance to the contraction however, the flow appears to be non-uniform.

Pressure distribution studies with the closed test section also show a difference in the static pressure drops across the first and second set of turning vanes. The drop in pressure across the second set of vanes appears larger than across the first set. Both the static and the total pressure losses were larger at the second corner.

Open test section

When operating with the open test section, flow and pressure distribution around the tunnel circuit differ from the results obtained with the closed test section. These differences appear at various locations and are mainly affected by the complex flow pattern inside the open test section. The resistance of the circuit increased, resulting in a decrease in the rate of flow for the given power of the fan.

Application of the nozzle-diffuser markedly improves pressure recovery in the first diffuser and also improves the flow pattern inside the open test section itself. Figure 47 was prepared to compare recovery for various test configurations and the three horizontal lines represent various recoveries experienced with the "bare" open test section, with the collector installed in the open test section and with the closed test section. The "bare" open test section refers to tests performed without the collector and nozzle-diffuser. The curves representing results obtained with the nozzle-diffuser for various wall angles have already been shown in figure 20. At optimum angle setting, the nozzle-diffuser performance lies roughly halfway between the closed test section and the open test section having the collector only.

As to what extent the nozzle-diffuser widens the flow may be established from velocity traverses inside the open test section shown in figures 26 and 27. One may also recognize the central core region, the shear layer and the recirculating flow shown in figure 29. Of particular interest is to observe the flow pattern at five sections in plan view shown in figure 28. The data recorded right at entrance to the collector at

station 311 shows a core width of about 4 inches with the nozzle-diffuser but only about 2.5 inches width without it. Thus the jet width increased by about 60 percent.

Downstream from the open test section, at entrance to the first diffuser, at station 4 one may compare figure 14(a) with figure 21(a) and find an improved distribution with the nozzle-diffuser. Further downstream, at locations 6 and 9, the differences become much smaller. Thus one may conclude, that application of the nozzle-diffuser improves the flow distribution inside the open test section and at entrance to the first diffuser and both contribute to the increase of recovery in the first diffuser.

The nozzle-diffuser also increases the rate of flow by about 4.5 percent and the pressure distribution data also show a slight decrease in pressure loss inside the open test section amounting to about 3 percent.

Flow distribution at the fan location

The flow distribution at the fan location (#9) needs special consideration because the fan design is based on the velocity distribution at inlet to the fan. Since the fan power is partly based on the prevailing flow rate Q, in this instance it is more suitable to establish the average flow velocity V_{ave} and plot V/V_{ave} rather than $U=V/V_{max}$ against the normalized distance $X=x/w$ or $Y=y/w$. In fact, a truer physical picture is obtained when V is related to the same value, i. e., V_{ave}, which is independent of the plane where the measurement is made, while V_{max} varies around the circumference.

Several factors appear to influence the flow distribution, namely:

a) choice of closed or open test section

b) type of corner vane design

c) history of the flow

Consider first the Salter type vanes fitted to the first and second corner and compare the flow distribution between results obtained with the closed and open test section while operating in the first open circuit mode. To facilitate comparison, three sets of two diagrams appear side by side, the first being figure 48. Here the vertical and horizontal outer distributions appear as being similar, while the horizontal inner distributions differ. One may observe, that having attained a maximum at about x/w=0.15, all the three curves fall with increasing distance.

One may conclude, that the flow distribution is somewhat affected by the choice of test section.

Consider now the Dimmock vanes and compare results obtained with closed or open test section. While the vertical and inner horizontal curves gradually fall after attaining a maximum, the horizontal outer curves keep on rising and attain a maximum value at about x=0.7 as shown in figure 49. Since this result differs from the one obtained with the Salter vanes, one may conclude that flow distribution indeed depends on the corner vane design.

When considering the history of the flow, one may compare the flow distribution with the Salter vanes while operating with the open test section either in the mode of the first open or in the second open tunnel circuit. It is noted, that in the second open circuit the flow enters the fan section through a corner that is turned around by 180 degrees outwardly. Therefore a change in the horizontal distribution can be anticipated and this was clearly demonstrated by the tests as shown in figure 50 where the horizontal inner and outer distributions changed over, while the vertical distribution also changed its shape.

Finally, consider the flow distribution without a corner and compare it with a flow in presence of a corner, say, fitted with Salter vanes. It appears, that in the case of a

straight inflow the three distributions agree reasonably well and one may observe a uniform flow over about 80 percent of the distance, while a sharp decline was noticeable over the last 20 percent, as shown earlier in figure 46. When the corner is added a marked difference appears and thus the history of the flow has a major effect on the flow distribution.

Turning vanes

It appears first, that the losses in the second corner are much greater than in the first corner. Second, most losses appear to be larger than the values of similar vanes published in the literature.

First consider the "probable" causes of the discrepancies existing between observed results and data found in references [4] and [5].

Scale effects

Based on average velocity 128 ft/s, chord 1.5 inches, kinematic viscosity 1.67x10E=4 ft^2/s , one obtains a Reynolds number 0.95x10E+5, while based on center velocity Re=1.25x10E+5. Book-reference: Salter tested at Re=1.9x10E+5, giving a loss coefficient for circular arc sheet metal vanes the value of about 0.15; Dimmock gives for tests conducted in the range of Reynolds numbers 2.1=4.2x10E+5 values between 0.16 and 0.21 for the loss coefficient. At lower Reynolds numbers higher losses may be expected.

Static pressure readings

Incorrect reading of static pressures may be due to two causes:

a) Pressures measured outboard of a corner is reported by Salter as being slightly higher than inboard values;

b) Pressure ports may be located too close to the trailing edge of the vanes. Dimmock suggests 3 diameters downstream.

Blockage effects

These may be due to differences in vane material thickness and the number of vanes employed in a corner.

Flow distribution effects

These effects may be due to two causes:

a) Distortion of flow distribution upstream from the turning vane which usually manifests itself as a non-uniform flow, having one or more velocity peaks which results in a lower average flowrate; book-references cite uniform inflow for corners tested.

b) Fluctuating flow which, in a windtunnel, may be caused by one set of turning vanes closely following another. This too could probably increase vane resistance.

Dynamic head averaging effects

Consider first the difference between the test results as compared to the values presented in the book-references.

As far as the first corner is concerned, figure 51 shows the velocity distribution upstream when the corner was fitted with the Salter vanes. The velocity traverse across location 6 shows a uniform central region with a velocity of 161 ft/s. However, when calculating from the flow rate Q (by dividing Q with area A) the average velocity was 128 ft/s. Thus the dynamic head at central region qc=30.32 psf (assuming density

being 0.00234), while the dynamic head based on the average velocity q_{ave}=19.17 psf. The ratio of the two figures is roughly 1.58 in this case.

It is of interest to repeat the calculations for q_{ave} by employing the integrated average dynamic head $\bar{q} = 1/A \int q dA$. With the Salter vanes this $\bar{q}$ was calculated to be 24.57 psf while for the Dimmock vanes it was only 20.22 psf. This result shows that the integrated average q is larger than the one derived from the average velocity obtained by dividing the flowrate with the area.

Pressure distribution around the tunnel circuit with the Dimmock and Salter vanes are shown in figures 52 and 53. It is of interest to note that the combined static pressure changes across the vanes for both corners resulted in 11.2 psf for the Dimmock and 11.3 for the Salter vanes, and therefore are almost equal.

The results are perfectly clear:

1) The Salter vanes appear less resistant and therefore more efficient than the Dimmock vanes. For almost the same "suction power" produced by the fan, the flowrate was found greater with the Salter vanes. Furthermore, the variation of dynamic head across the flow was more uniform with the Salter vanes.

2) Both the Dimmock and the Salter vanes show a consistently higher loss in the second corner, which is most probably due to an unfavorable flow distribution upstream.

When comparing the Dimmock with the Salter vanes, consideration must be given to the blockage caused by the number of vanes in the corners. It appears from figures 30 and 31 that Dimmock's design has 7 vanes in contrast with Salter's 16. Obviously, the Salter design suffers from a disadvantage. In order to calculate the

blockage caused by the vanes, establish the total length L of the vane leading edges facing the stream and multiply this with the vane thickness, t. Details of this calculation is given in APPENDIX III(b). The results show that the average dynamic head in the Salter vane corner increased by about 25 percent owing to the blockage. This would be less if the vanes were made of thinner material and the question is: what would be the practical limit to vane thickness? While the answer is partly a technological one, the vanes should be strong enough to withstand the forces due to momentum changes of the flow.

CONCLUSIONS

Various tests were performed on the 1:60 scale model of the proposed High Speed Acoustic Wind Tunnel facility in order to determine its performance.

When the tunnel was operating in the first open circuit mode, the following conclusions were reached:

(a) Closed test section

1. Both the first and second diffusers performed satisfactorily. No separation in the second diffuser was experienced. (See Table of Diffuser performance in APPENDIX II).

2. The flow distribution from entry to exit of the closed test section proved to be uniform except for a small build-up of the boundary layer, which was found turbulent.

3. The flow distribution at the fan location was depending on turning vane design. The distribution was found less uneven downstream from the corner fitted with Salter type. However, in the velocity distribution the deviation from the average

velocity V_{ave}=1 was found to be ±0.15 for the Dimmock vanes while it was about ±0.25 for the Salter vanes. Both deviations are considered large.

4. Pressure changes across both sets of turning vanes proved larger in the second corner, hence the second corner was found considerably less efficient than the first corner.

5. Corners fitted with Salter vanes showed a smaller total pressure drop as compared to corners fitted with Dimmock vanes. Also the flow rate around the tunnel circuit increased when Salter vanes were used.

(b) Open test section

1. Both the first and second diffusers performed satisfactorily and no separation in either diffusers was observed.

2. Application of the nozzle-diffuser resulted in a sizeable increase in the pressure recovery of the first diffuser. Best results were obtained when the side angles of the nozzle-diffuser and the gap of the collector were at their optimum setting.

3. With the nozzle-diffuser, the flow inside the open test section widened thus producing a wider uniform width of the core-flow in the open jet. It is anticipated, that eventually the turbulence level would also decrease to some extent.

4. As compared to the flow-rate in the closed test section, while maintaining constant fan pressure, the rate of flow decreased by about 9 percent with the Dimmock vanes and 17 percent with the Salter vanes. This large difference appears unreasonable and may be due to loose or worn-out Vee belts.

(c) Turning vane efficiency

1. The tests showed that the total pressure loss across the Salter vanes were lower than with the Dimmock vanes. Since there were more vanes in the corner fitted with Salter vanes, it stands to reason that the flow downstream was also more uniform.

2. The flow distribution downstream from the second corner, that is at the fan section, was markedly influenced by the type of vanes employed in the corners.

3. Decreasing the total head loss across the turning vanes is desirable as it would enhance the energy efficiency of the circuit.

PROBLEM AREAS

1. Turning vanes

Since the tests showed a larger pressure drop across the turning vanes of the second corner, further studies are needed. It may ultimately be necessary to establish an improved design of vanes which would offer reduced resistance to flow across the second corner.

2. Flow distribution

a) At the fan section (location #9) the flow distribution needs improving, because the prevailing variation of speed around the circumference could have undesirable effects on the fan performance.

b) At inlet to the wide angle diffuser and at the entrance to the contraction, the flow appears to be non-uniform and this may need correction in the future.

REFERENCES

1. Barna, P. S.: Experimental Investigations on the V/STOL Tunnel at NASA/LaRC. NASA CR165655, February 1981.

2. Ditshuisen, J. C. A.: Design and Calibration of the 1/10th Scale Model of the NLR LS Tunnel. NLR Agard-CP-No. 174, 1975.

3. Rundstadler, P. W., et al: Diffuser Data Book. TN-186, CREARE, May 1975

4. Dimmock, N. A.: The Development of a Simply Constructed Cascade Corner for Circular Cross Section. NGTE Memo M78, 1950.

5. Salter, C.: Experiments on Thin Turning Vanes. R&M No. 2469, 1946 (Great Britain).

6. Barna, P. S.: Aerodynamic Effects of the Jet-Flow in the Open Test Section of the 4x7m Tunnel at NASA/LaRC. Progress Report, February 1983

7. Barna, P. S.: Flowfield Studies on the 60th scale (4x7m) Tunnel to Establish the Optimum Recovery of Pressure in the First Diffuser. Progress Report, July 31, 1989.

SYMBOLS

A	area, sq ft
c	specific heat, Btu/lb/°F
L	length, ft.
M	Mass, lb.
p	static pressure lb/ft^2
pt	total pressure, lb/ft^2
q	dynamic head, $1/2\ \rho\ V^2$, lb/ft^2
Q	heat, Btu
t	time, hr.
S	surface area, ft^2
V	velocity, ft./sec.
W	electric heat energy, Watts
$\dot{W}$	massflow, lb/hr
x	horizontal distance, ft.

Abbreviations

HP	horsepower
Btu	british thermal unit
Hz	frequency, Herz
rpm	revolution per minute
Re	Reynolds number

Greek letters

α	heat transfer coefficient, Btu/hr, deg F, ft^2
δ	boundary layer thickness
ρ	density, $slugs/ft^3$
υ	kenematic viscosity, ft^2/sec
η	efficiency in recovery
θ	static temperature, °F

Subscript

ave	average
max	maximum

APPENDIX I

BOUNDARY LAYER ALONG THE CLOSED TEST SECTION

To establish the nature of the boundary layer build-up along the closed test section, calculations were made using data obtained from the N series of tests.

Boundary layer thickness at inlet to test section = 0.1 ins.

ditto at outlet = 0.4 ins.

Air velocity at section center V = 234 ft/sec.

Test section length L = 16 ins. = 1.333 ft.

Kinematic viscosity of air $\nu = 1.67 \times 10^{-4}$ ft^2 / sec.

Boundary layer thickness (based on 1/7 power law) $\delta = 0.377\, x \,/\, R_{ex}^{0.2}$ where $R_{ex} = Vx/\nu$.

Calculations:

First calculate the "run-up" length over which the 0.1 in. layer build up occurs. Substitute for δ =0.1 ins= 0.00833 ft. Since $R_{ex_o} = 234\, x_o / 1.67 \times 10^{-4} = 1.404 \times 10^6\, x_o$, one obtains $R_{ex_o}^{0.2} = 16.96\, x_o^{0.2}$.

Therefore $\delta = 0.00833 = 0.377\, x_o / 16.96\, x_o^{0.2}$, resulting in $x_o = 0.293$ ft. This distance need to be added to the test section length 1.333 + 0.293 = 1.626 ft, hence for the total length $R_{eL} = (234)(1.626)/ 1.67 \times 10^{-4} = 2.3 \times 10^6$

With this value one obtaines the boundary layer thickness at exit from the test section as being

$$\delta = 0.377\ (1.626\ )/(2.3 \times 10^6)^{0.2} = 0.0327 \text{ ft}$$
$$= 0.393 \text{ ins}$$

This result is close to 0.4 ins and the boundary layer is considered turbulent. Based on the horizontal width of the test section, 4.40 ins.,the value of 0.4 ins. represents about 9 percent of the width.

APPENDIX II.

DIFFUSER EFFICIENCIES

Formula for calculating diffuser efficiency:

First diffuser: $\eta = 1.037 \, (p_4 - p_6) / (p_3 - p_2)$ (*)

Second diffuser: $\eta = 4.074 \, (p_{10} - p_{13}) / (p_3 - p_2)$ (*)

TEST RESULTS:

CLOSED TEST SECTION

First diffuser

L Tests Dimmock vanes	p_4	p_6	p_3	p_2	η%
	64.6	29.3	66.1	4.6	59.52
N Tests Salter vanes	77.8	35.7	79.9	5.3	58.52

Second diffuser

L Tests Dimmock vanes	p_{10}	p_{13}	p_3	p_2	
	42.7	31.7	66.1	4.6	72.87
N Tests Salter vanes	44.9	31.8	79.9	5.3	71.54

OPEN TEST SECTION

First diffuser

J Tests Dimmock vanes Coll. gap 0.25 ins Noz. Diff. optimum	p_4 66.5	p_6 31.9	p_3 54.9	p_2 3.8	70.22
S Tests Salter vanes	65.8	31.8	55.2	3.9	68.73

Second diffuser

J Tests Dimmock vanes	p_{10}	p_{13}	p_3	p_2	
	40.8	31.3	54.9	3.8	75.74
S Tests Salter vanes	40.8	31.4	55.2	3.9	74.65

(*) For details see APPENDIX IV.

APPENDIX III(a)

PRESSURE LOSSES ASSOCIATED WITH TURNING VANES.

Tests were also perfomed to establish the integrated average dynamic pressure $\bar{q}$, calculated from traverses taken up-and downstream from each set of vanes. The losses then may be expressed in terms of total pressure changes across the vanes.

Denoting upstream location with sub- n and downstream with sub- n+1, one obtains for each corner the loss

$$\Delta p_t = (p_n - p_{n+1}) + (\bar{q}_n - \bar{q}_{n+1}) = \Delta p + \Delta \bar{q}$$

where $\bar{q} = {}^1/_A \int q dA$, p= static pressure, psf., q = dynamic pressre.

Table I.

RESULTS WITH TEST SECTION CLOSED

Dimmock vanes "L"

Corner	Station #	$-p_n$	$\bar{q}_n$ (*)	Δp	$\Delta \bar{q}$	Δp_t	$\Delta p_t / q_n$
	6	29.3	20.22				
First				3.5	2.75	6.25	0.309
	7	32.8	17.47				
Second				7.7	1.79	9.49	0.543
	8	40.5	15.68				

Salter vanes "N"

	6	35.7	24.57				
First				2.9	0.96	3.86	0.157
	7	38.6	23.61				
Second				8.4	-1.41	6.99	0.296
	8	47.0	25.02				

Table II.

RESULTS WITH TEST SECTION OPEN

Dimmock vanes "J"

	6	31.9	13.36				
First				3.0	3.61	6.61	0.495
	7	34.9	9.75				
Second				5.7	-1.67	4.03	0.414
	8	40.6	11.42				

Salter vanes "S"

	6	31.8	15.03				
First				3.9	-.33	3.57	0.237
	7	35.7	15.36				
Second				6.8	-2.54	4.26	0.277
	8	42.5	17.9				

(*) $\bar{q}$ results were communicated by Mr. E. Booth

APPENDIX III(b)

EFFECTS OF VANE THICKNESS ON DYNAMIC HEAD.

Sketch A shows a circle being the cross section of the duct leading to the set of vanes. Consider SALTER vanes first, assuming 16 gaps between 15 vanes in a 6.25 ins. dia. circle, thus having r=3.125 ins. radius. Pitch = 6.25/16= 0.3906 ins. between vanes. Writing the equation for the circle : $x^2 + y^2 = 3.125^2 = 9.765$, $y = \sqrt{9.765 - x^2}$, where y is the 1/4 length of the vane edges facing the stream, the edge having 0.0625 width. Thus the total length of turning vanes edges facing the flow

$$L = \sum_{1}^{8} 4\sqrt{9.765 - x^2}$$

where: Vane #	x	4y
0	0	12.5
1	.39	12.4
2	.78	12.1
3	1.17	11.6
4	1.56	10.8
5	1.95	9.77
6	2.34	8.27
7	2.73	6.08
8	3.12	.71
		84.2

Vane area facing flow:
$A_v = 84.2 \times 0.0625 = 5.263 \text{ in}^2$
Area of circle $30.66 \text{ in}^2 = A_c$
Area open to flow
$A_{eff} = 30.66 - 5.263 = 25.397 \text{ in}^2$
Thus blockage $B = 1 - A_{eff} / A_c = 0.172$

(17.2%)

Sketch B shows the circle with the Dimmock vanes facing the flow. This time the circle is displaced with its center at radius distance from origin for convenience, because the vanes are un equally placed. Writing the equation of the circle $(x - 3.125)^2 + y^2 = r^2$, one obtains $y = \sqrt{6.25x - x^2}$ and thus $L = \sum_{1}^{7} 2\sqrt{6.25x - x^2}$

where: Vane #	x	1
1	.42	3.13
2	.95	4.49
3	1.57	5.43
4	2.30	6.03
5	3.14	6.25
6	4.07	5.95
7	5.11	4.82
		36.1

Vane area facing flow:
$A_v = 36.1 \times 0.0625 = 2.256 \text{ in}^2$
Area open to flow:
$A_{eff} = 30.66 - 2.256 = 28.4 \text{ in}^2$
Thus blockage $B = 1 - A_{eff} / A_c = 0.0737$
(7.37%)

Thus the dynamic head ratio

$$\frac{q_{Salter}}{q_{Dimmock}} = (28.4/25.39)^2 = 1.25$$

APPENDIX IV

CALCULATION OF THE AVERAGE DYNAMIC HEAD AT THE CONTRACTION EXIT

To establish the dynamic head q, write Bernouilli's equation for locations 2 and 3

$$p_2 + 1/2\rho V_2^2 = p_3 + 1/2\rho V_3^2 + \text{losses } 2\text{-}3$$

Assume losses 2-3 $= 0.05\ 1/2\rho V_3^2$, hence

$$p_2 - p_3 = 1/2\rho V_3^2\ (1+0{,}05) - 1/2\rho V_2^2 \qquad \ldots.1$$

By continuity

$$A_2 V_2 = A_3 V_3,$$

hence

$$V_2^2 = (A_3/A_2)^2\ V_3^2$$

Since the contraction ratio is 9:1, $A_3/A_2 = 1:9$

Upon substitution into Eq.1 one obtains

$$p_2 - p_3 = 1/2\rho\ V_3^2 (\ 1.05 - 1/81\ ) = 1.0377\ q_3$$

Where $q_3 = 1/2\ \rho\ V_3^2$

Hence, $$q_{3\ av} = 0.964\ (\ p_2 - p_3)$$

Since all the pressures are negative, being sub-atmospheric,

$$q_{3ave} = 0.964\ (\ p_3 - p_2\ )$$

With this value of q, average dynamic head around the tunnel circuit can be calculated at any paricular point when knowing the area ratio related to A_3 .

Diffuser efficiency (See APPENDIX II)

Let diffuser efficiency be defined as the pressure rise divided by the average dynamic head,

$$\eta = (\ p_e - p_1\ ) / q_{ave}$$

Thus for the first diffuser

$$\eta = (\ p_6 - p_4\ ) / q_{3ave} = 1.0377\ (\ p_6 - p_4)/(\ p_3 - p_2)$$

Since the area at the second diffuser inlet relates to the area at the first diffuser inlet in an area ratio of 3.92/ : 1, one obtains for the second diffuser

$$\eta = 3.927\ (\ p_{13} - p_{10}\ ) / q_3 = 4.074\ (p_{13} - p_{10})/(p_3 - p_2).$$

APPENDIX V.

ELECTRIC MOTOR COOLING

The electric motor driving the proposed ax 1 flow fan of the model tunnel was specified for a shaft power output 2.5 HP at a rotational speed of of 11,700 r.p.m. Suppliers of the motor specified 180 Watts for internal heat generation, allowing a maximum "total" temperature rise not to exceed 150 ^{o}C when operating with 200 volts and frequency 400 Hz.

The cooling of motors of similar designs is generally achieved by using extended surfaces externally added to the housing. External fins or ribs are generally arranged radially around the circumference of the housing along the length of the motor for heat dissipation. A cross section of such an arrangement is shown in figure V/1.

Generally, removal of the heat causes no problem if the motor is operated in open space and free convection suffices. However, problems occur in windtunnels when the motor is housed inside the nacelle and the fan is directly driven by the motor. In such a case some form of forced convection is required.

For cooling the motor it was proposed in this case to use a cross -flow arrangement and create currents inside the spaces between fins by blowing air over the tips of the fins. This was achieved by leaving a narrow gap inbetween the fin tips and the nacelle "skin" and introducing air flow through a streamlined tubing extending through the fan annulus shown in figure V/1. It was proposed to employ a blower fan to force air through the tubing and meter the flow rate and measure the temperature rise of the air.

Test model for motor cooling

For testing the effectiveness of the proposed cooling arrangement, a model was built. A 1 inch wide section of the actual motor housing was obtained from the manufacturers and this was heated from the inside by an electric element embedded in an aluminum disc tightly fitted into the place of the motor. To form an air passage, an outer ring surrounded the section, leaving an 1/8 ins. gap inbetween. At inlet to the passage, the flow of air was divided and was allowed to branch into two halves only to be collected at the outlet. Thermocouples were used to measure the disc temperature as well as the temperature rise of the air, while the flowrate was measured with an orifice.

Finally, the section was sandwiched between two endplates and was insulated. Ambient air temperature was monitored from time to time. A volt and an ampere meter established the heat input in Watts. Air flow was obtained from the main air line in the laboratory, and the pressure change around the perimeter was measured.

Theory

The heat absorbtion dQ_1 of a given mass M of a material through a temperature rise $d\theta$ is given by

$$dQ_1 = cMd\theta$$

where c is the specific heat of the material.

The heat input (electric) dQ_2 in dt time

$$dQ_2 = 3.4Wdt$$

where W is in watts and Q is in Btu.

The heat transferred to the ambient air in dt time

$$-dQ_3 = \alpha(\theta - \theta_{air}) Sdt$$

where α is the heat trasnfer coefficient and S is the heat trasfer contact surface.

Thus the net heating effect

$$dQ_1 = dQ_2 - dQ_3$$

or

$$cMd\theta = 3.4Wdt - \alpha(\theta - \theta_{air})\,Sdt$$

It follows that

$$dt = d\theta / (A - B\theta^*)$$

where $A = 3.4W/cM$, $B = \alpha S/cM$, $\theta^* = \theta - \theta_{air}$

Upon integration, one obtains

$$t+C = -\frac{1}{B} \ln (A - B\theta^*)$$

When $t=0$, $\theta^* = \theta - \theta_{air} = 0$, hence $C = -1/B \ln A$

Therefore

$$t = 1/B \ln A / (A - B\theta^*)$$

For the temperature difference θ^* one obtains

$$\underline{\theta^* = A/B (1 - e^{-Bt})}$$

The curve θ^* vs. t approaches the limit A/B if t is large, thus $\theta^* \rightarrow A/B = 3.4W / \alpha S$

From this formula the heat transfer coefficient α can be calculated when measuring θ^* and W over a period of time. If α is large enough, t=1 hr. may be sufficient.

Results of experiments

Two sets of test were performed: in the first set of tests the air supply for cooling was turned off and in the second set, the cooling air supply was turned on. Results of the tests are plotted in figure V/2 , where the "core" disc temperature rise is plotted against time. It appears that in the first set of tests temperature kept rising and it was estimated that the value of

= 2 approximately. In the second set of tests, three values

of air mass flow was used, $\dot{W}$ = 10.42, 12.52 and 14.8 lbs/ hour. These curves show common characteristics: all rise fast at start and reach equilibrium after about one hour of operation.

From the results obtained with $\dot{W}$=12.52 lbs/hr air flow the heat transfer coefficient was established as being α = = 14.2 Btu/ hr, sqft., ^{o}F , using the physical constants shown below. With this value of α the temperature rise curve may be expressed as

$$\theta^{*} = 50.5 \left(1 - 1/ e^{5.86t} \right)$$

It appears from figure V/3 that values obtained from theory agree very well with those obtained from the experiments.

Without using airflow the calculations of temperature rise agree well with the experiments if a heat transfer coefficient α = 1.55 is used. It appears that after one hour the temperature still kept rising.

Data:

Mass of aluminum parts = 1.344 lbs
Mass of bakelite covers= 0.515 lbs } Total weight M = 1.86 lbs.

Surface areas: in the case of forced convection S = 0.167 ft^2
without air cooling S = 0.51 ft^2

Electric heat input: 0.32 Amps. at 110 Volts. = 35.2 Watts.

Specific heat of aluminum parts is 0.23 Btu/lb/oF

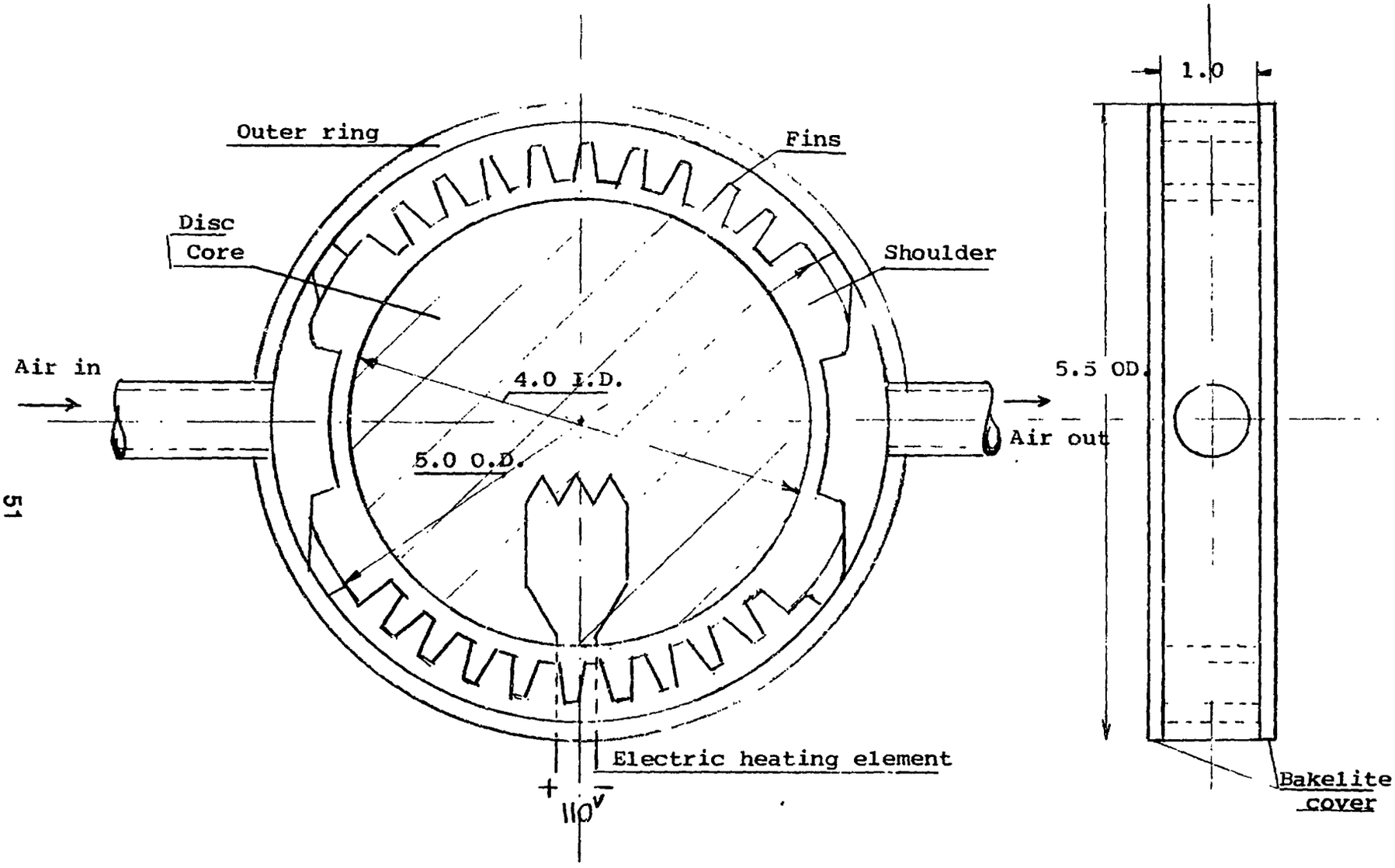

Figure V/1. Experimental set-up for determination of motor cooling

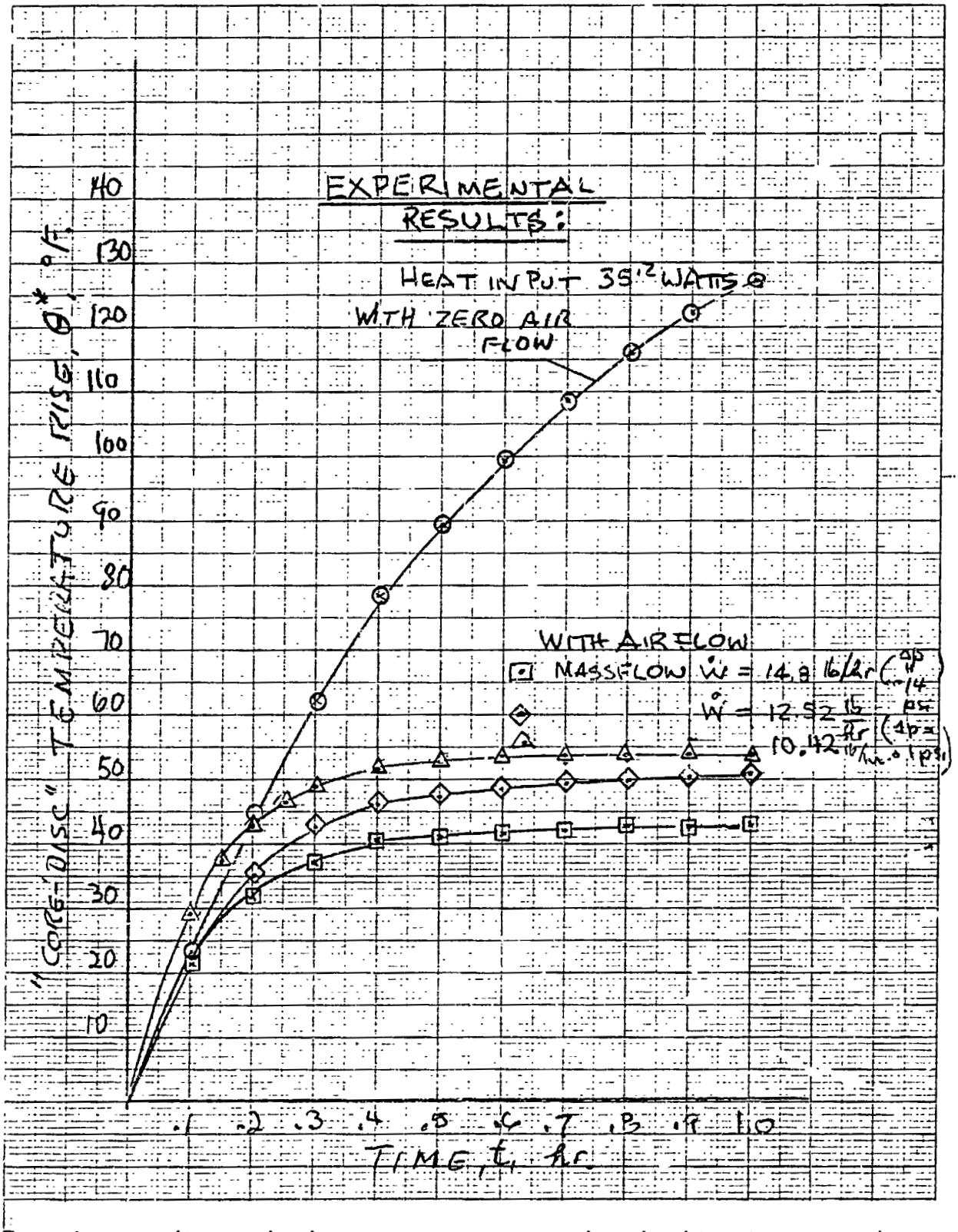

Figure V/2. Variation of temperature rise inside the core disc with and without air cooling

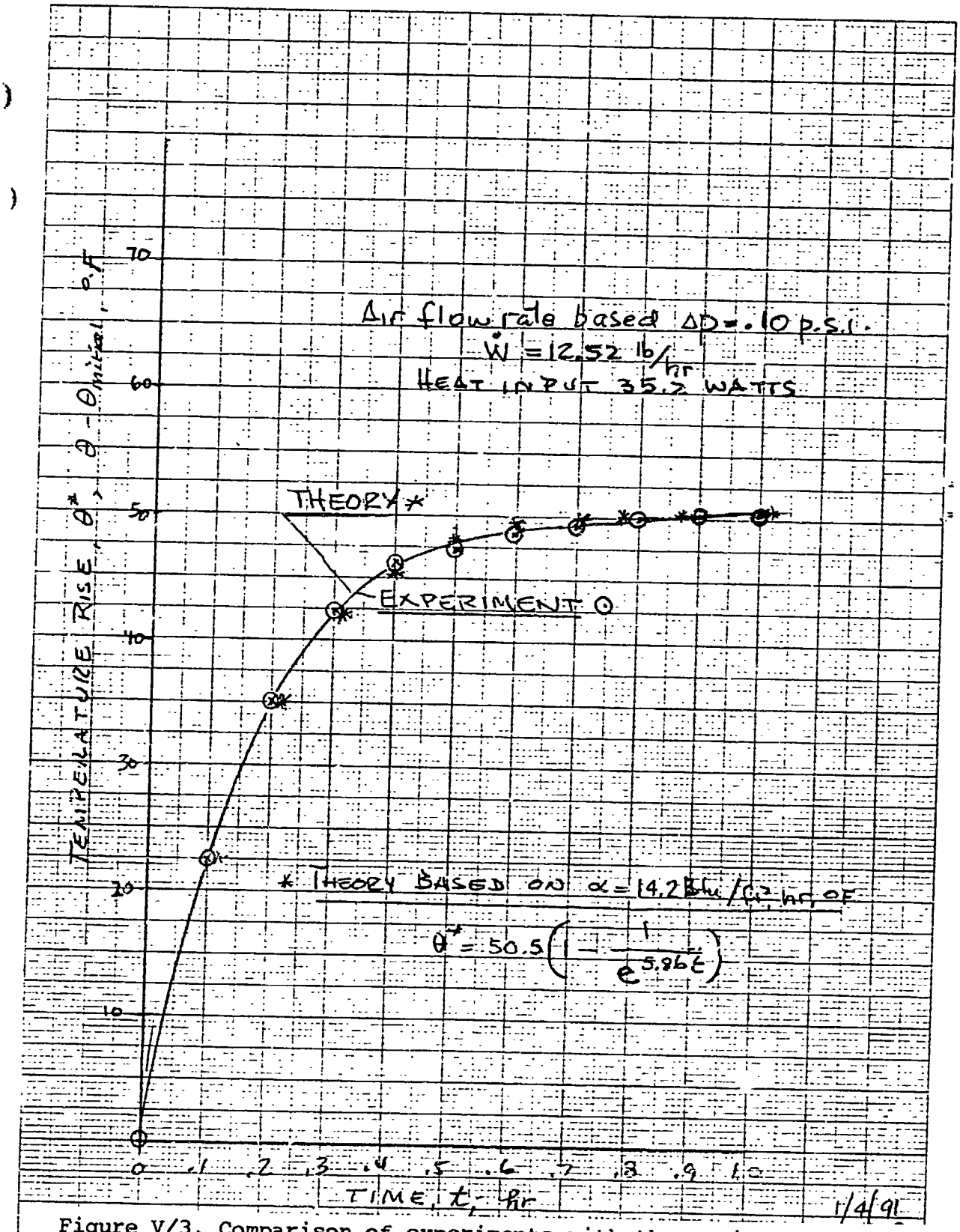

Figure V/3. Comparison of experiments with theoretical prediction of temperature rise

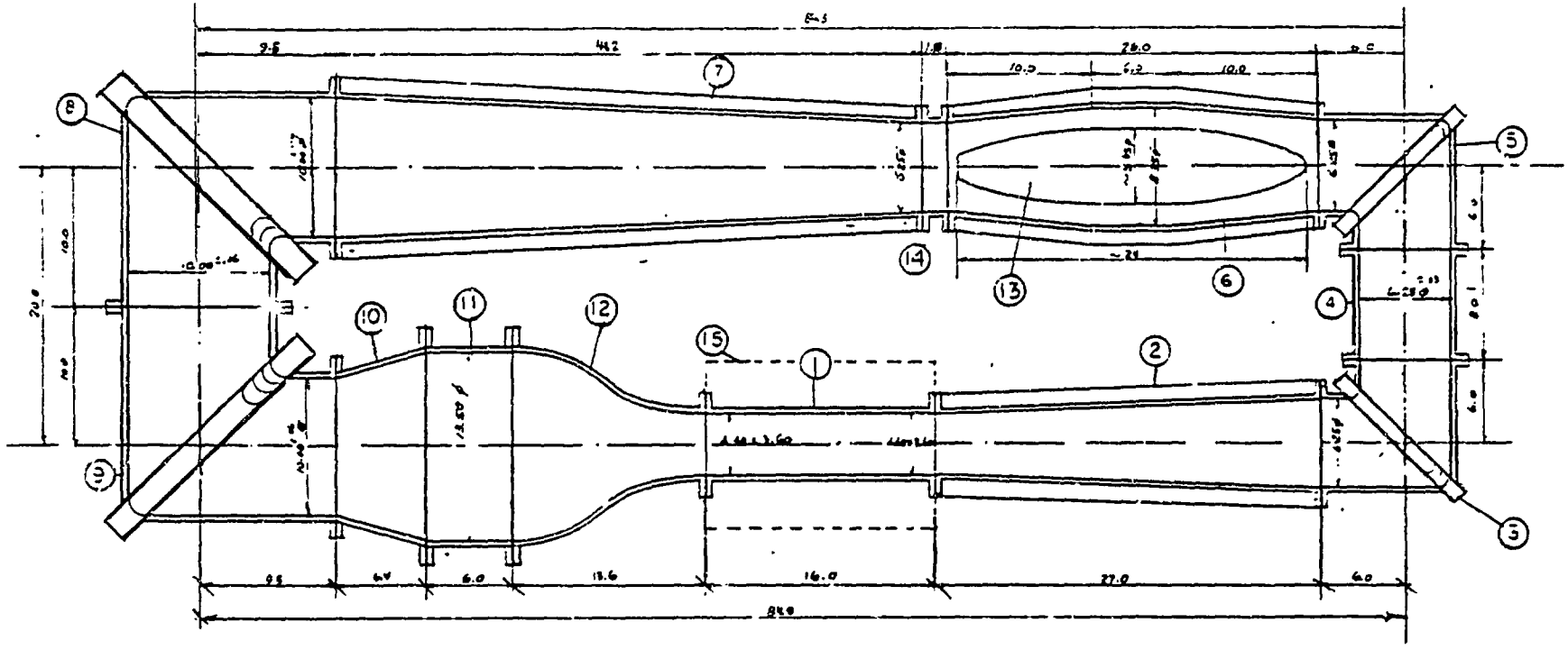

Figure 1. Plan view of the H.S.A.W.T. 1/60th scale model

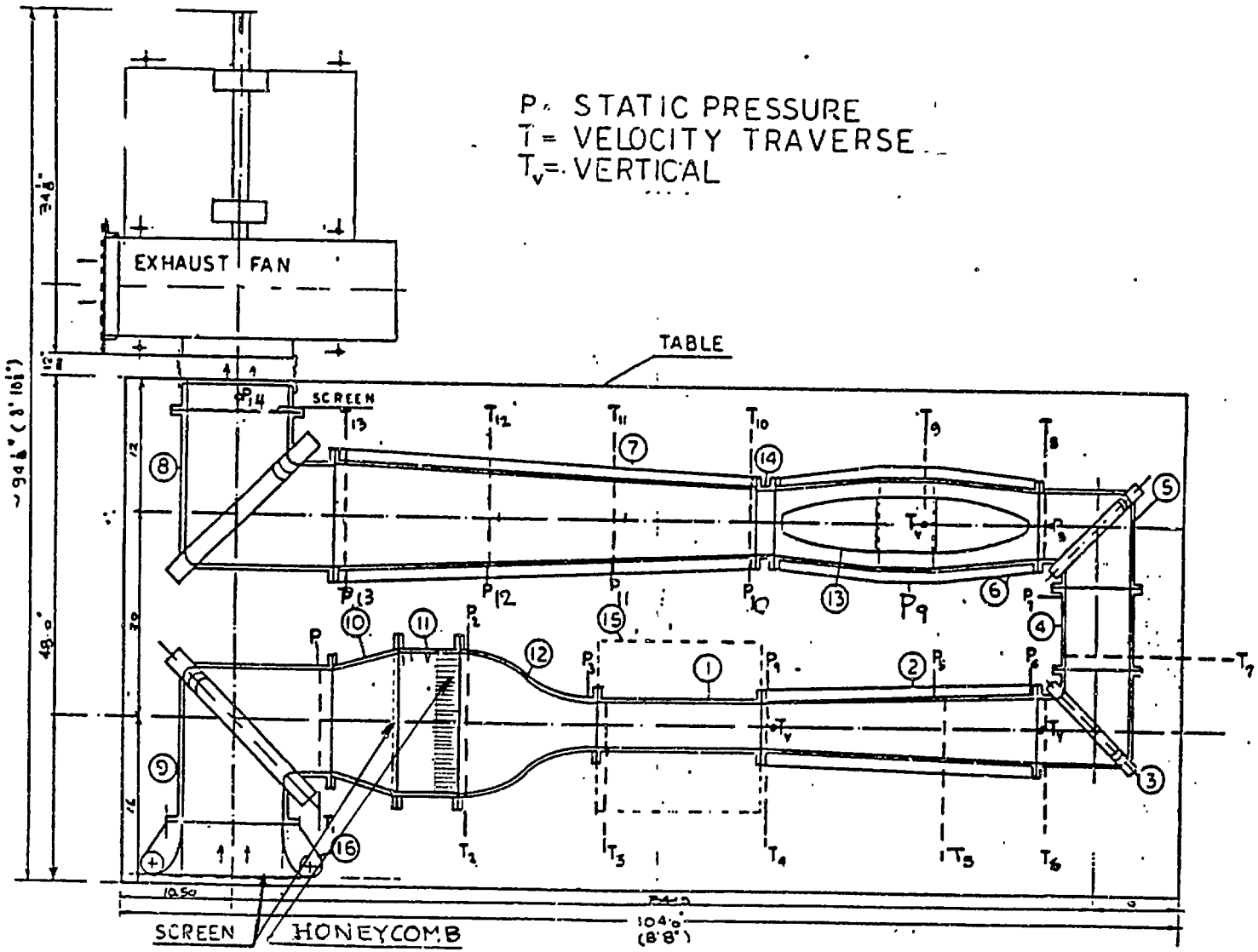

Figure 2. Plan view of the open circuit model tunnel showing induction fan, pressure ports and traverse locations. Closed Test Section.

H.S.A.W.T. 1/60 SCALE MODEL

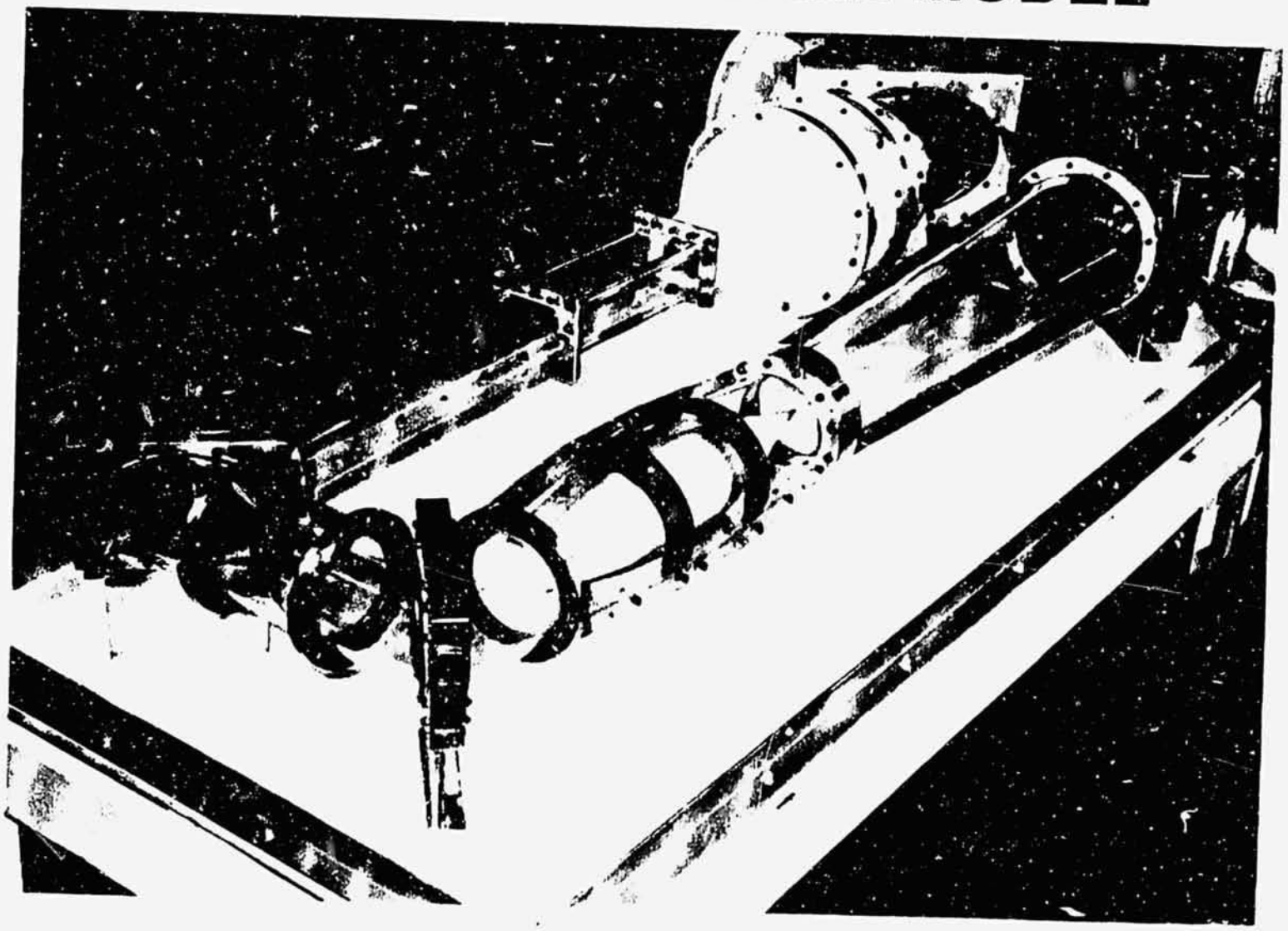

Figure 3. Photographic view of the tunnel with closed test section

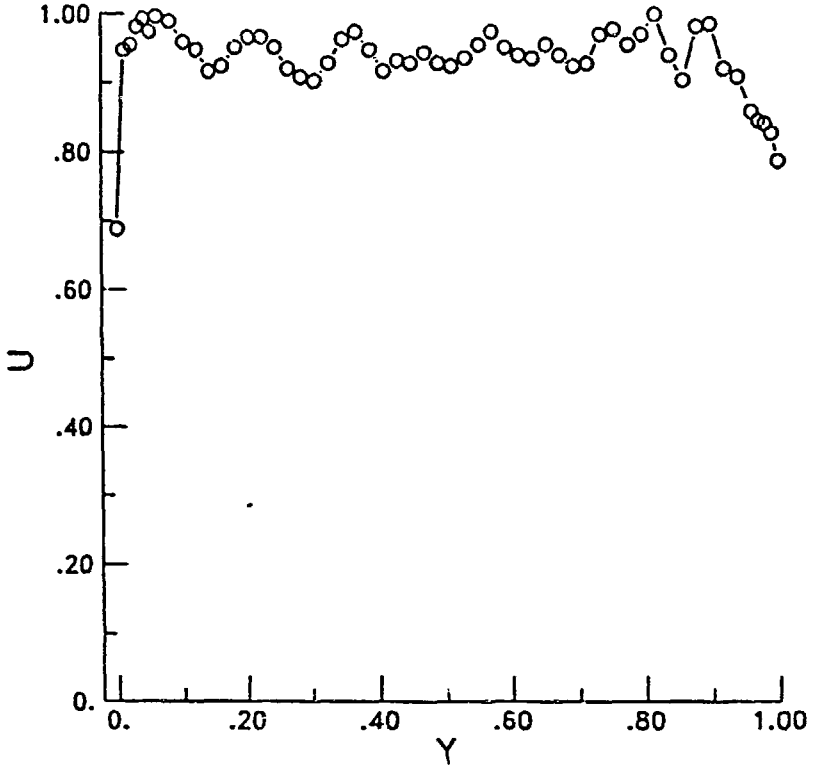

Figure 4a. Location #1

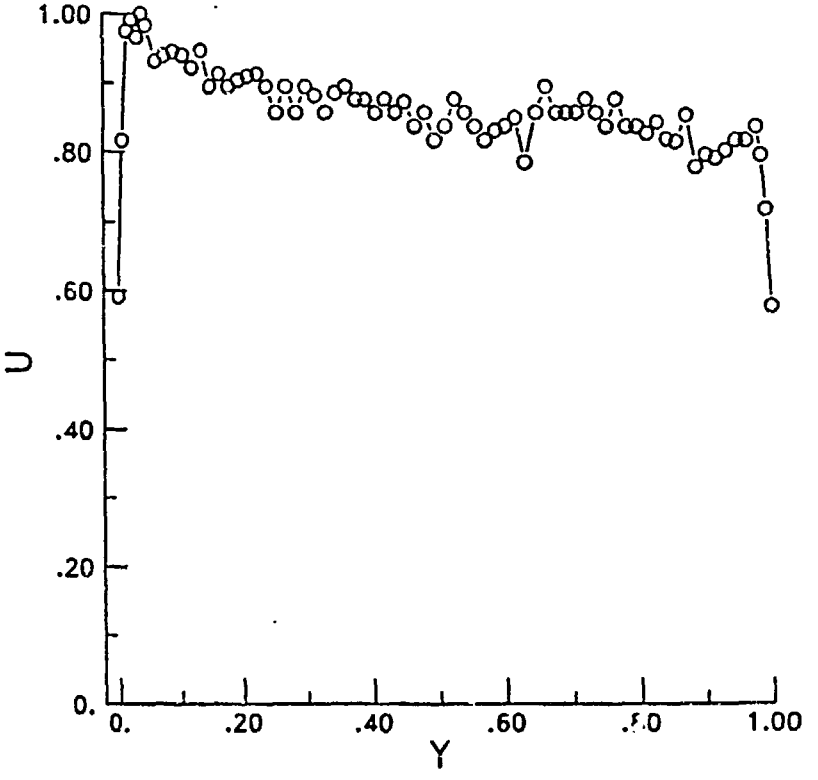

Figure 4b. Location #2

Figure 4. Horizontal velocity traverses around tunnel circuit

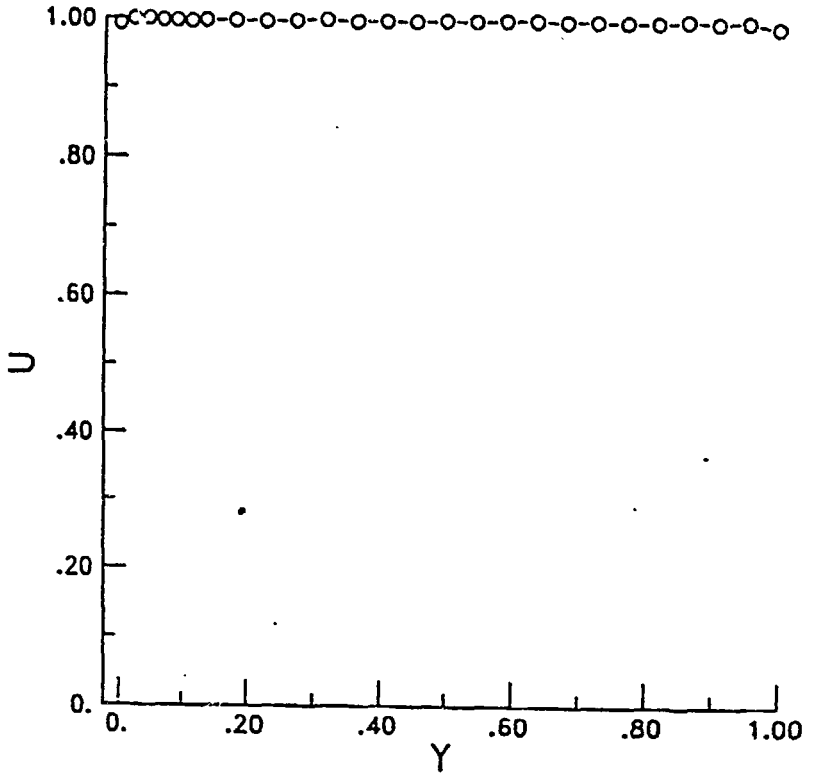

Figure 4c. Location #3

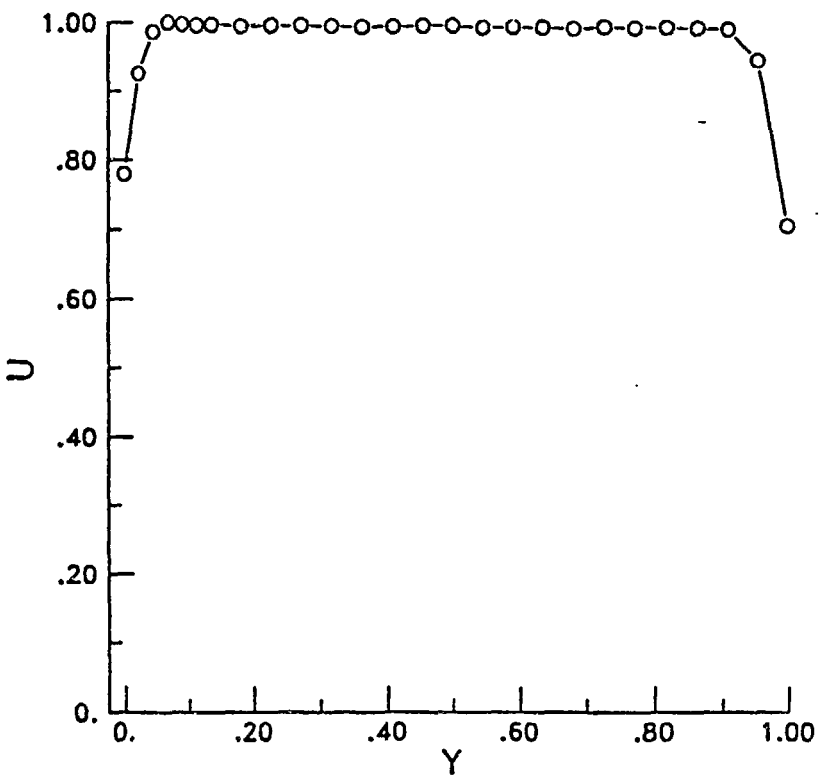

Figure 4d. Location #4

Figure 4-Continued

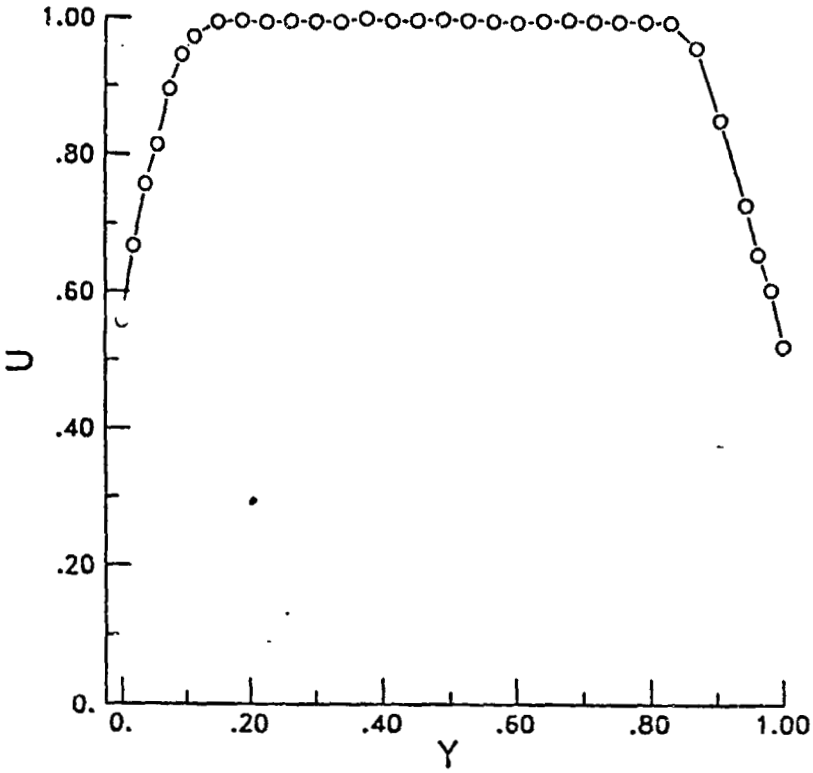

Figure 4e. Location #5

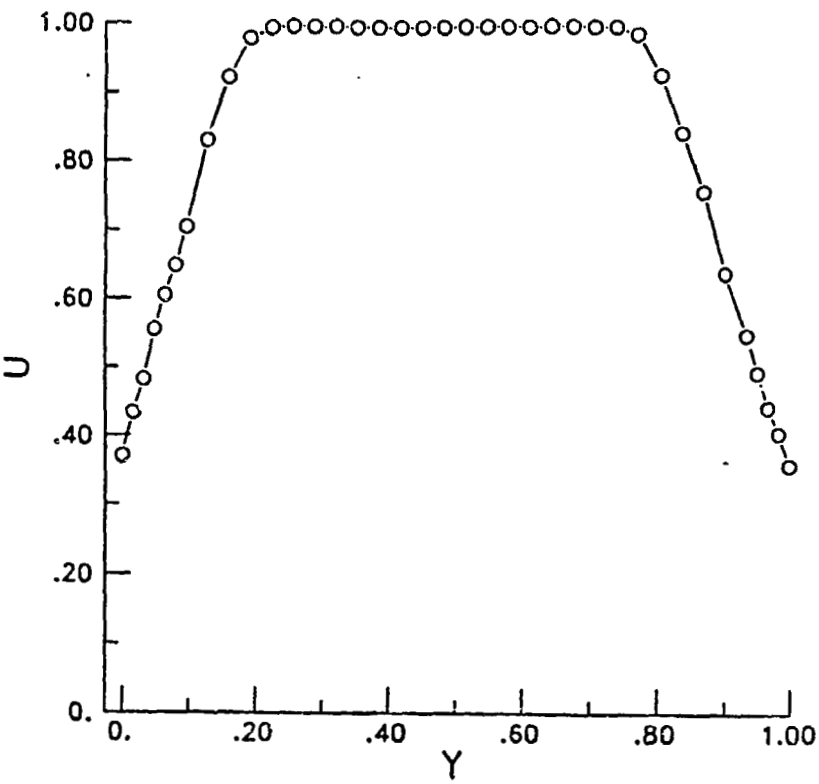

Figure 4f. Location #6

Figure 4-Continued

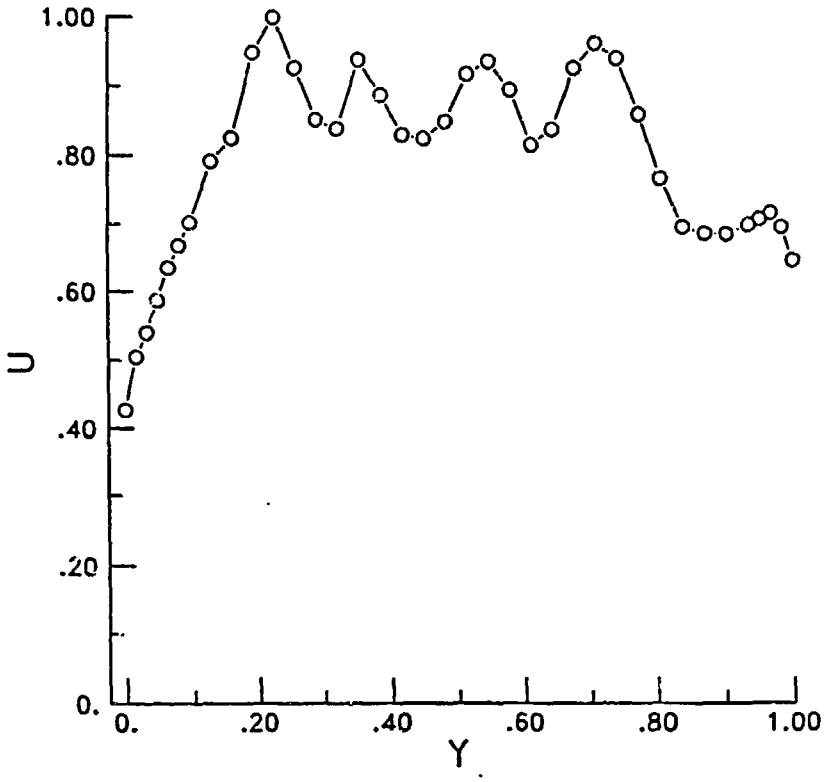

Figure 4g. Location #7

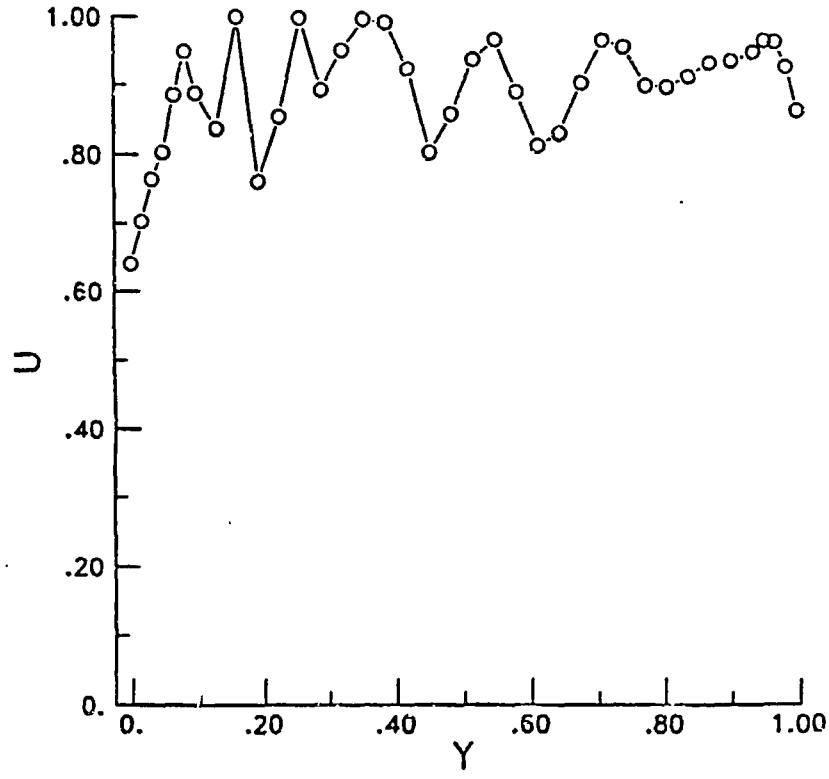

Figure 4h. Location #8

Figure 4-Continued

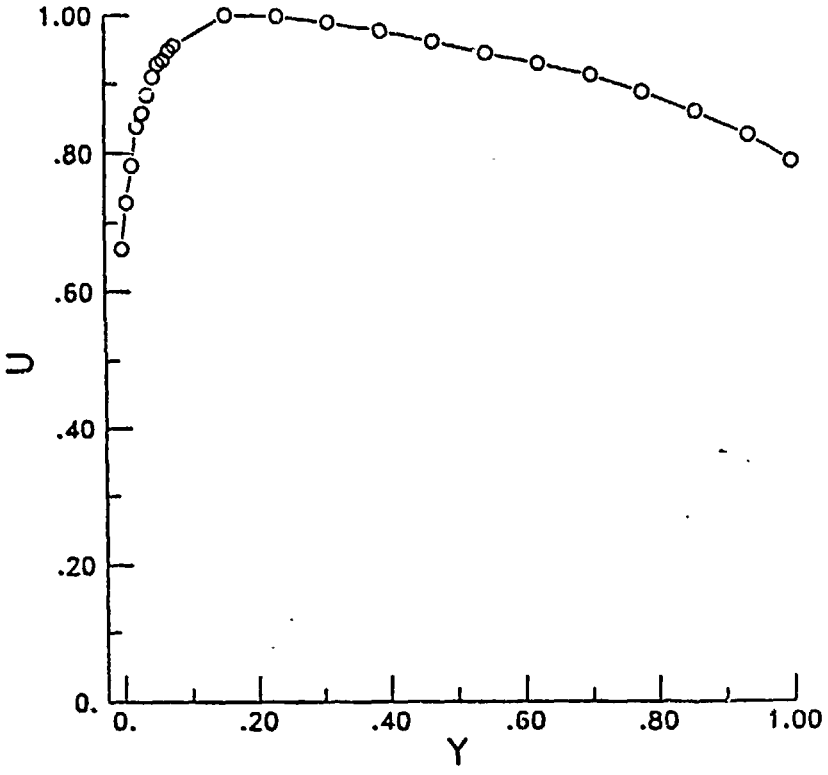

Figure 4i. Location #9- Inboard

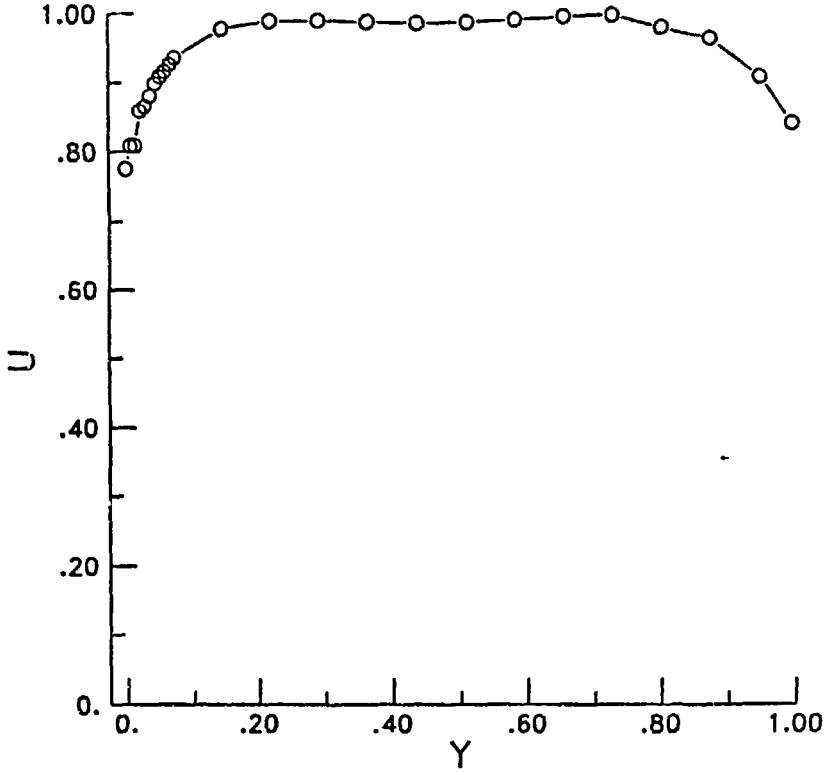

Figure 4j. Location #9- Outboard

Figure 4-Continued

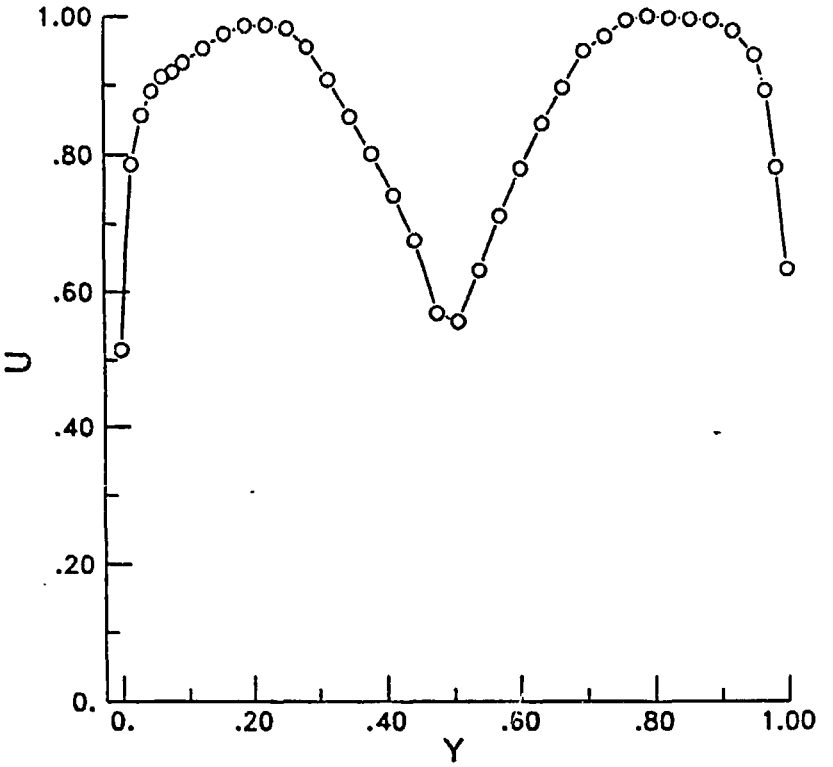

Figure 4k. Location #10

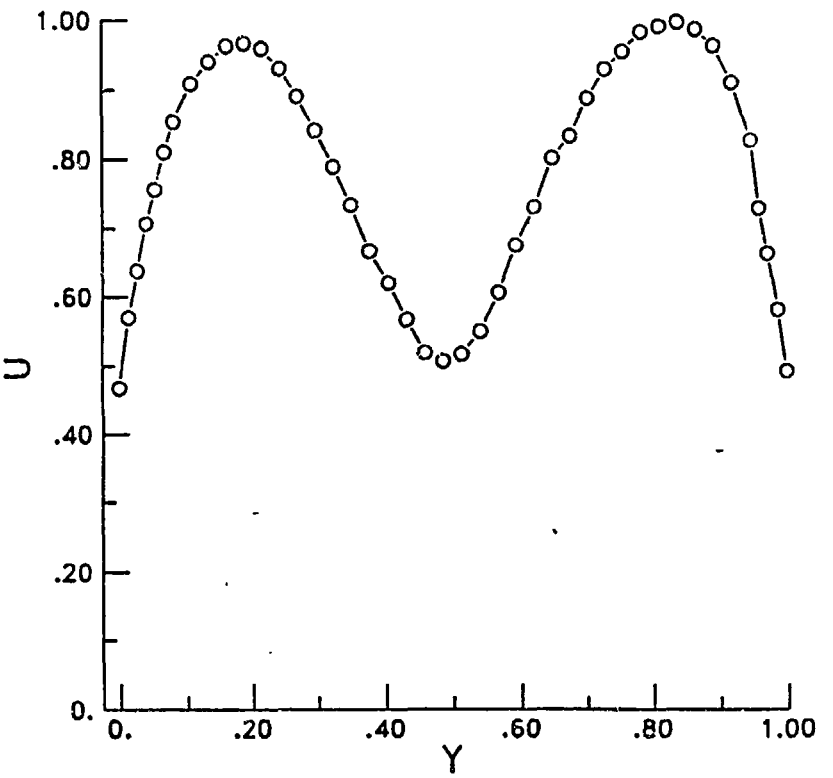

Figure 4m. Location #11

Figure 4-Continued

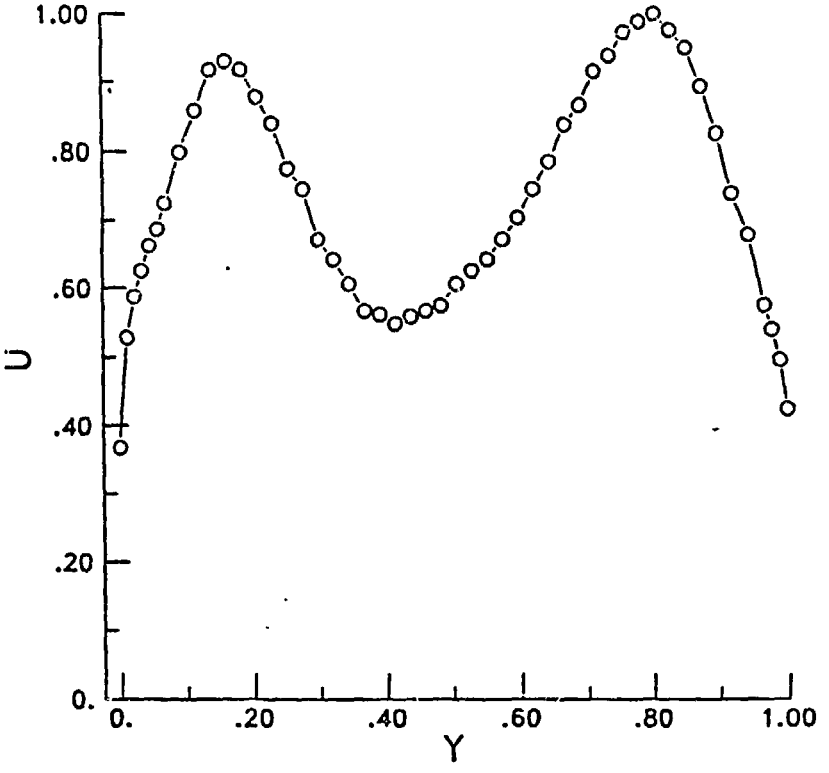

Figure 4n. Location #12

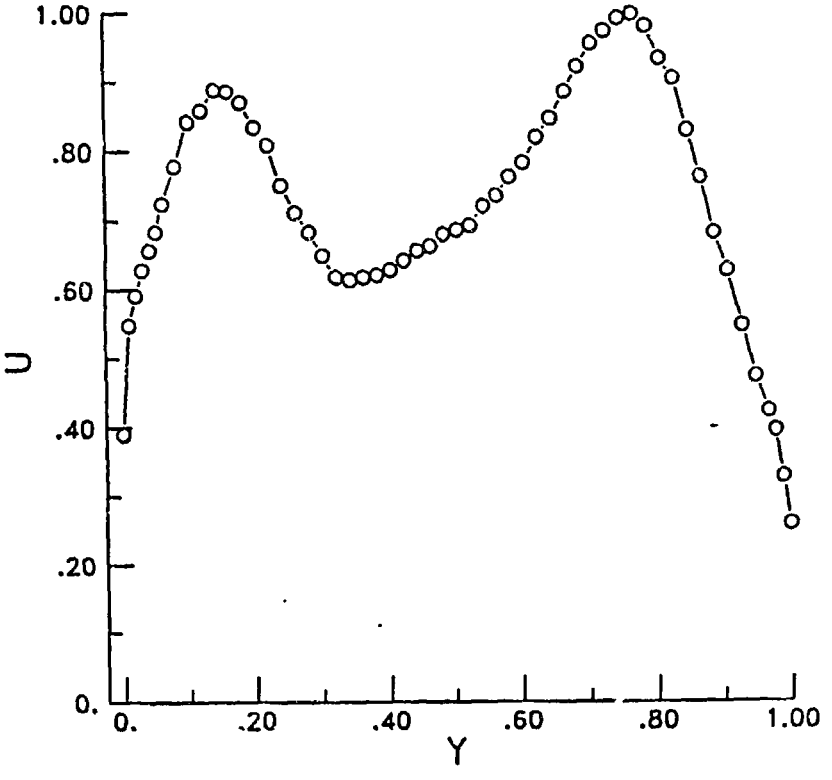

Figure 4o. Location #13

Figure 4-Concluded

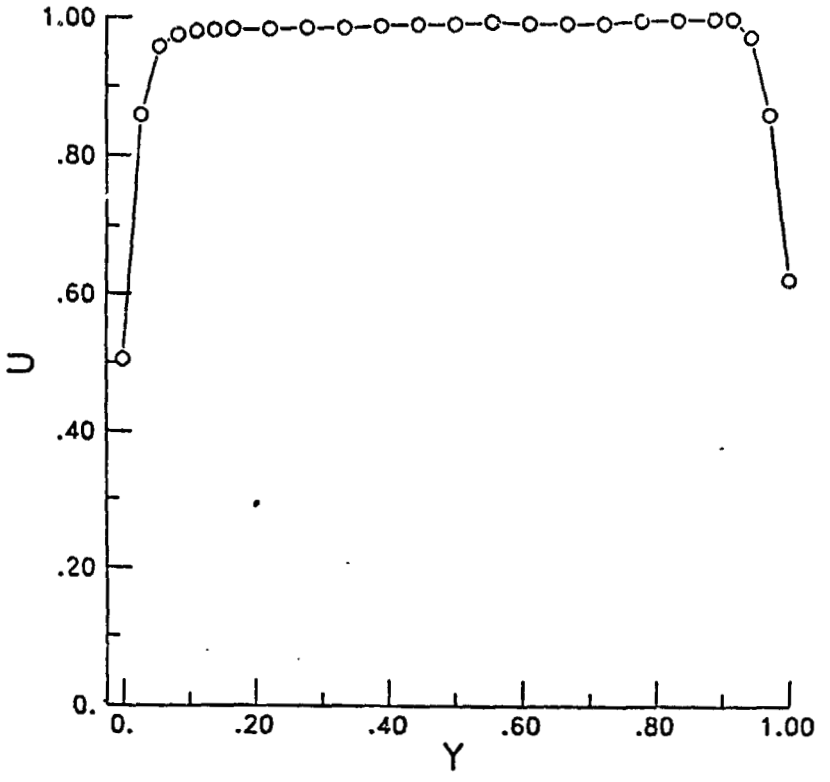

Figure 5a. Location #4

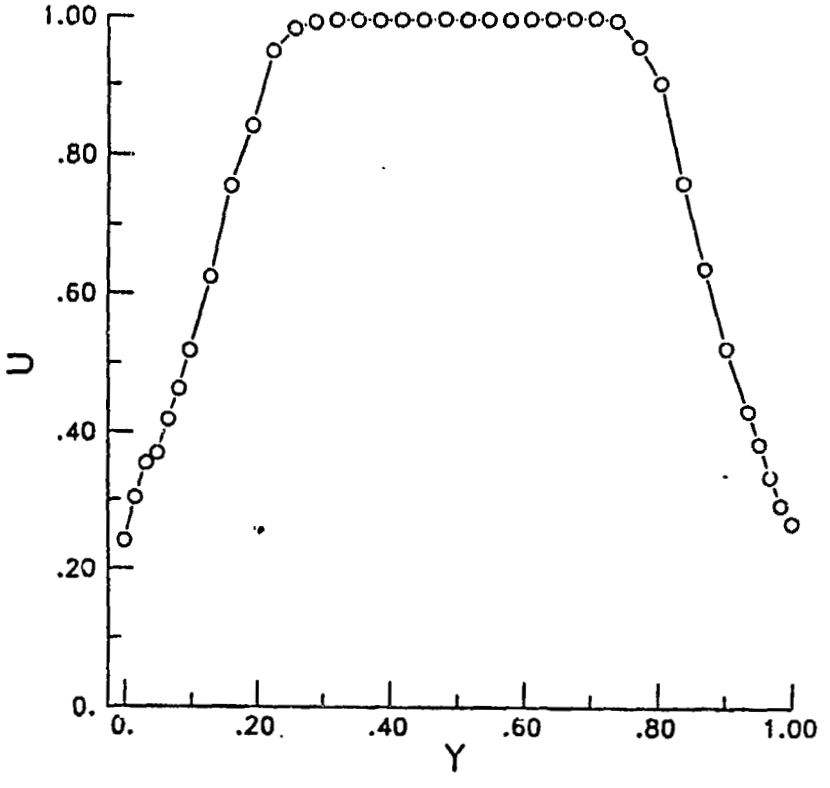

Figure 5b. Location #6

Figure 5. Vertical velocity traverses at various locations

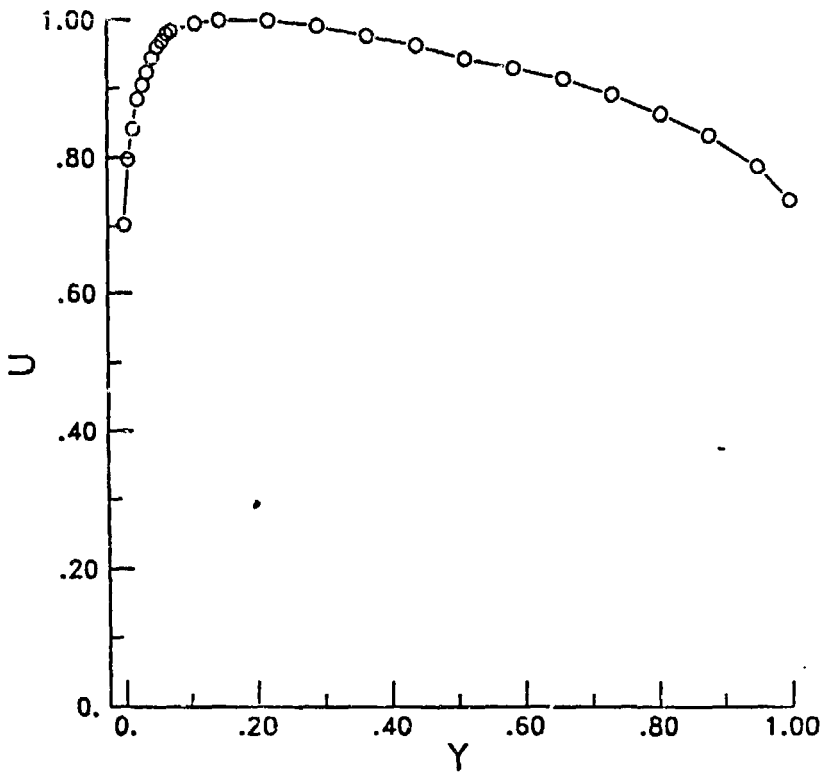

Figure 5c. Location #9

Figure 5 - Concluded

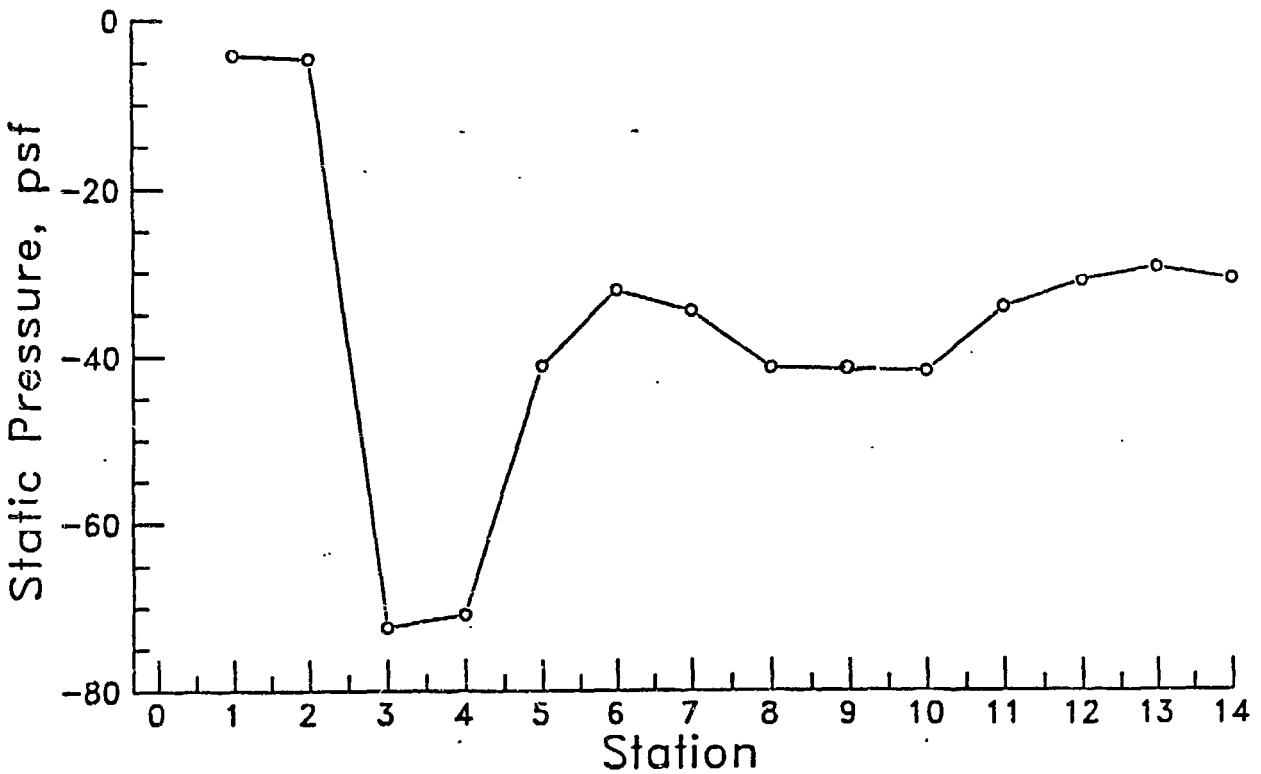

Figure 6. Pressure distribution around the tunnel circuit (closed test section)

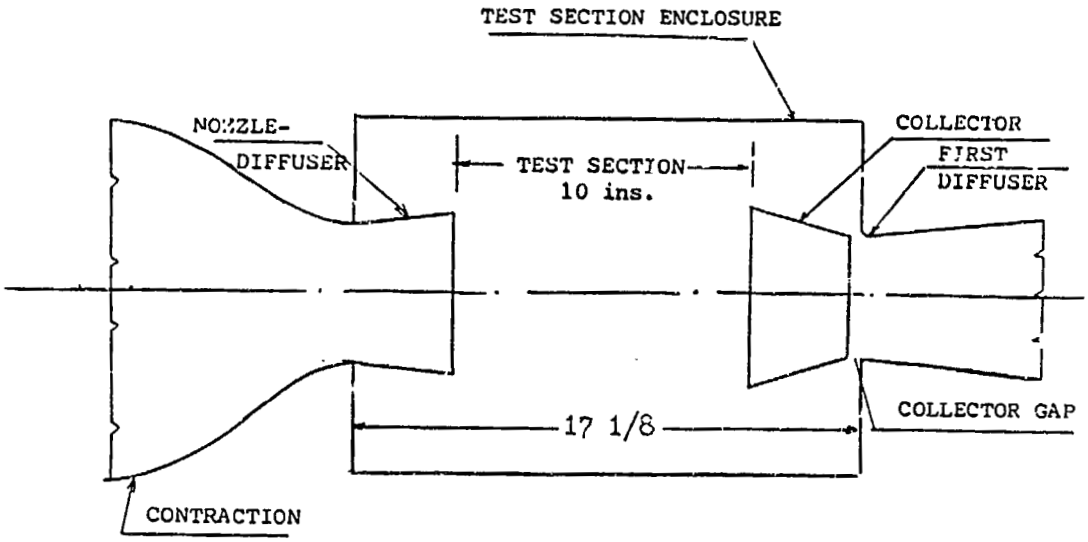

a: Schematic outline of the open test section

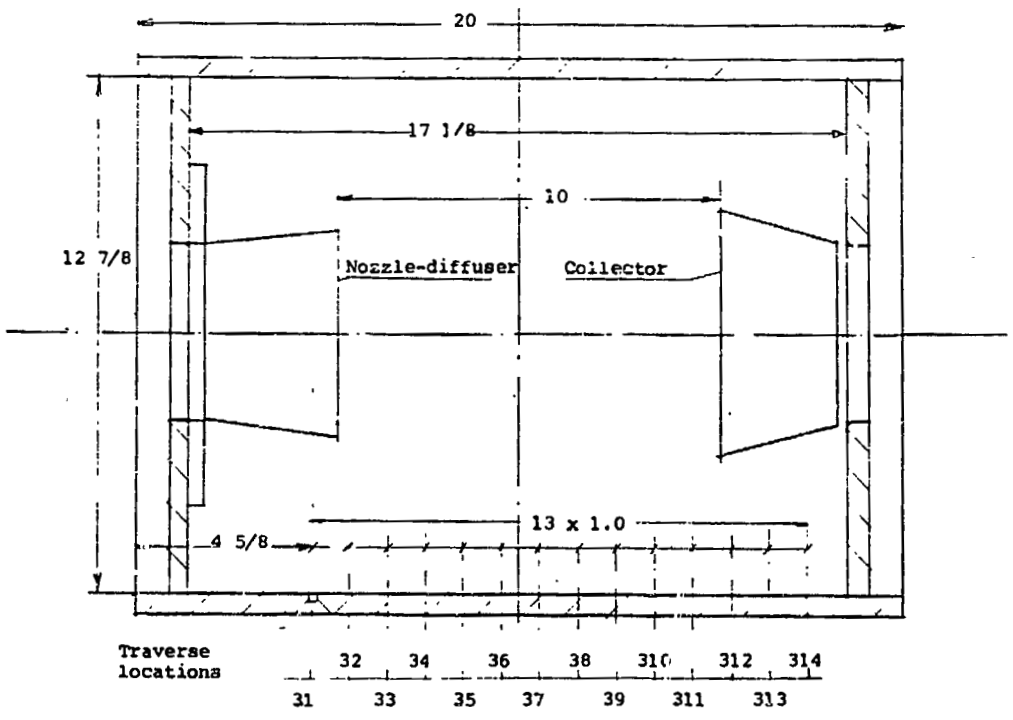

b: Plan view of the Open Test Section showing velocity traverse locations

Figure 7

Figure 8. Overall view of the H.S.A.W.T. model tunnel with open test section

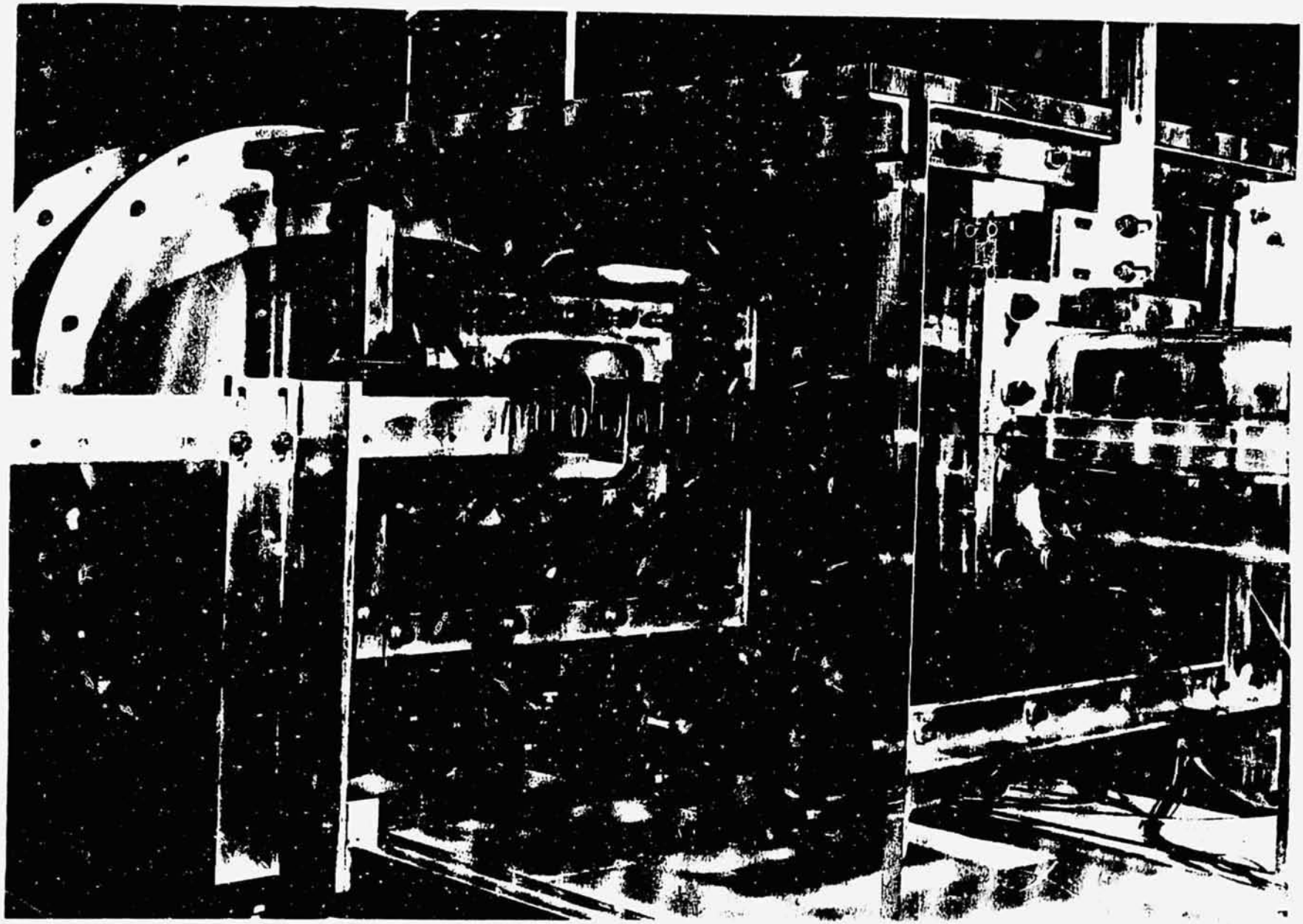

Figure 9 Side view of the Open Test Section

Figure 10, Top view of the Open T.S. with the lid removed

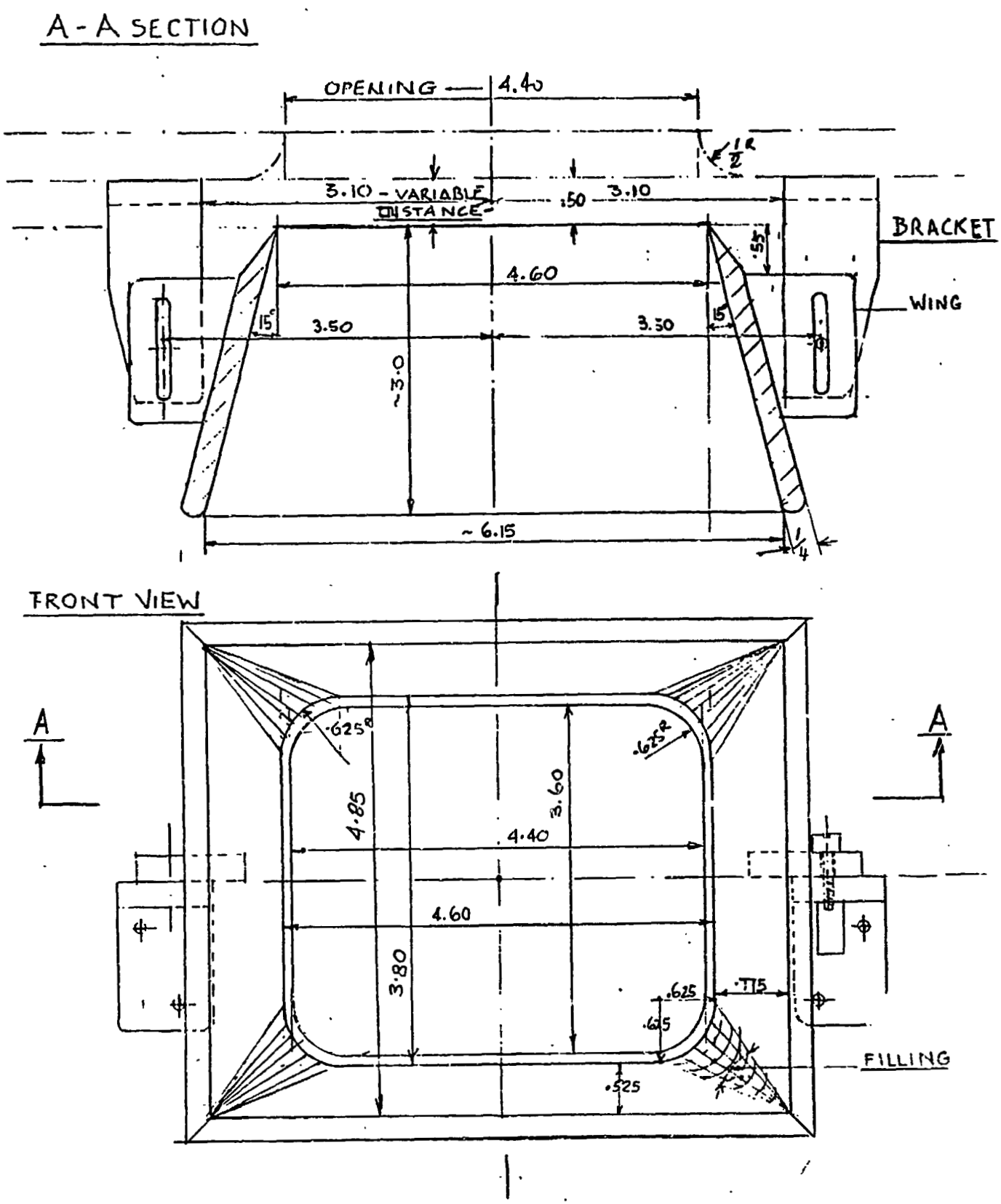

Figure 11. Details of the Collector design

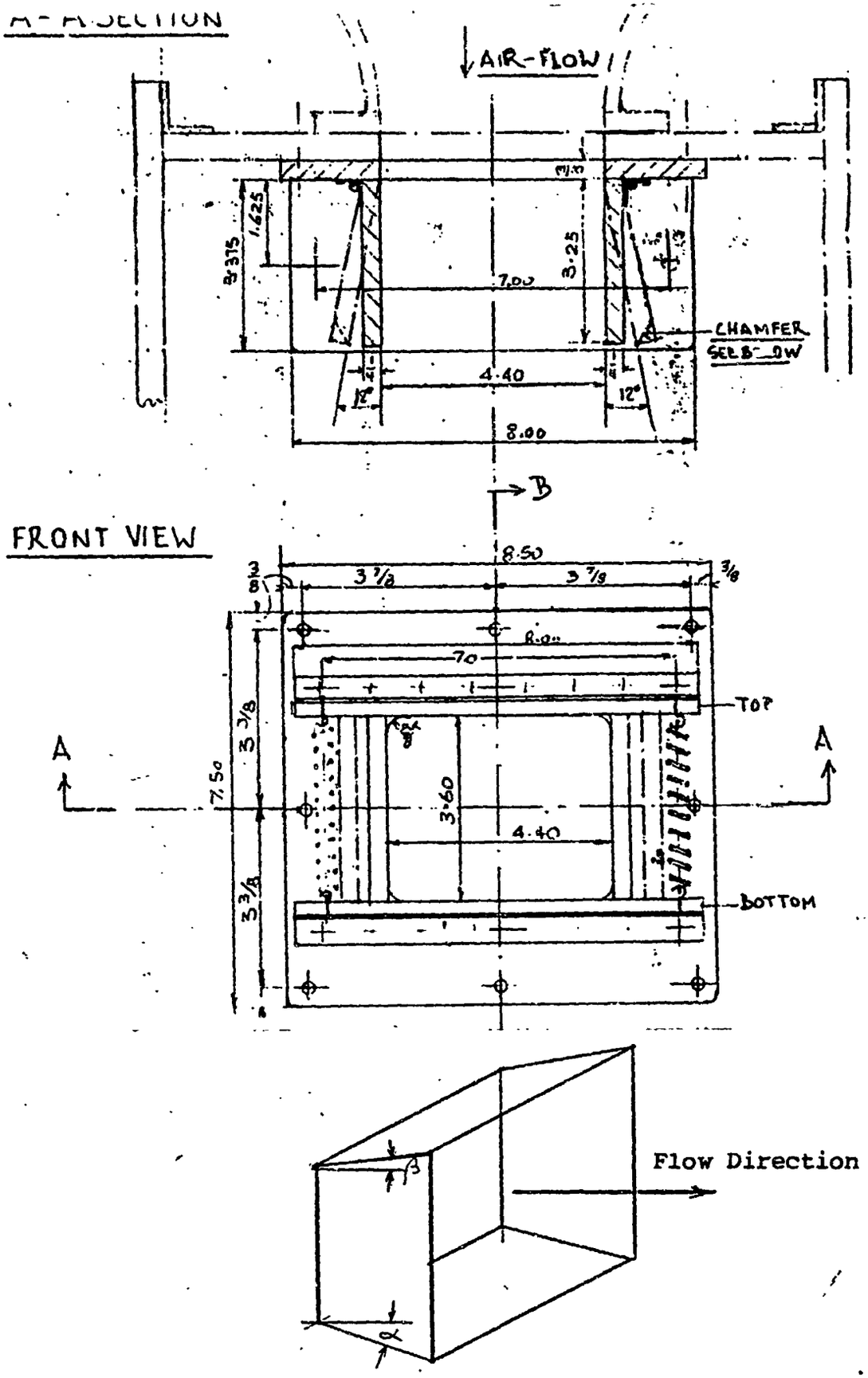

Figure 2. Details of the Nozzle-Diffuser design

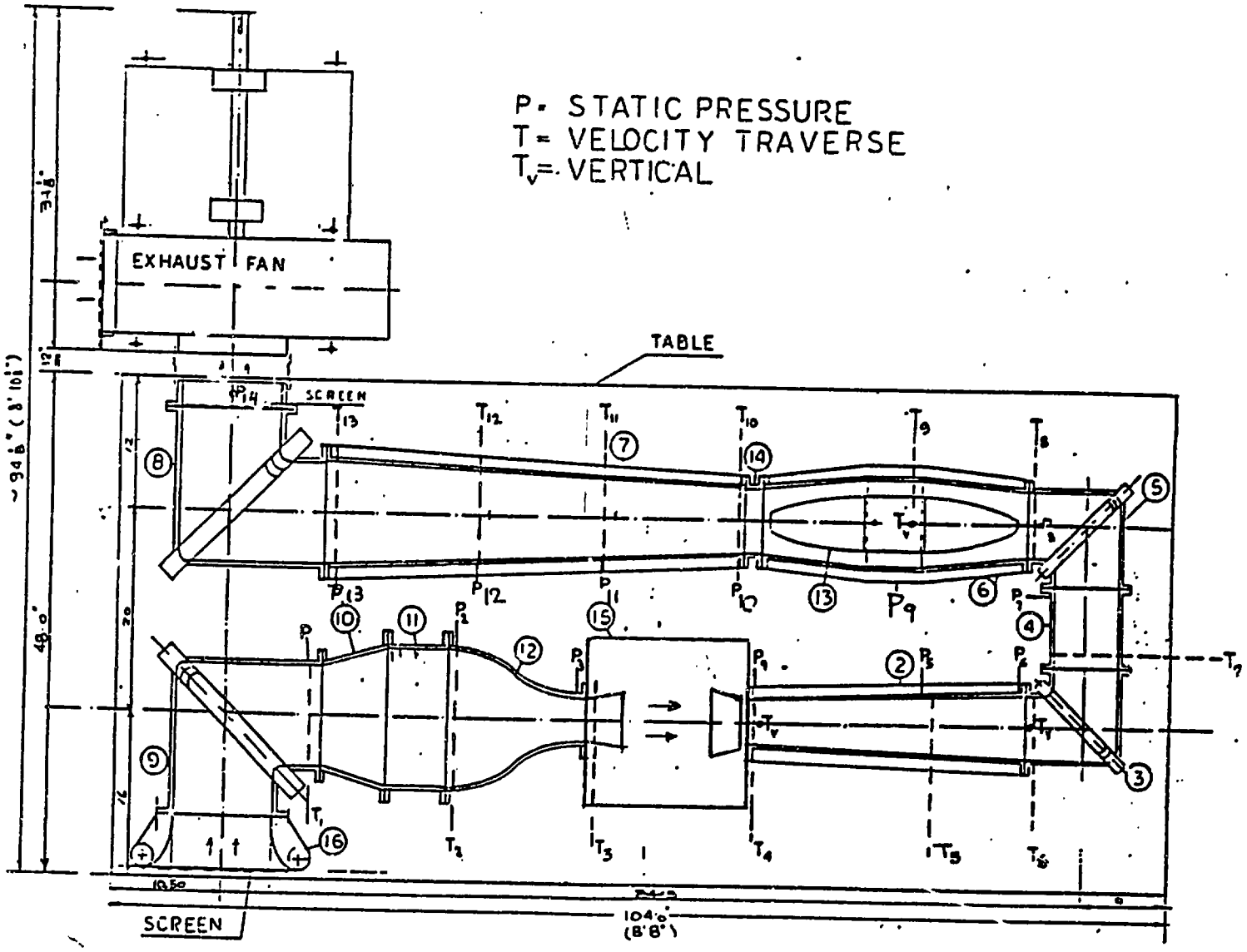

Figure 13. Plan view of the model tunnel circuit with Open Test Section

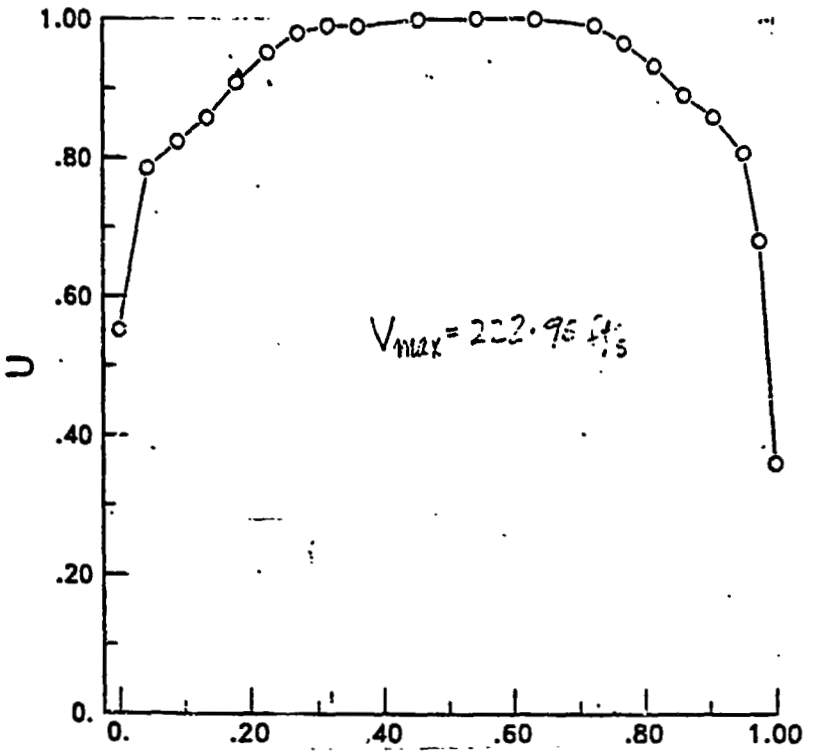

a) Horizontal

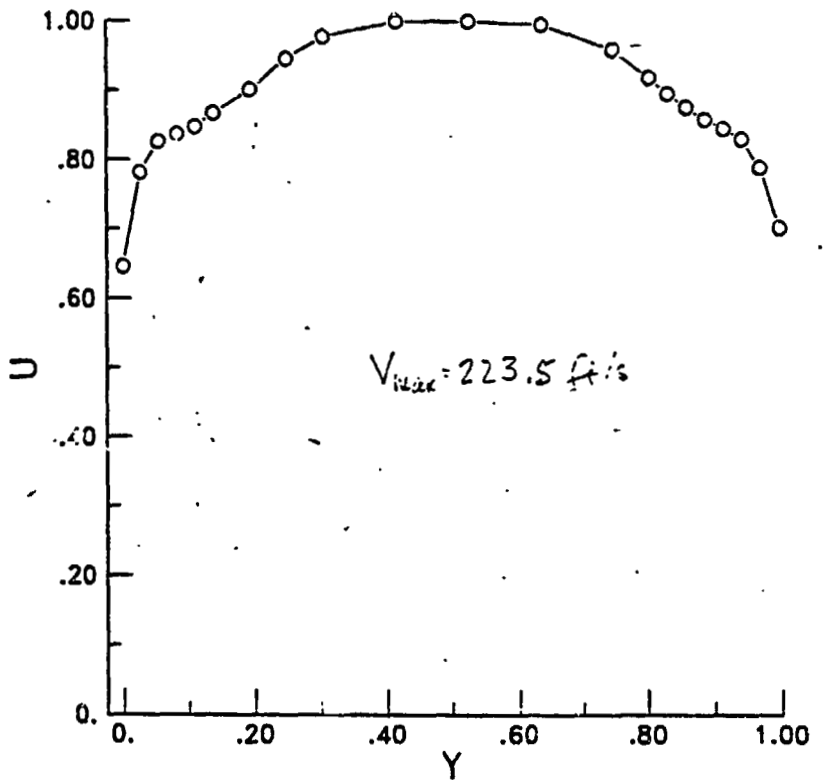

b) Vertical

Figure 14. Velocity traverses at location #4

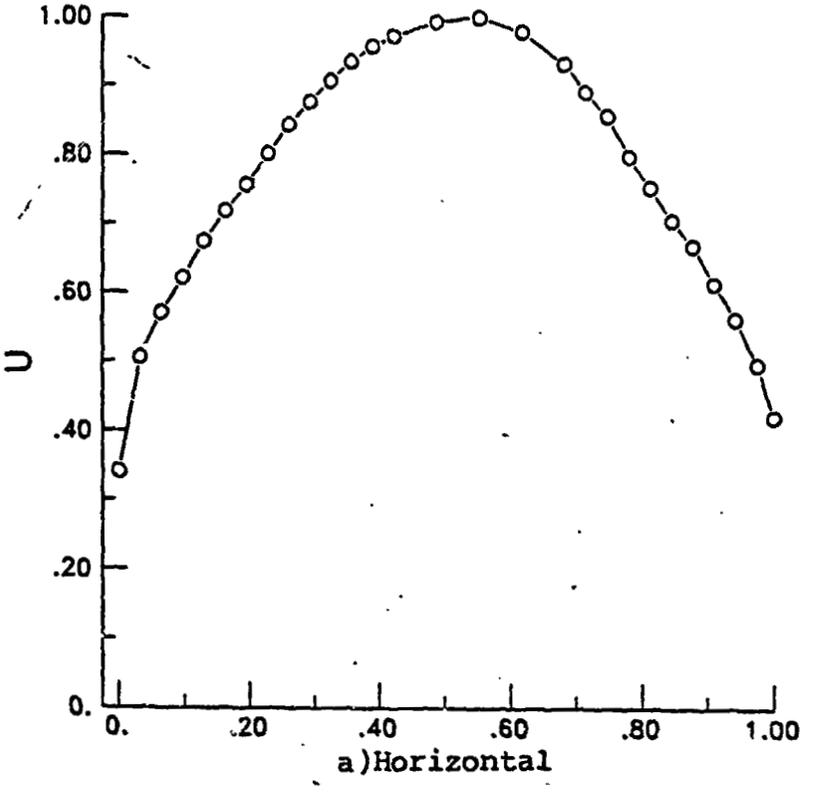

a)Horizontal

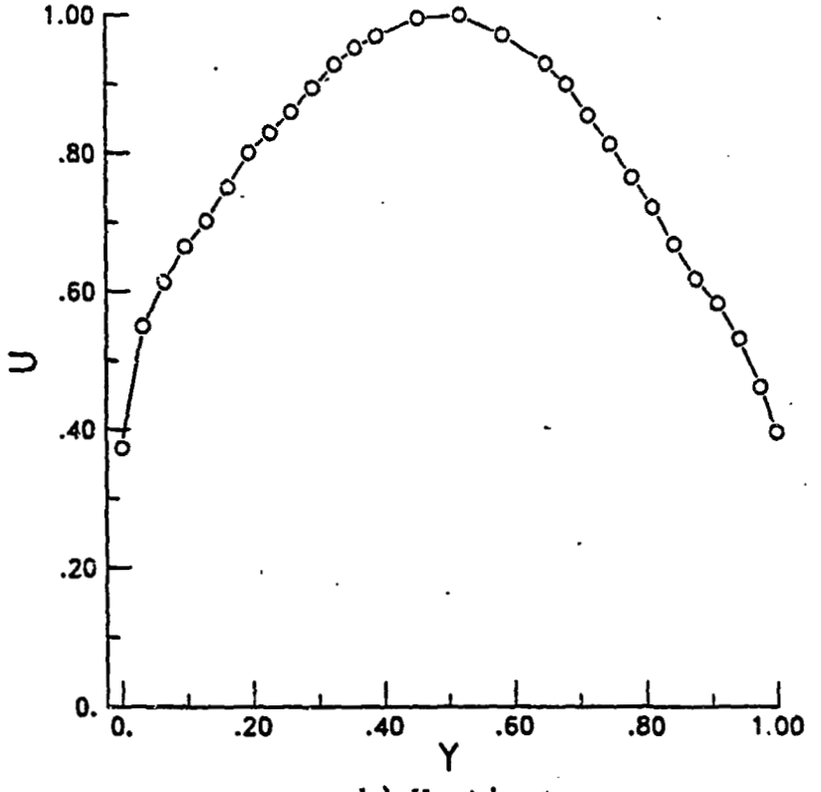

b) Vertical

Figure 15. Velocity traverses at location #6

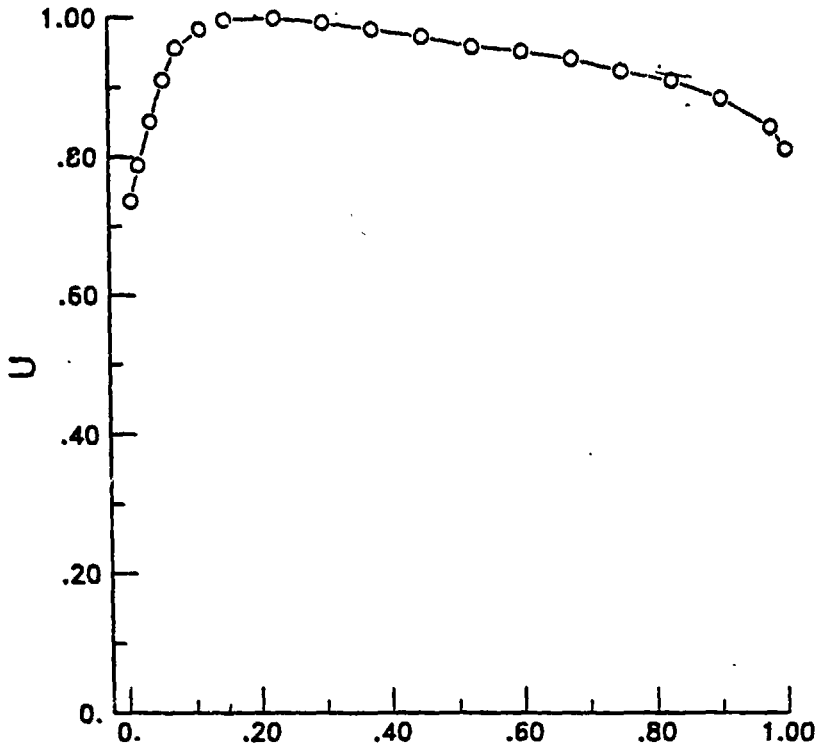

a) Inner horizontal

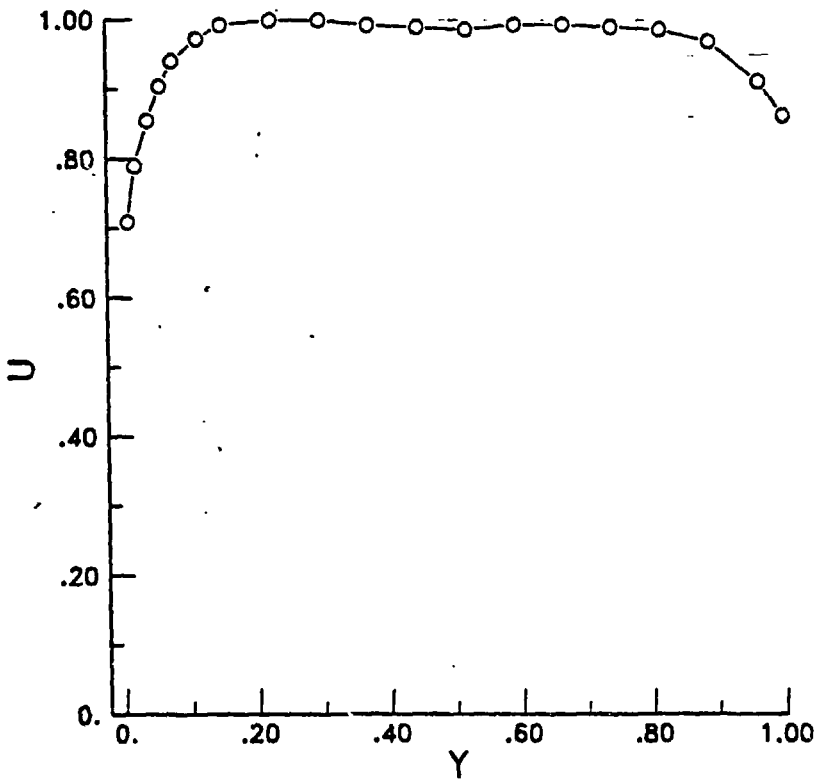

b) Outer horizontal

Figure 16. Velocity traverses at location #9 (fan annulus)

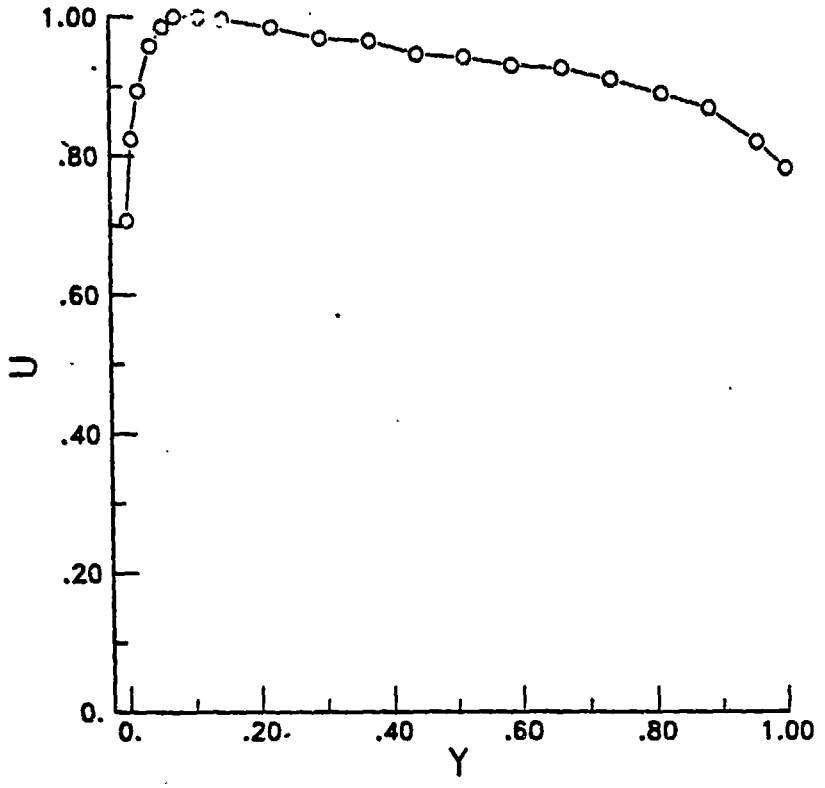

c) Vertical (top only) -Figure 16- CONCLUDED

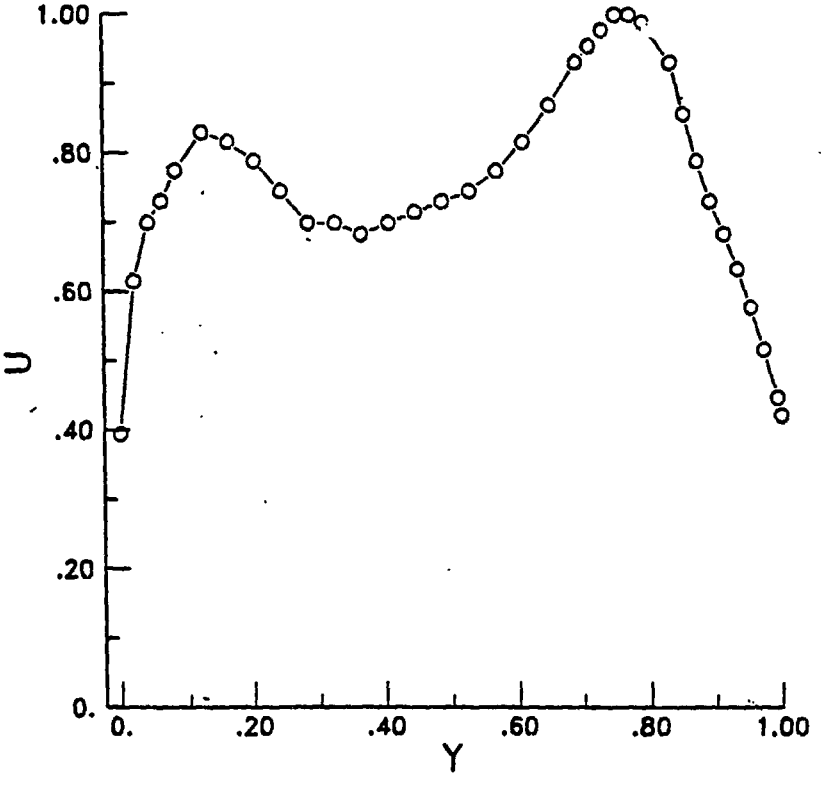

Figure 17. Velocity traverse at location #13

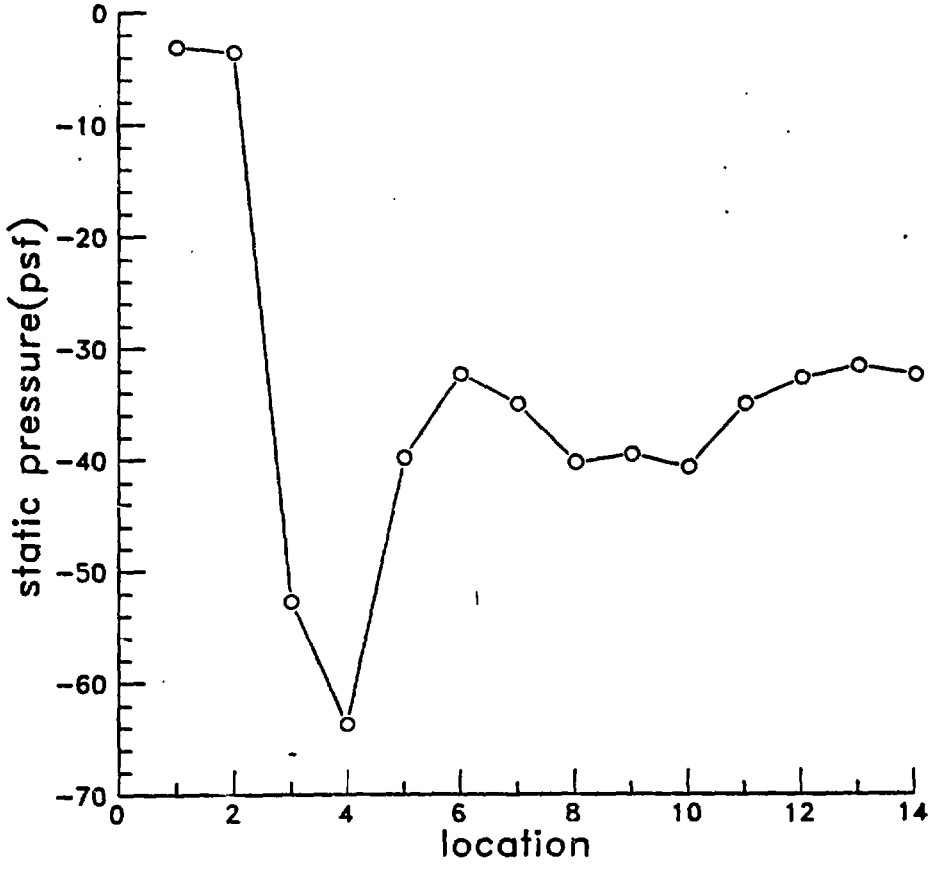

Figure 18. Pressure distribution around tunnel circuit with collector alone

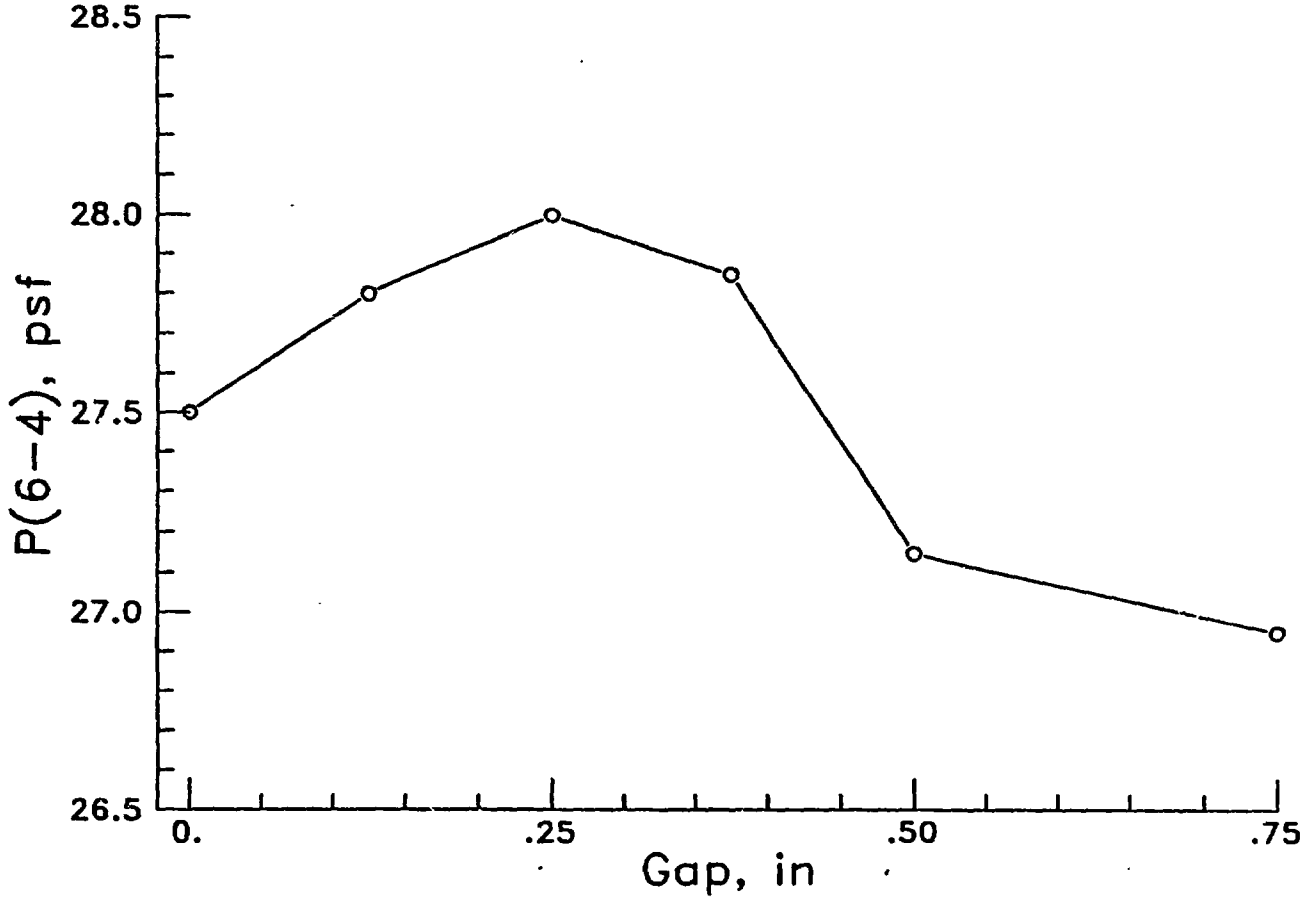

Figure 19. Collector gap calibration curve

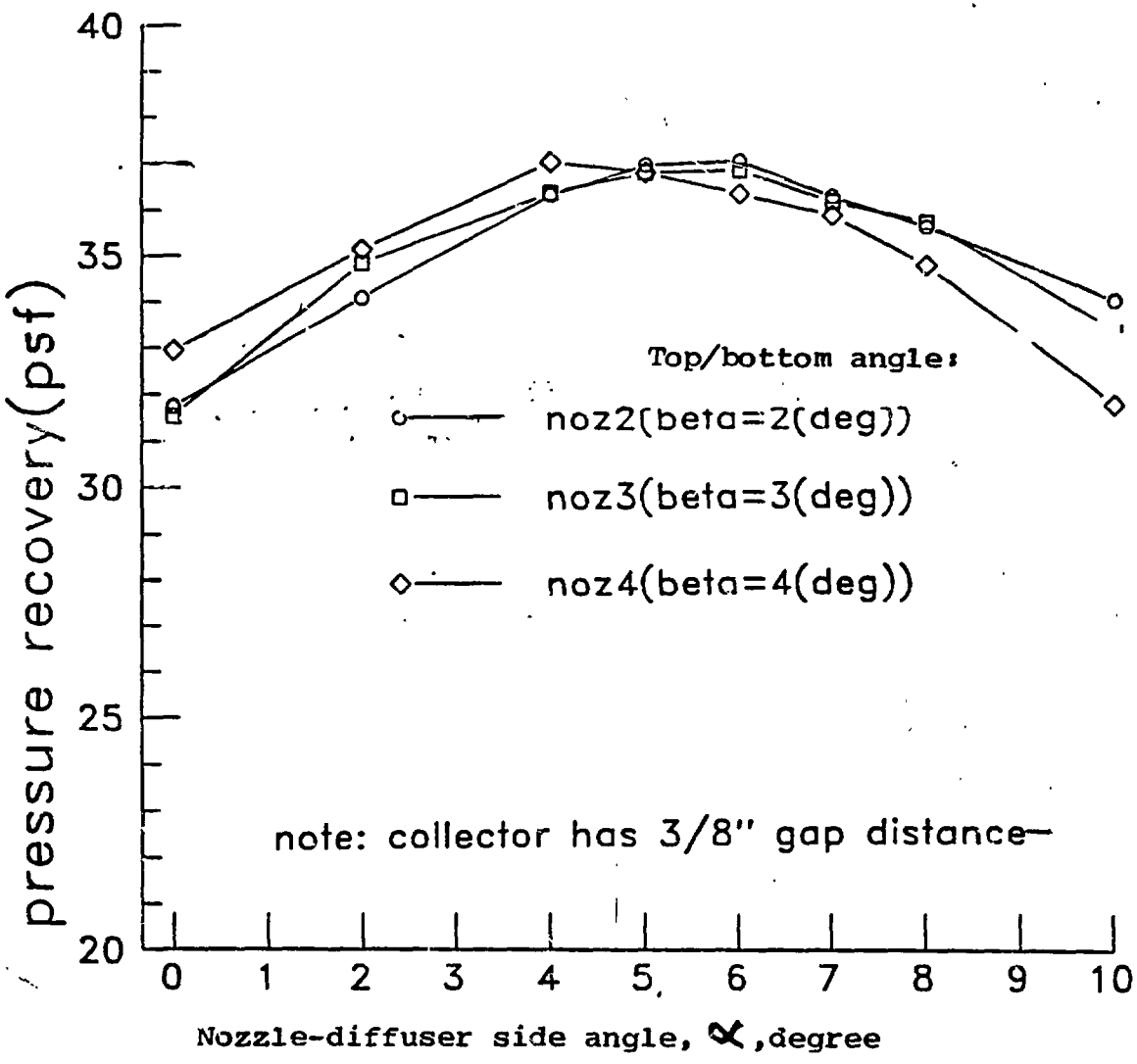

Figure 20. Nozzle Diffuser calibration. Pressure rise in first diffuser vs. side angle α, for β=2,3,4°

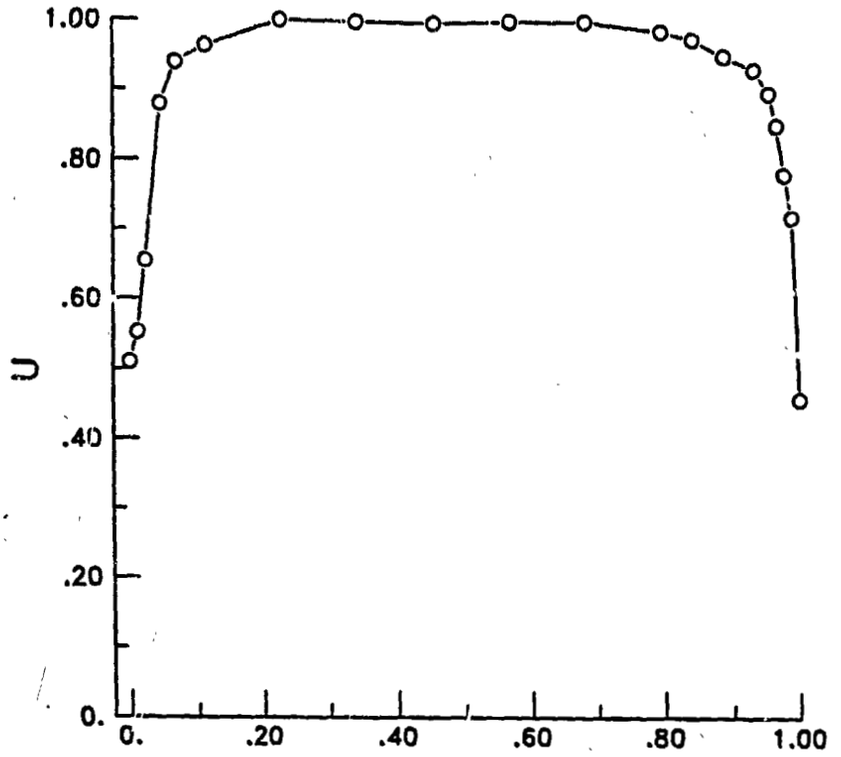

a) Horizontal

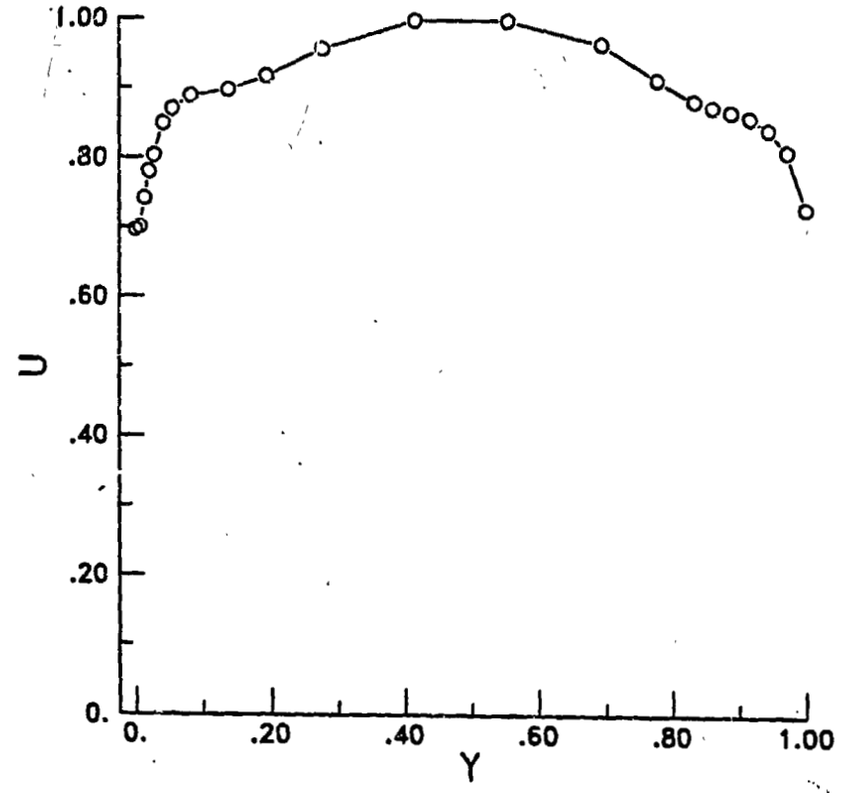

b) Vertical

Figure 21, Velocity traverses at location #4. Collector and nozzle-diffuser at optimum

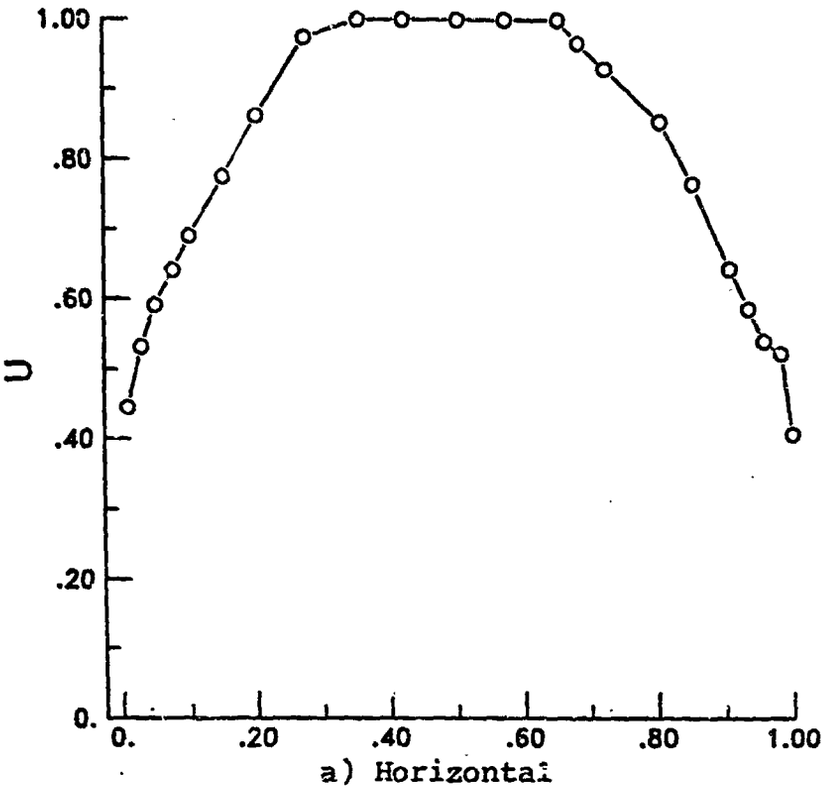

a) Horizontal

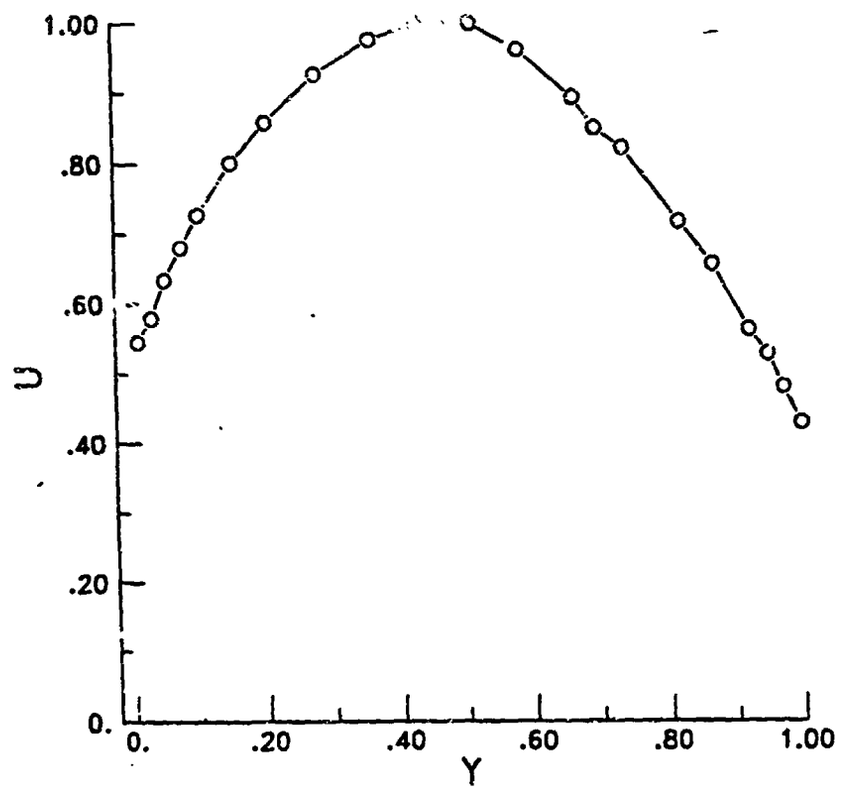

b) Vertical

Figure 22. Velocity traverses at location #6. Collector and nozzle-diffuser at optimum

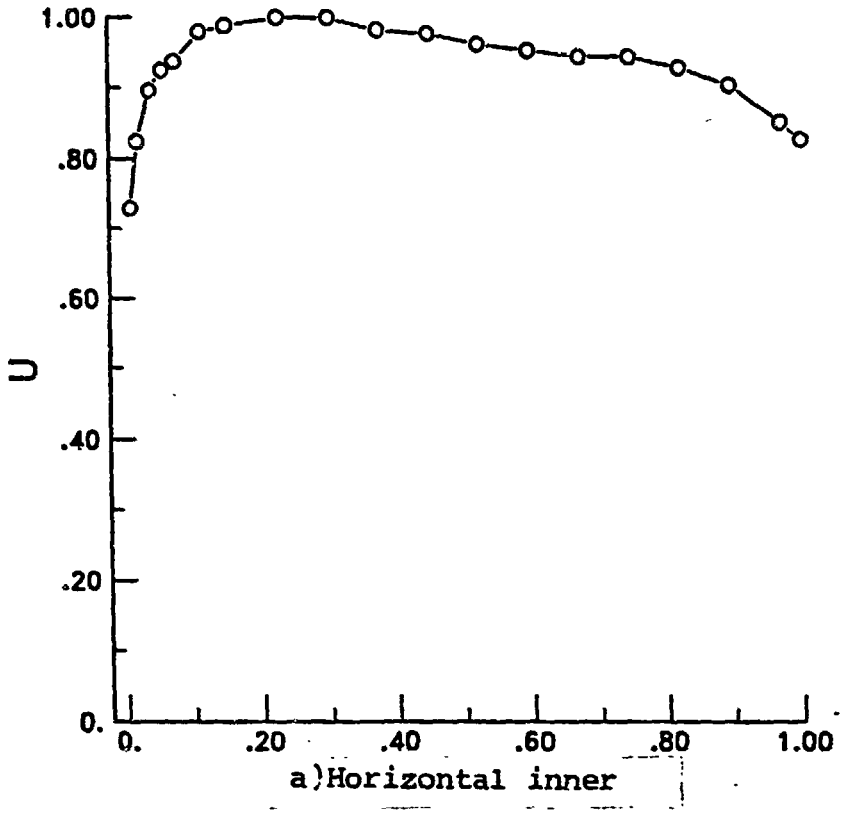

a)Horizontal inner

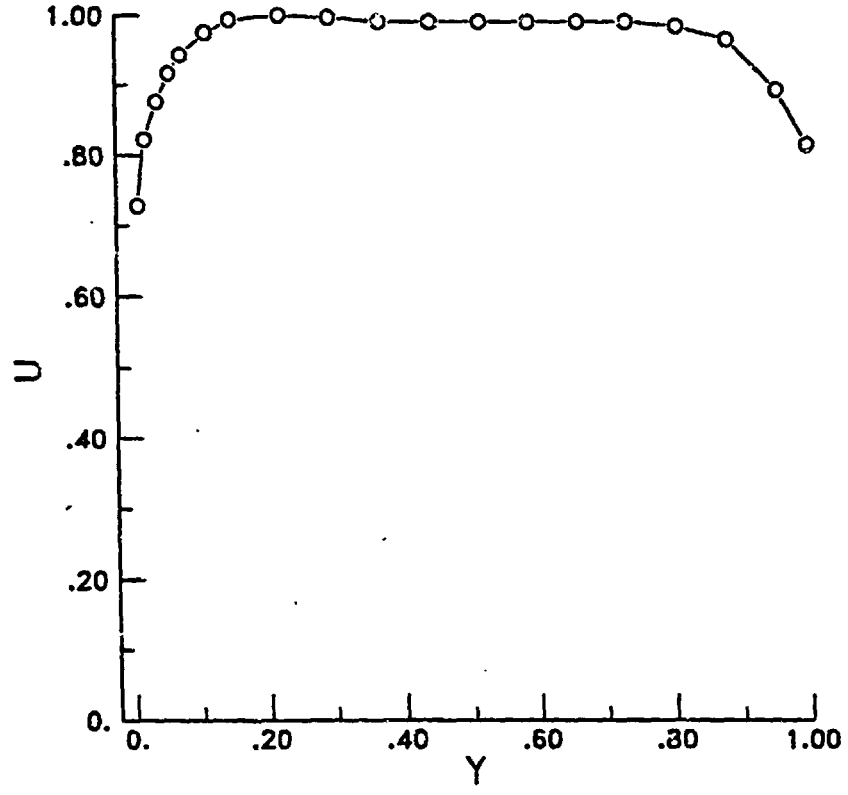

b) Horizontal outer

Figure 23. Velocity traverses at location #9. Collector and nozzle-diffuser at optimum

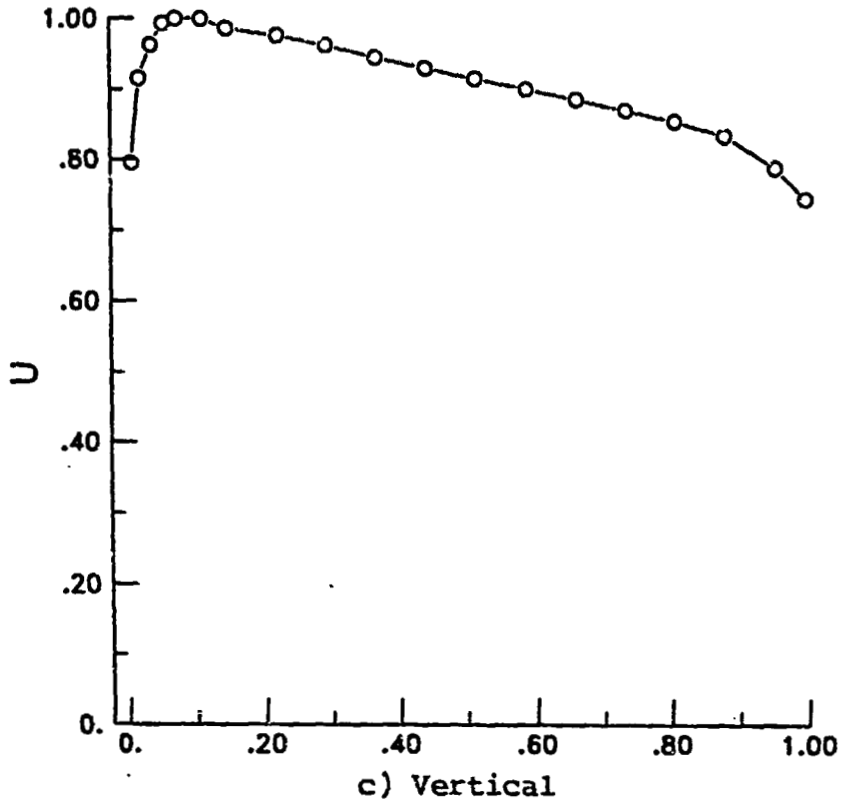

c) Vertical

Figure 17-CONCLUDED

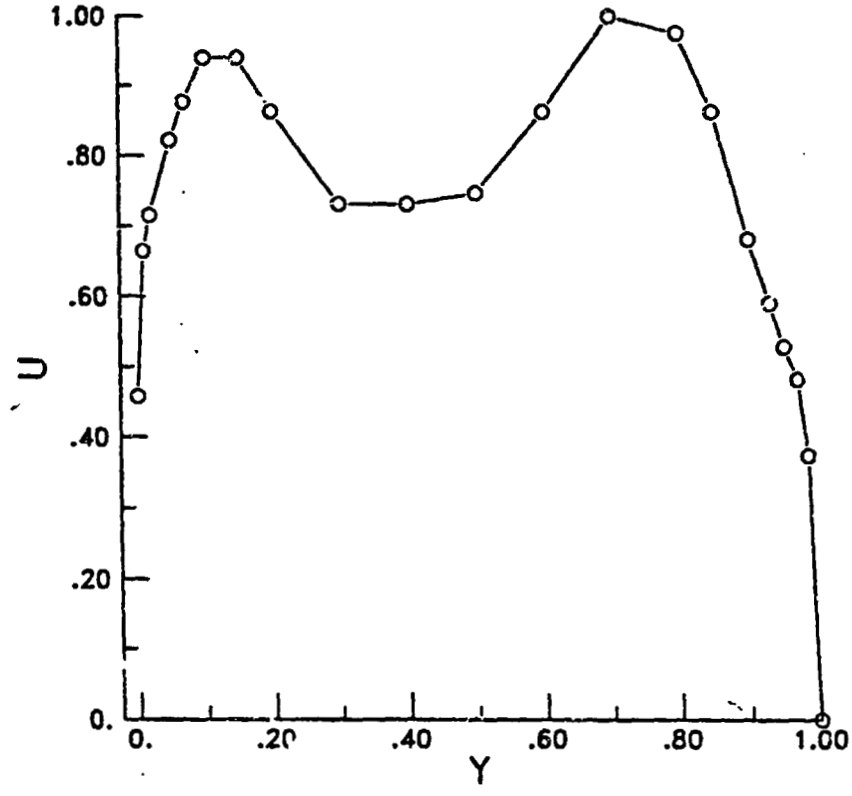

Figure 24. Horizontal velocity traverse at location # 13. Collector and nozzle-diffuser at optimum

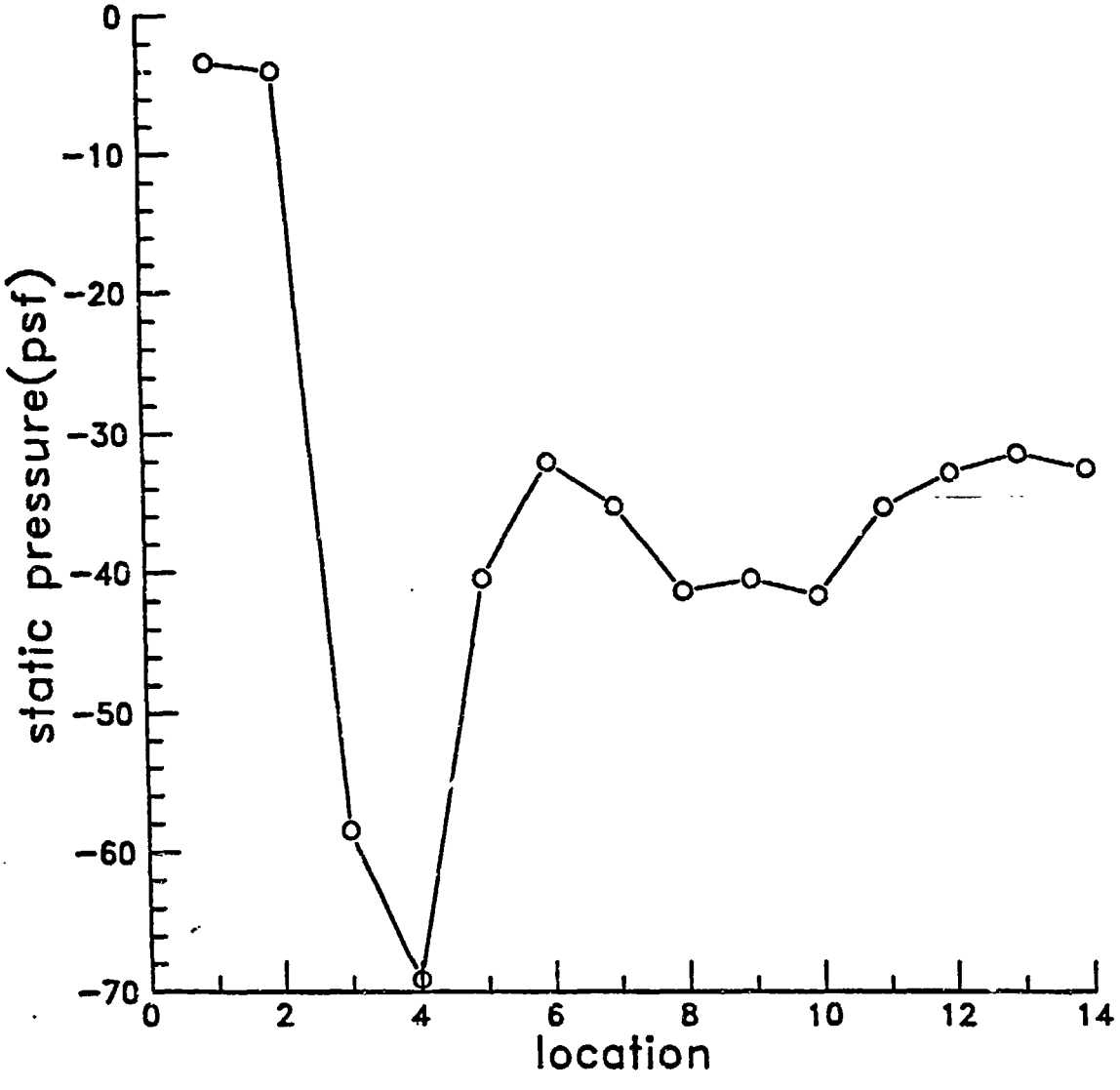

Figure 25, Pressure distribution around tunnel circuit. Collector and nozzle-diffuser at optimum

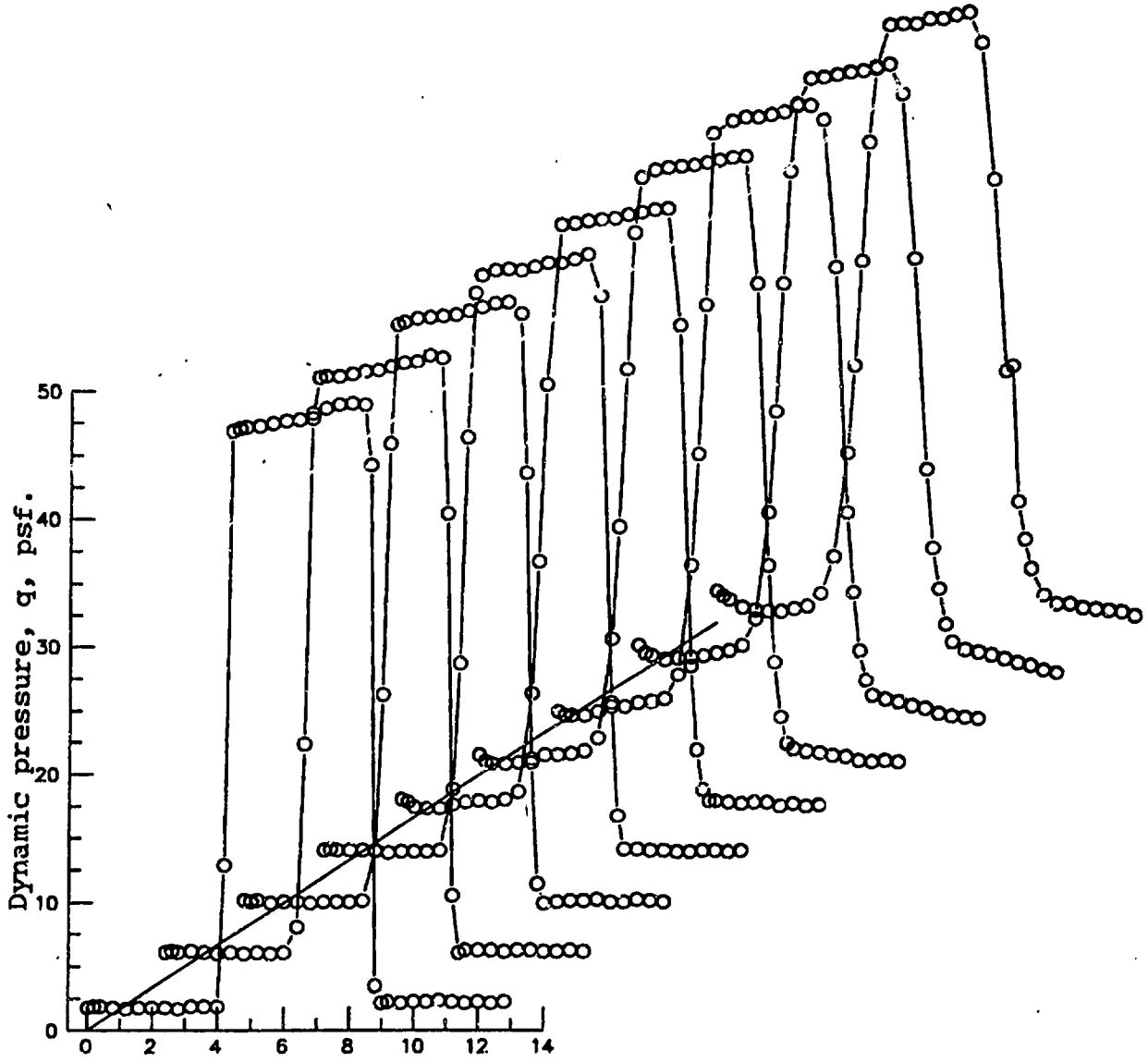

Figure 26. Velocity distributions inside the O.T.S. Collector only

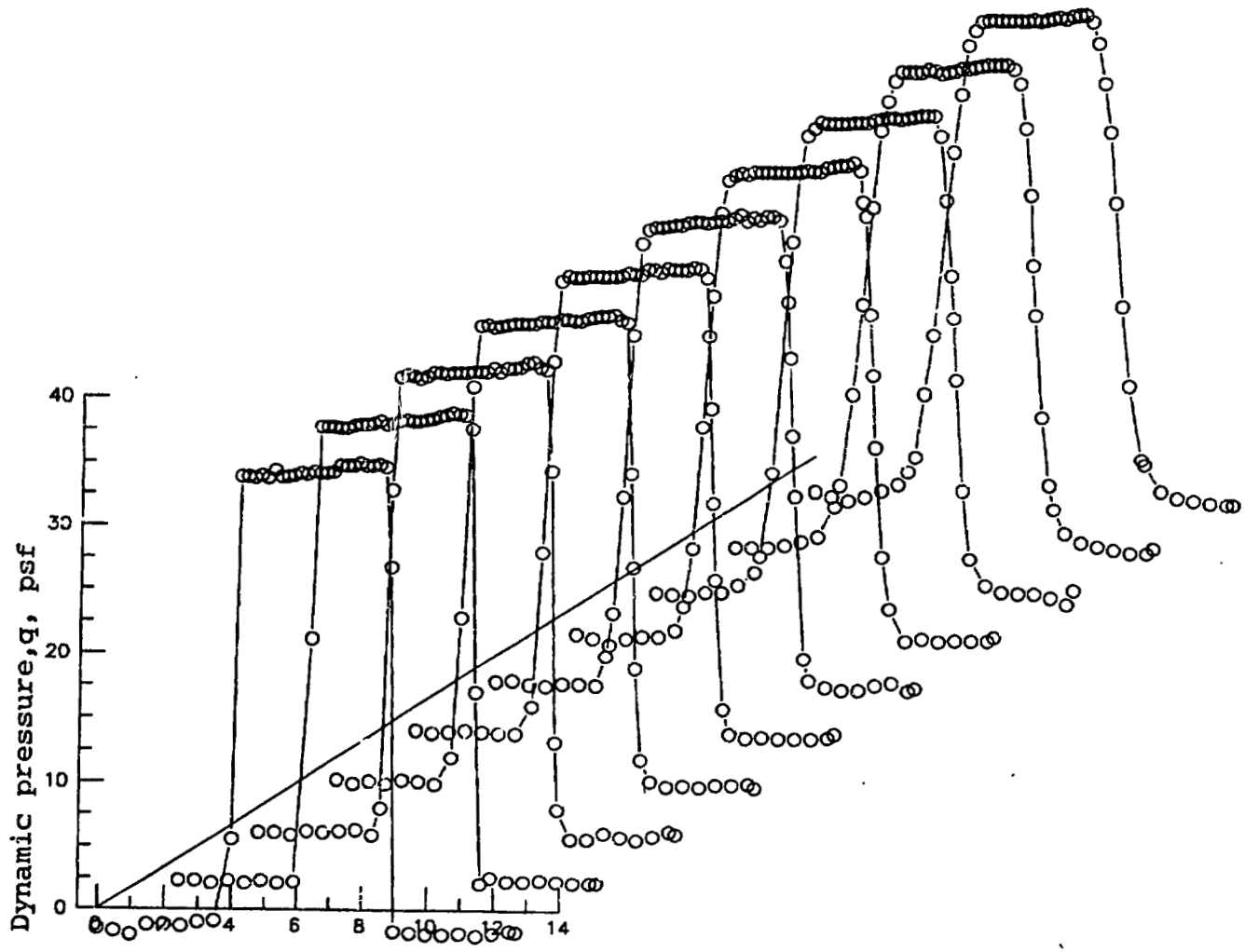

Figure 27. Velocity distributions inside the O.T.S. Collector and nozzle-diffuser at optimum

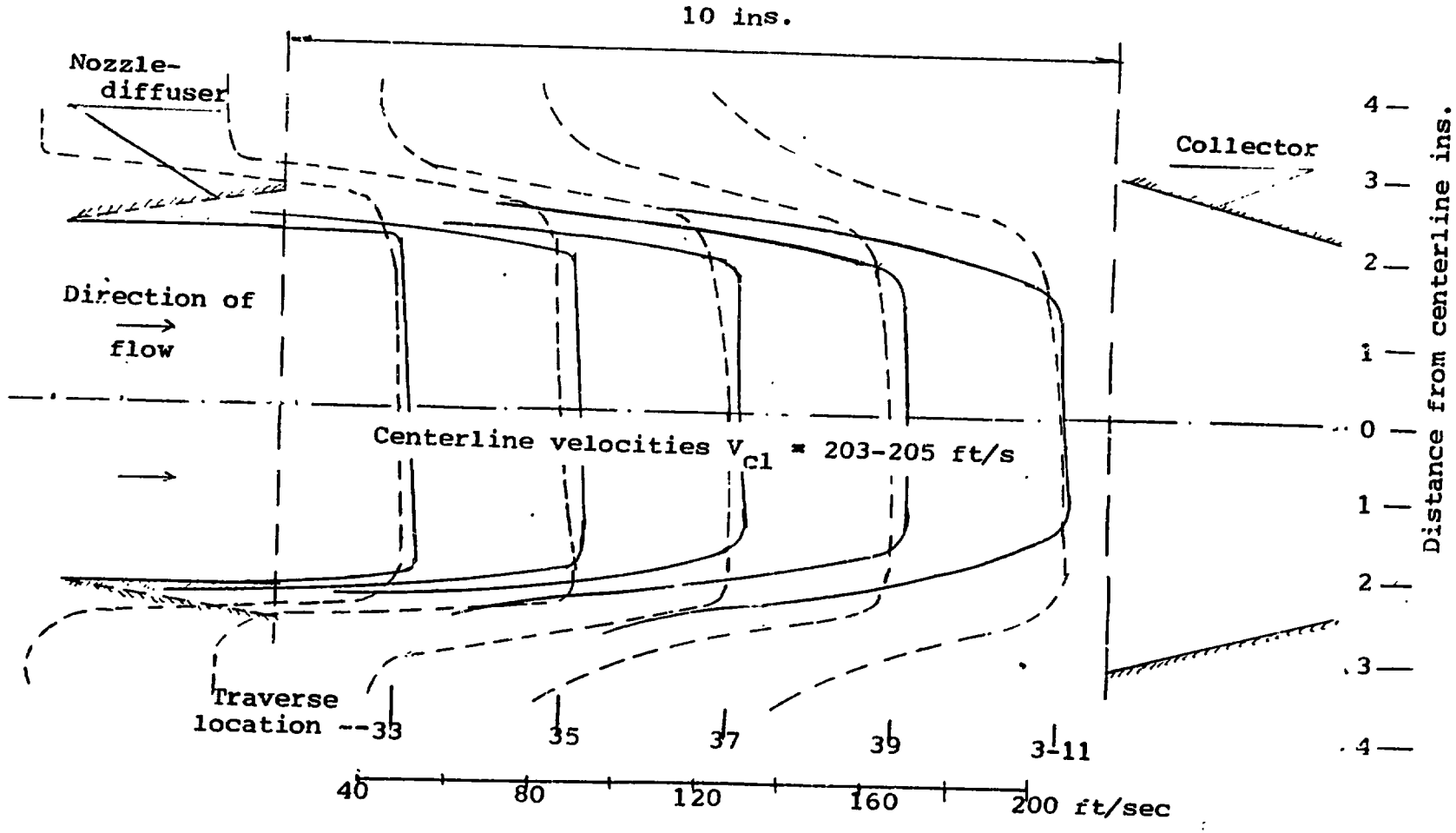

Figure 28. Superposition of two flow fields in plan view inside the open test section

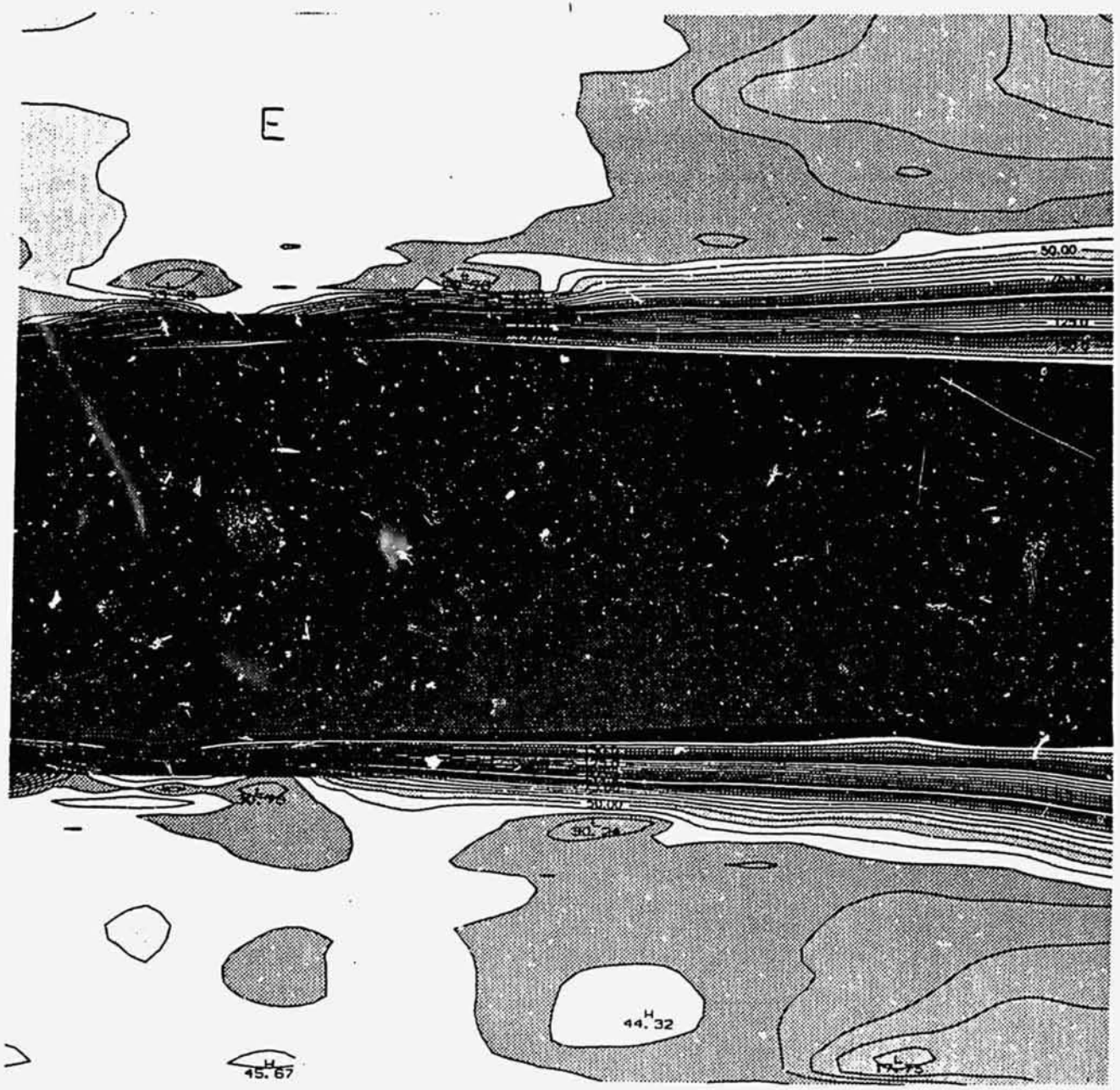

Figure 29. Velocity contour representation of the flow with collector and nozzle-diffuser

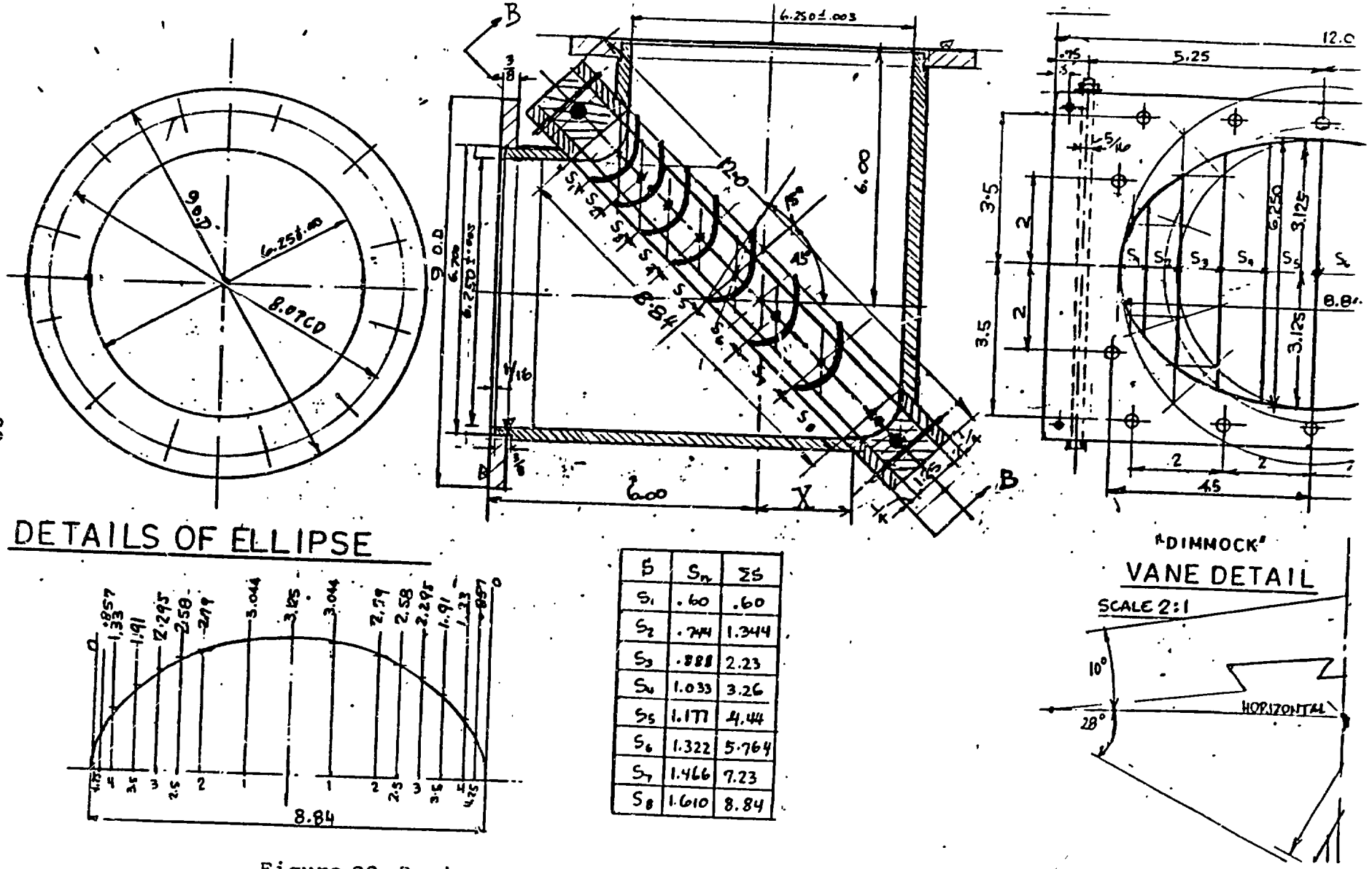

S	S_n	ΣS
S_1	.60	.60
S_2	.744	1.344
S_3	.888	2.23
S_4	1.033	3.26
S_5	1.177	4.44
S_6	1.322	5.764
S_7	1.466	7.23
S_8	1.610	8.84

Figure 30. Design details of the Dimnock type corner vanes

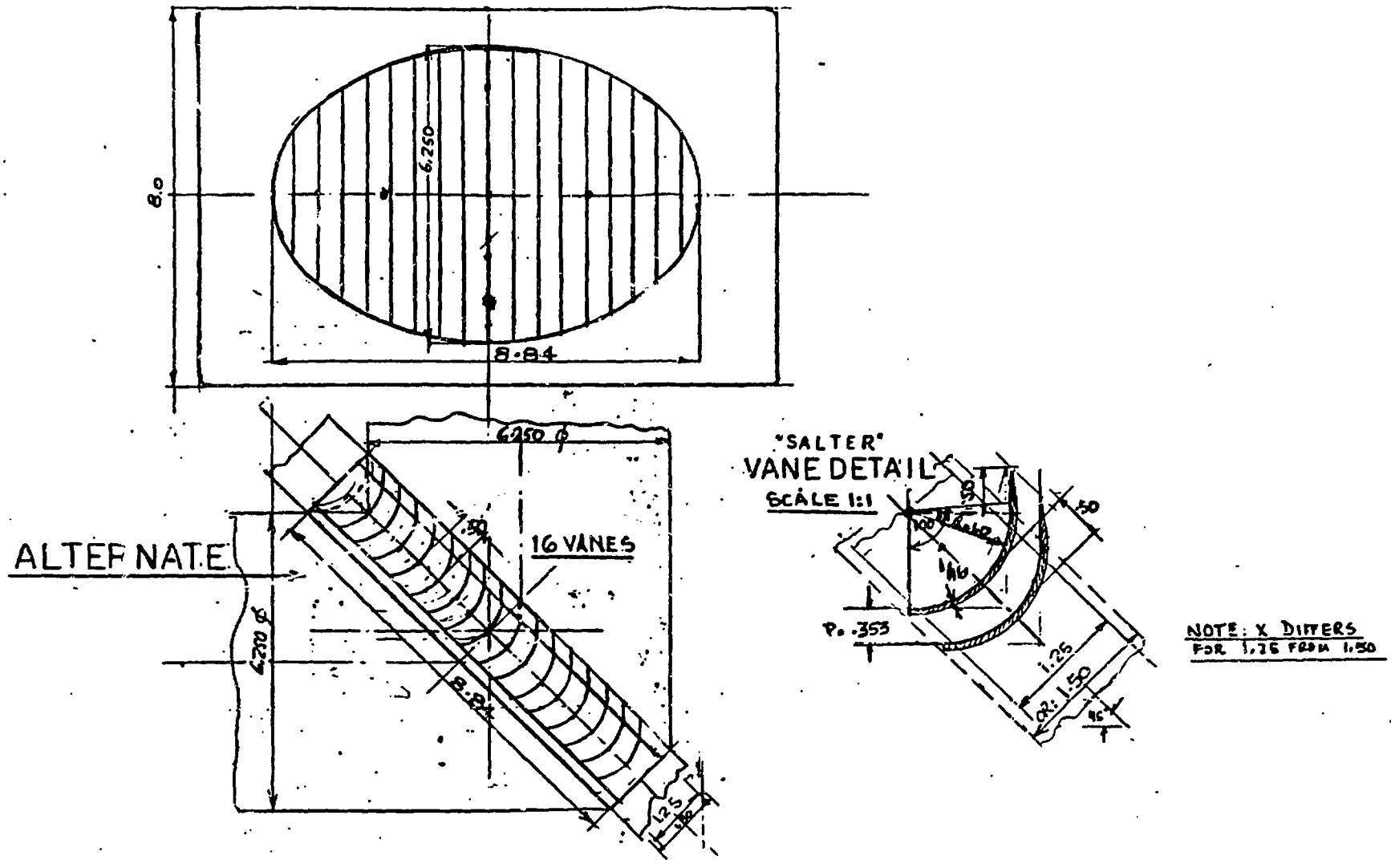

Figure 31. Design details of Salter type corner vanes (originally designed)

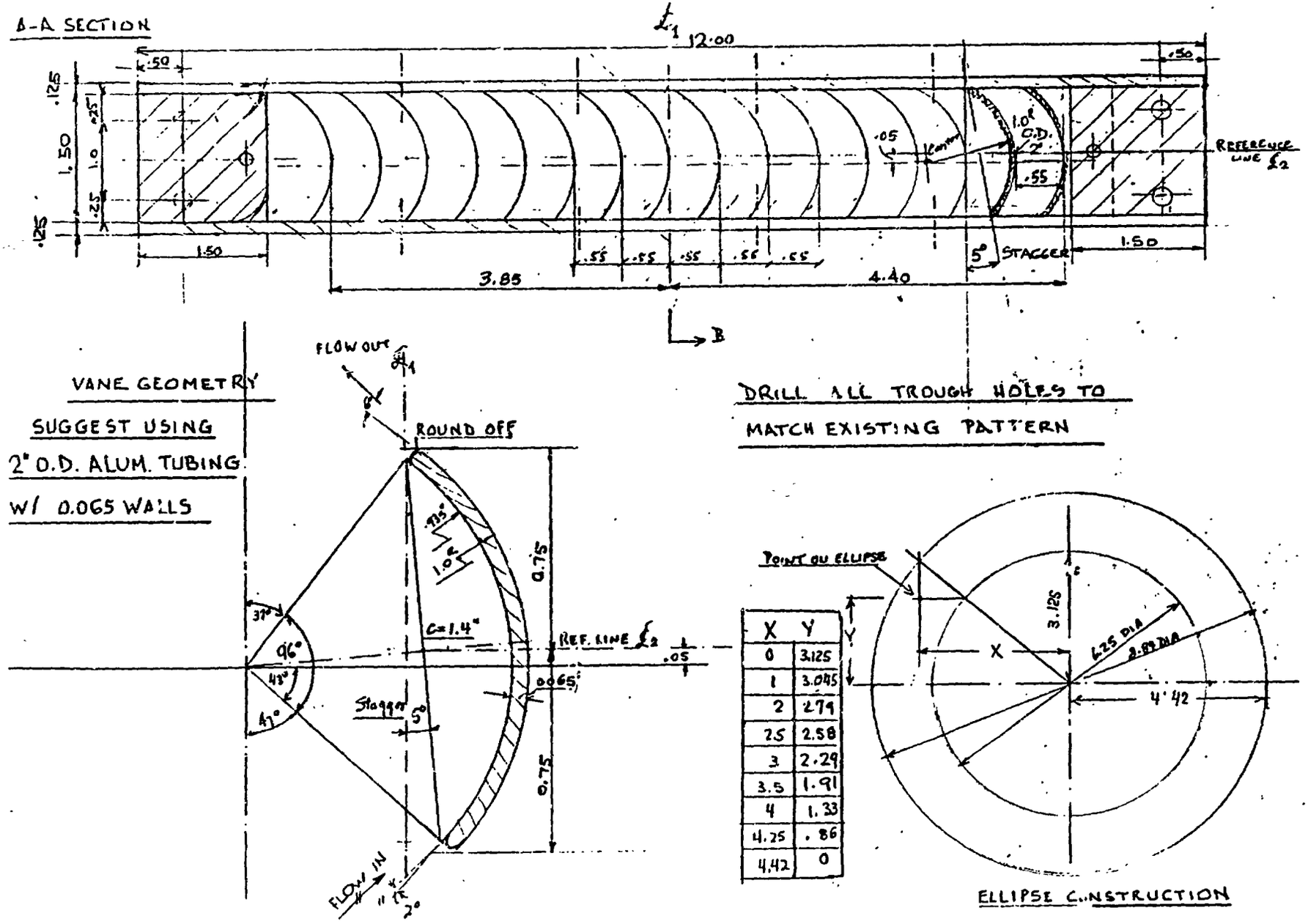

X	Y
0	3.125
1	3.085
2	2.79
2.5	2.58
3	2.29
3.5	1.91
4	1.33
4.25	.86
4.42	0

Figure 32. Design details of Salter type vanes used in test

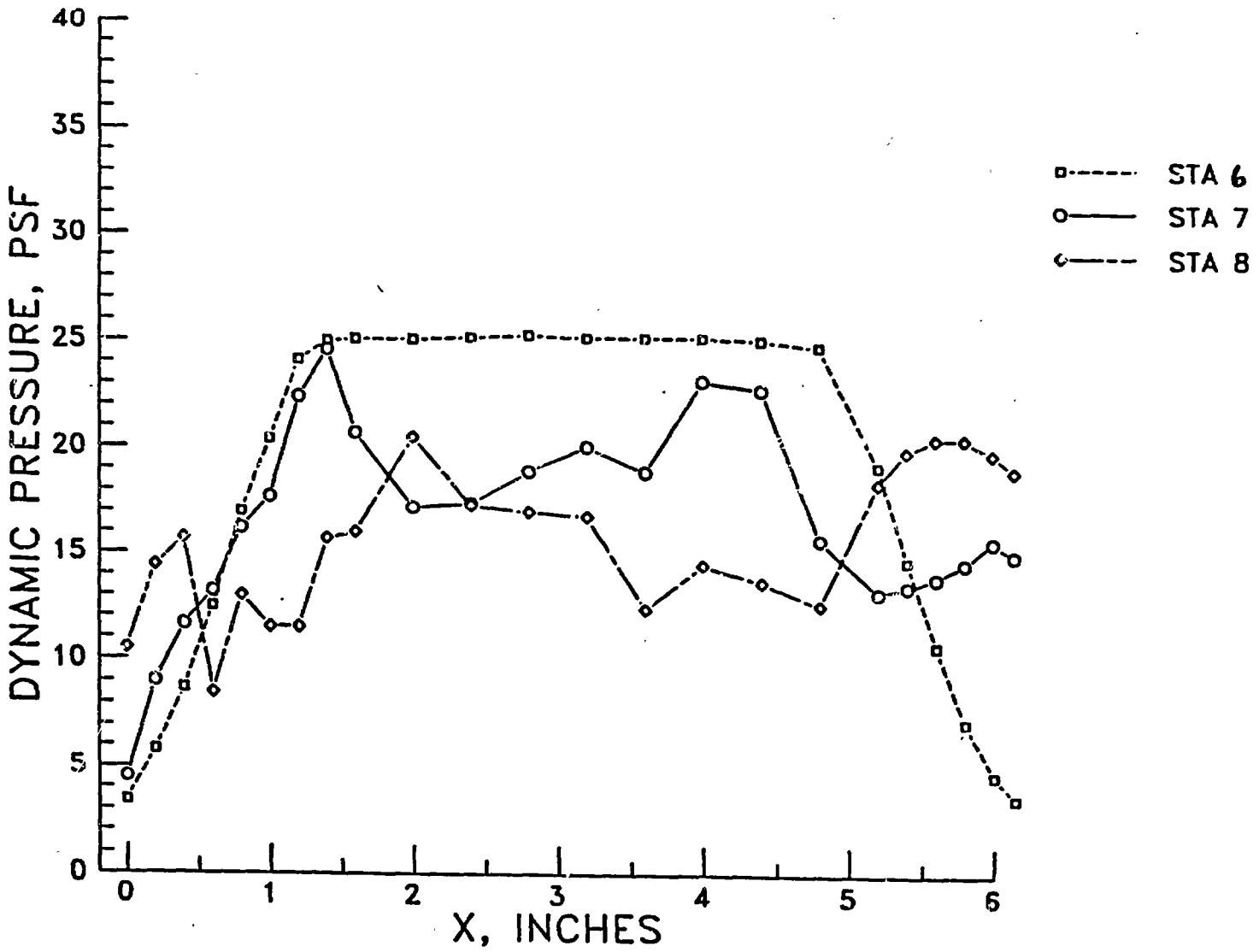

Figure 33. Variation of dynamic pressure across locations 6,7,&8.
Closed test section-Dimmock vanes

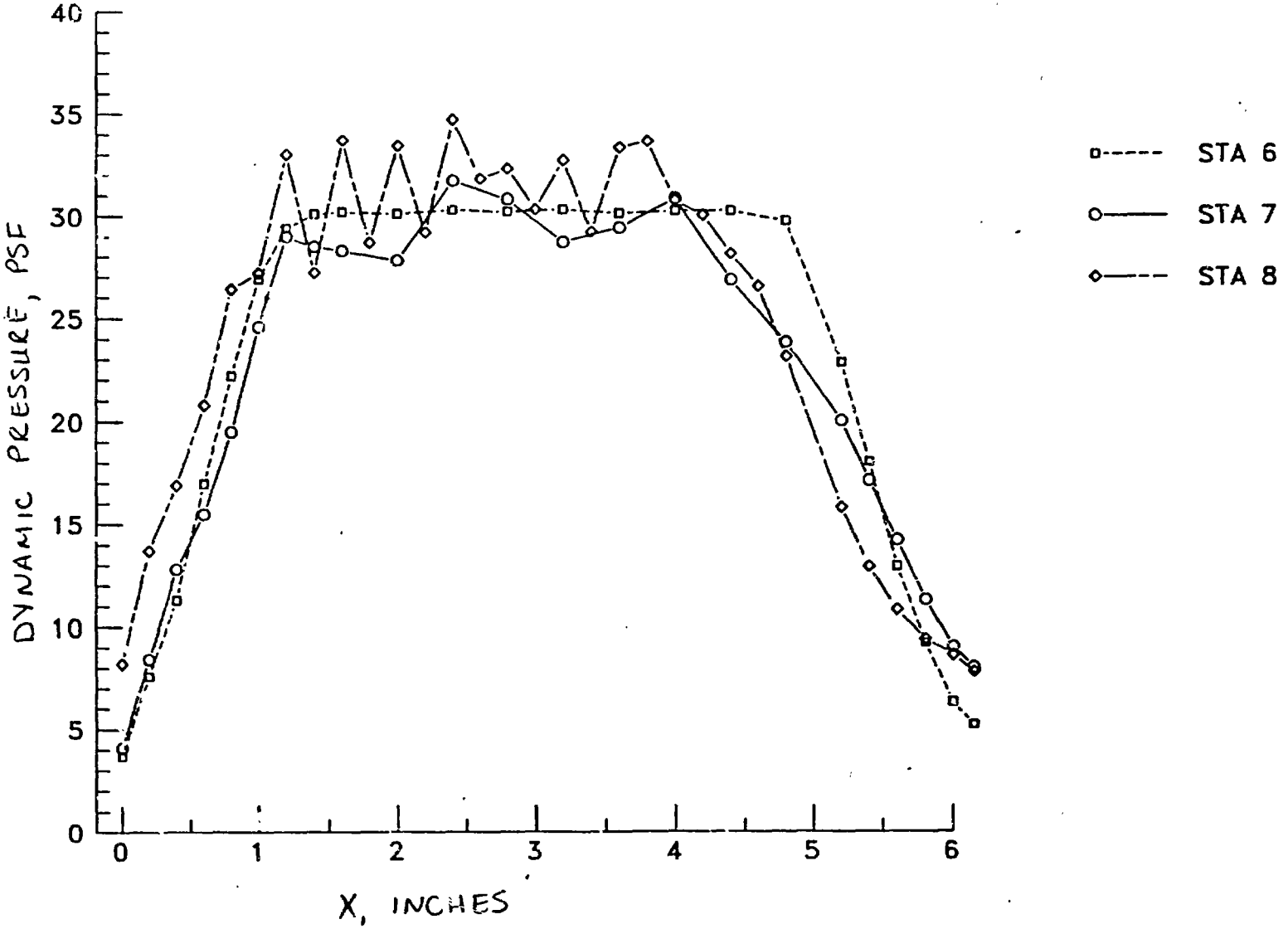

Figure 34. Variation of velocity across location 6. Closed T.S. Salter vanes

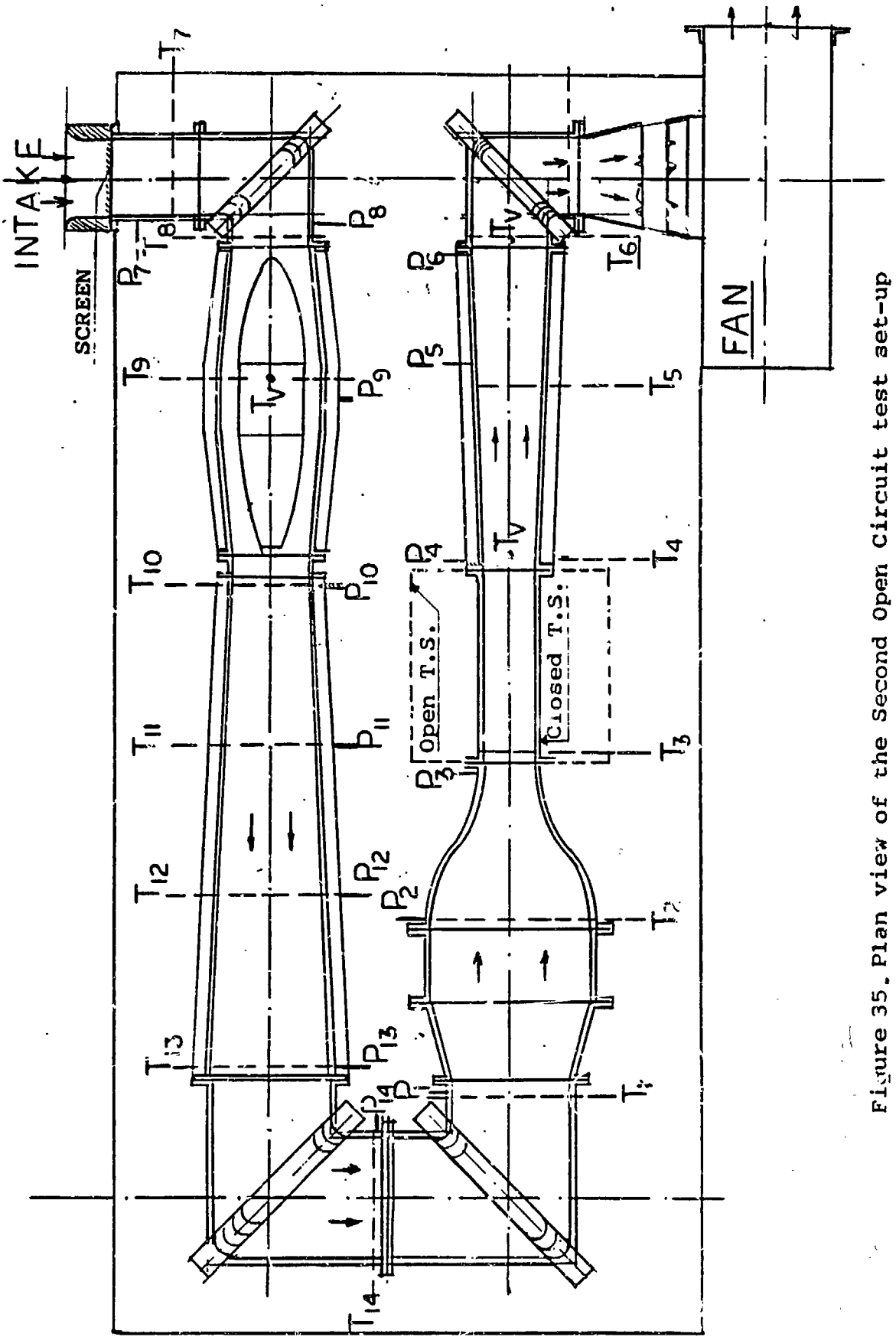

Figure 35. Plan view of the Second Open Circuit test set-up

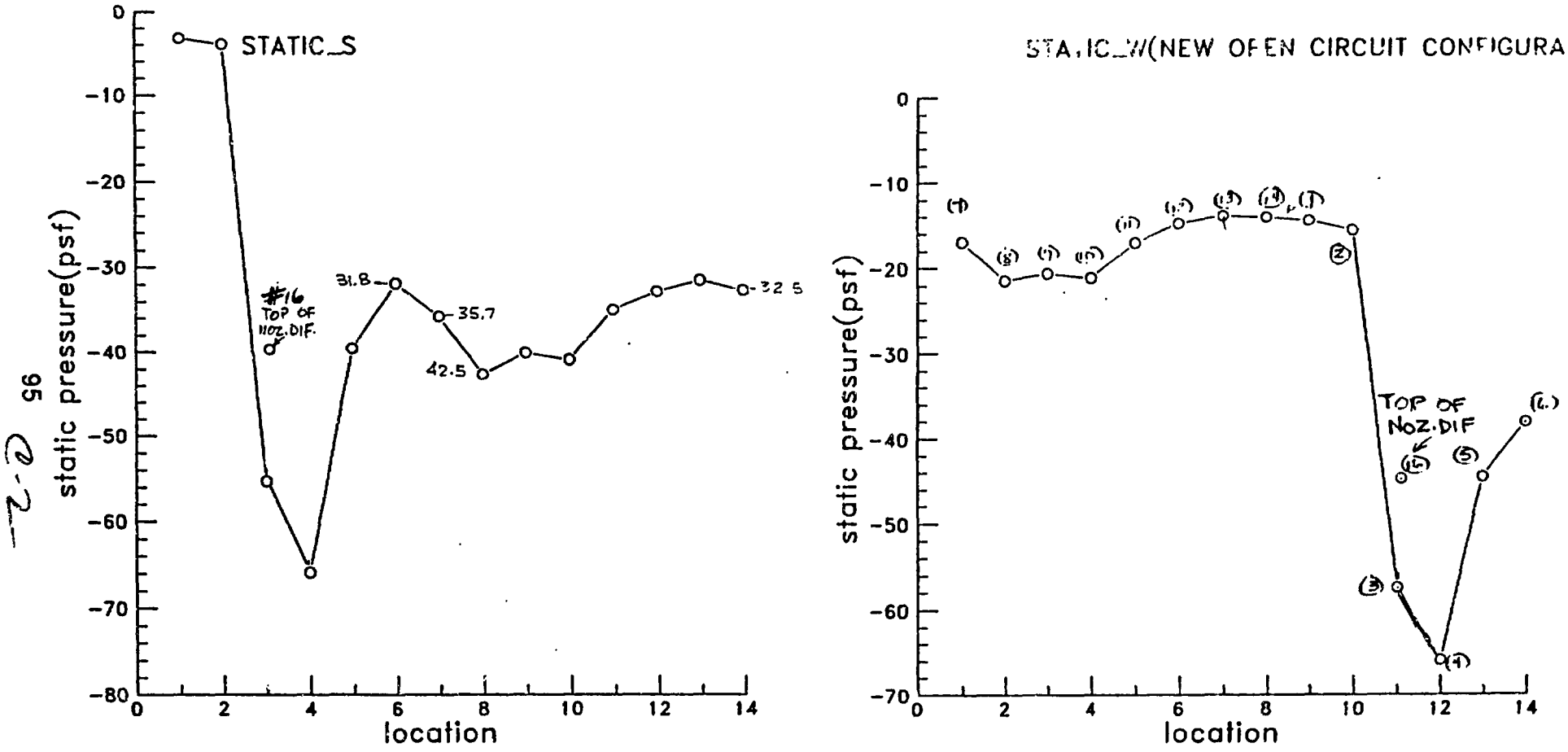

Figure 36 Pressure distribution around the tunnel circuit for the first and second open circuit

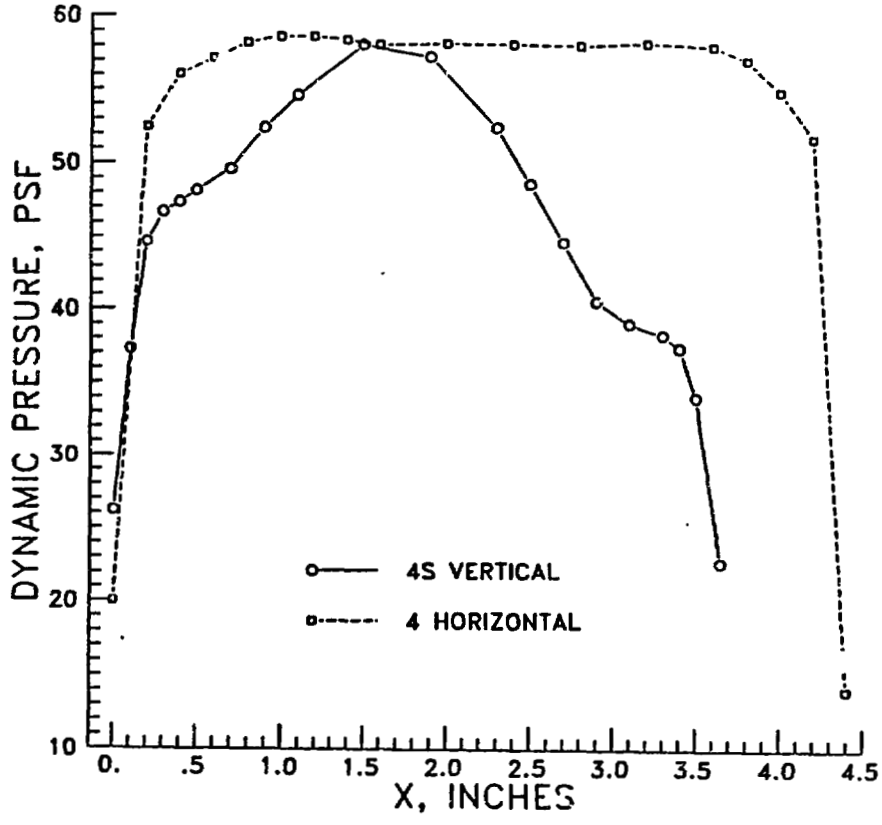

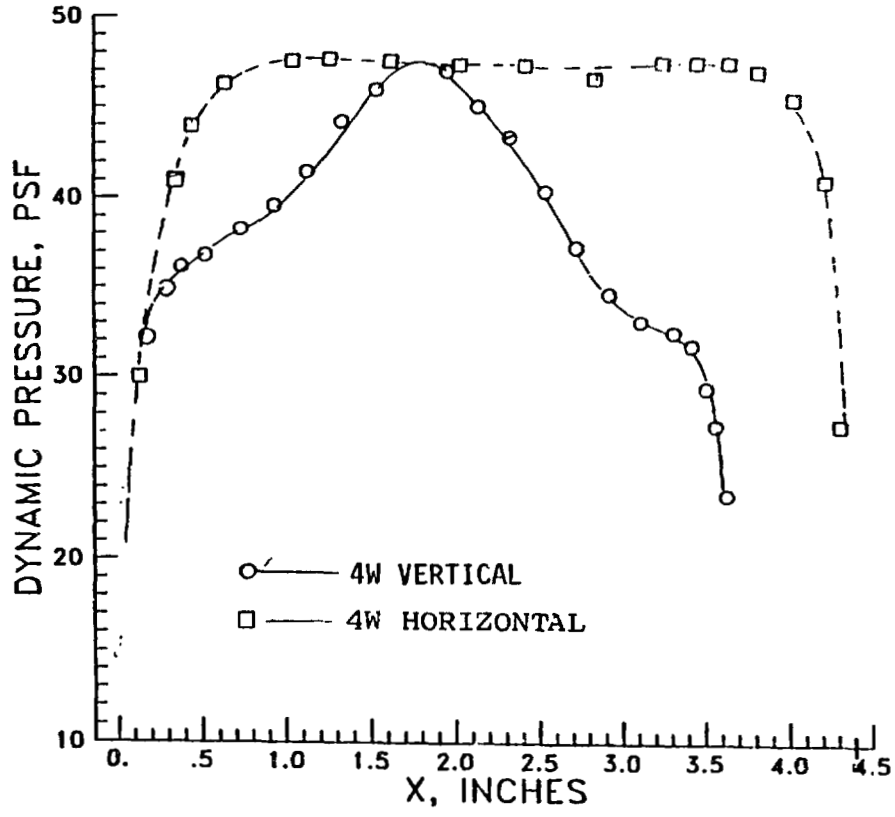

Figure 37. Dynamic pressure distribution at location 4

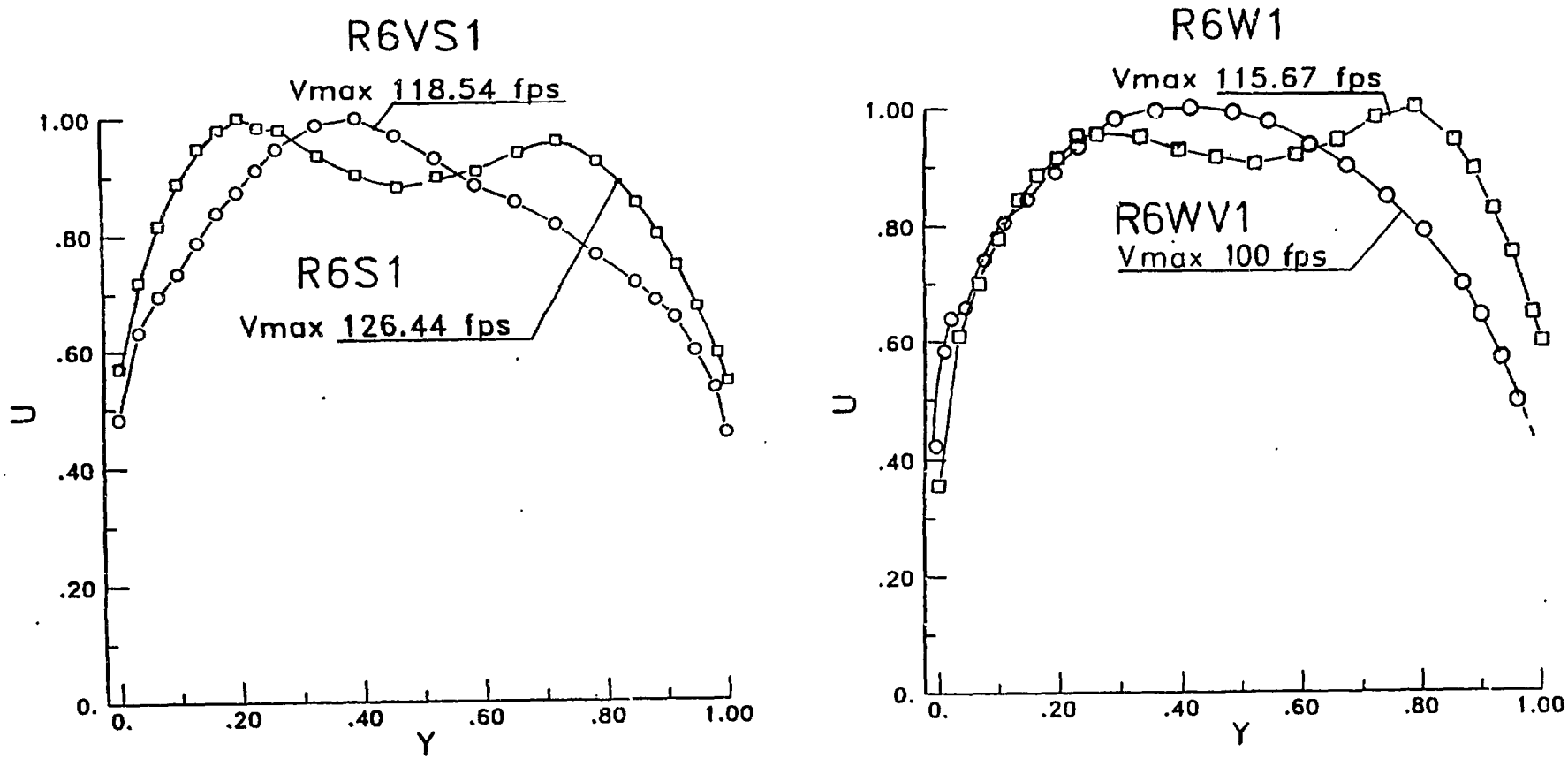

Figure 38. Velocity distribution at location 6.

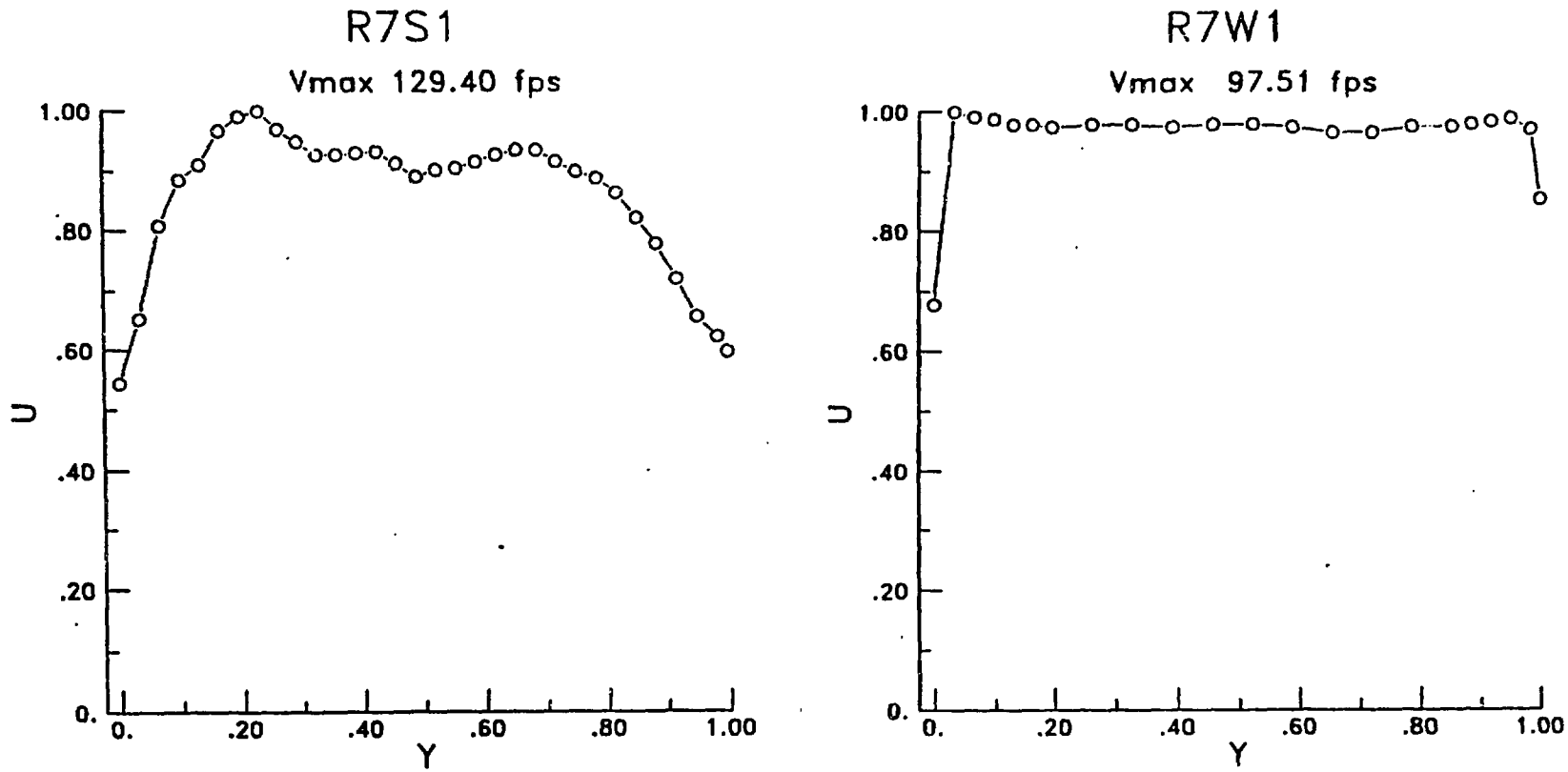

Figure 39. Velocity distribution at location 7

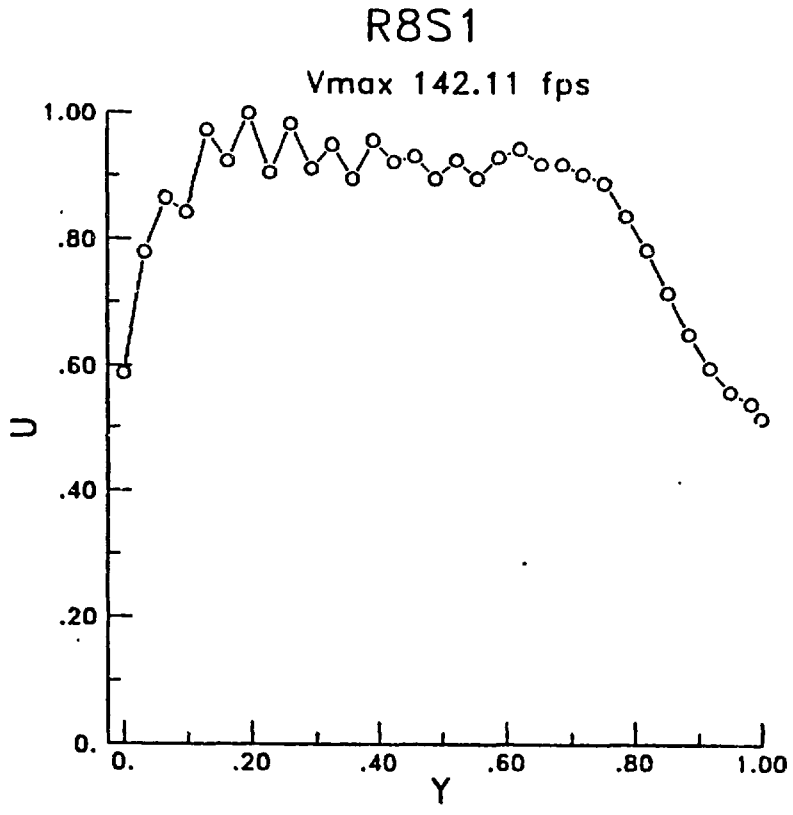

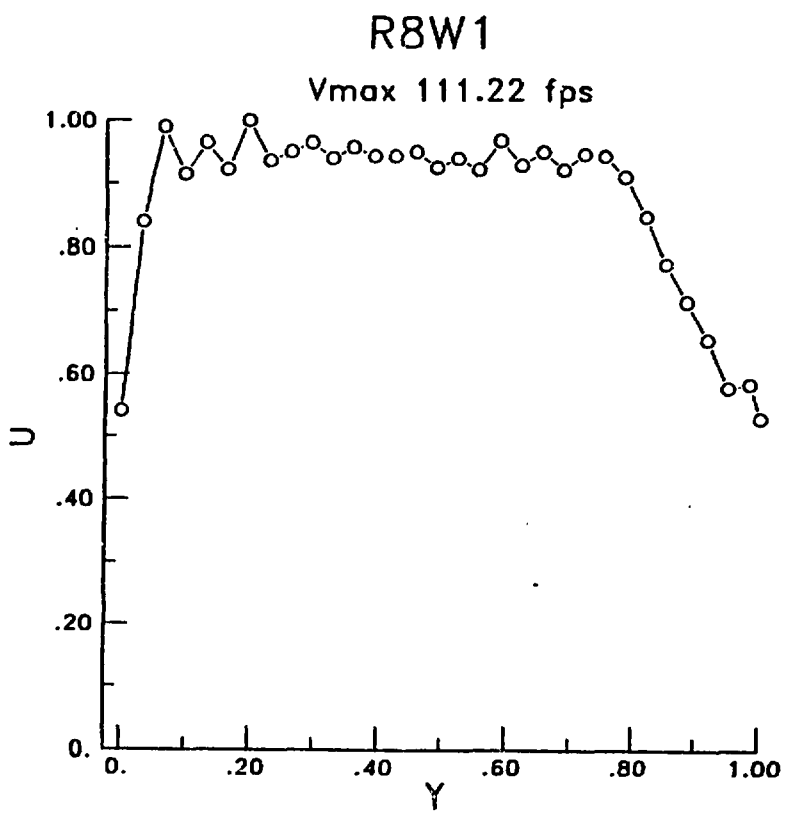

Figure 40, Velocity distribution at location 8

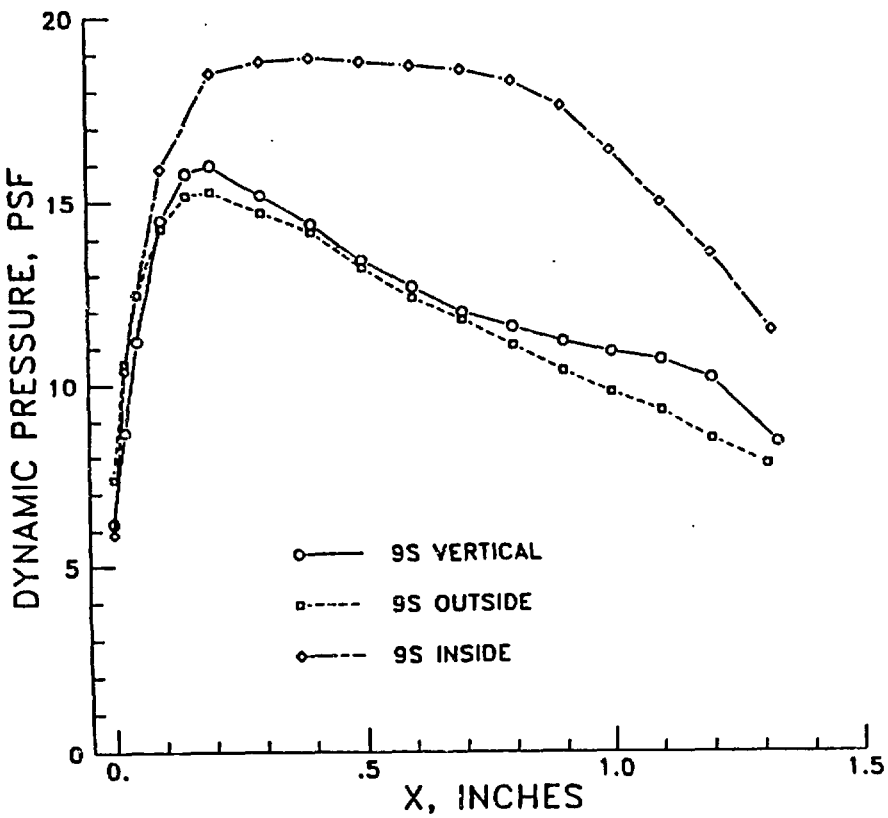

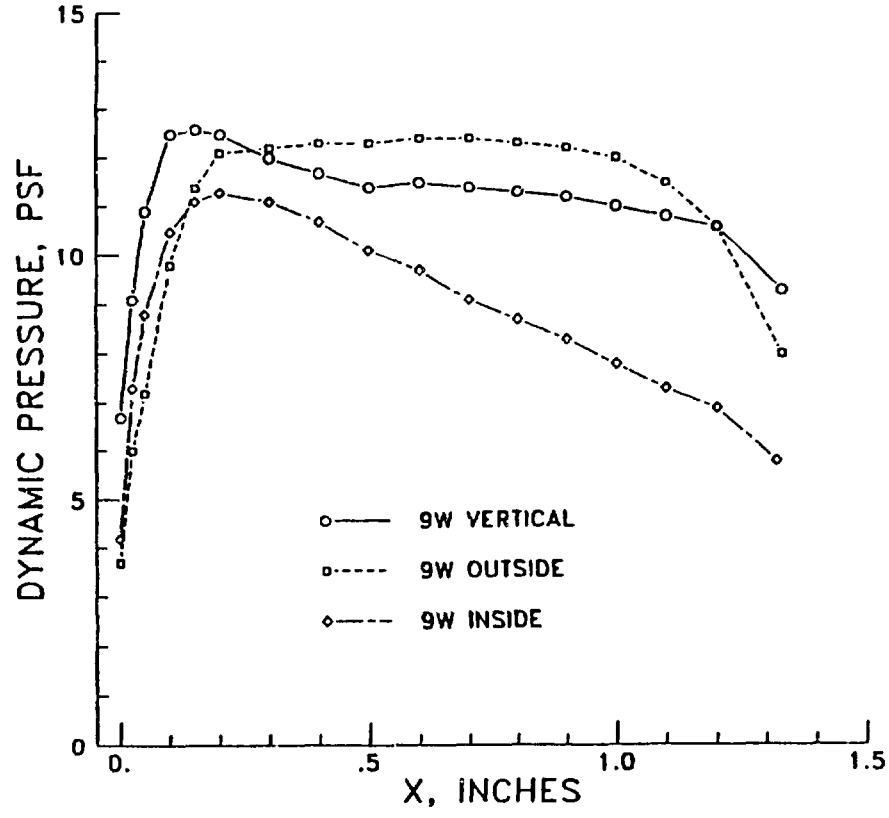

Figure 41. Dynamic pressure distribution at location 9

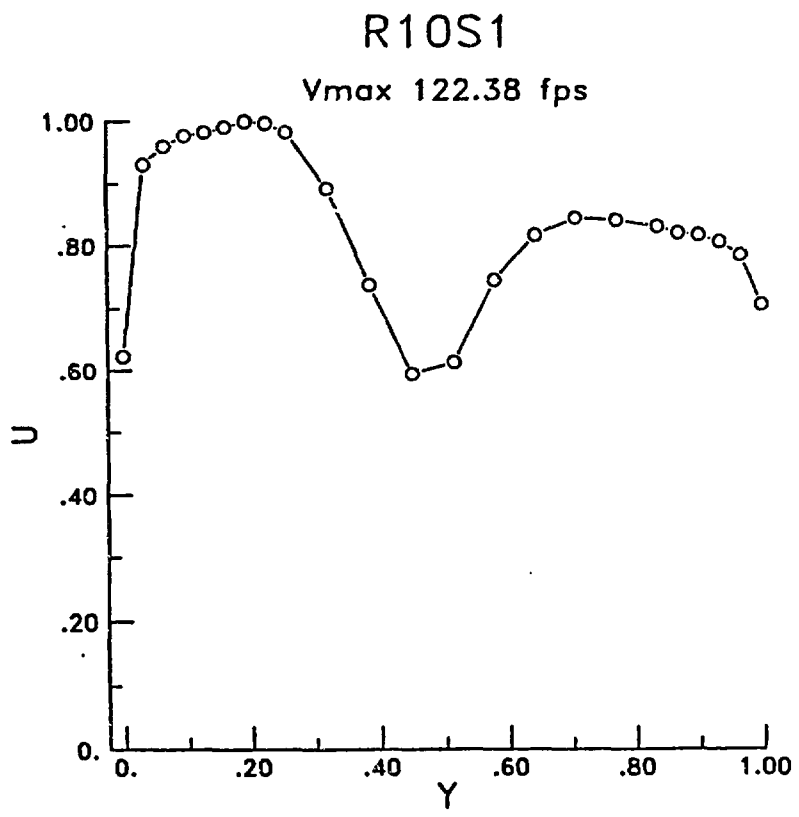

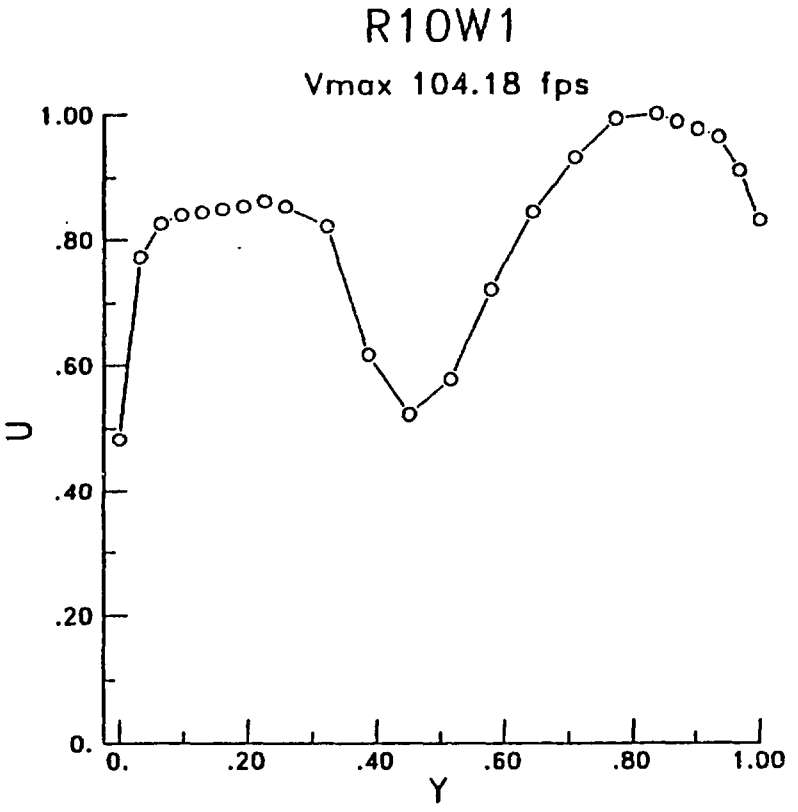

Figure 42. Velocity distribution at location 10

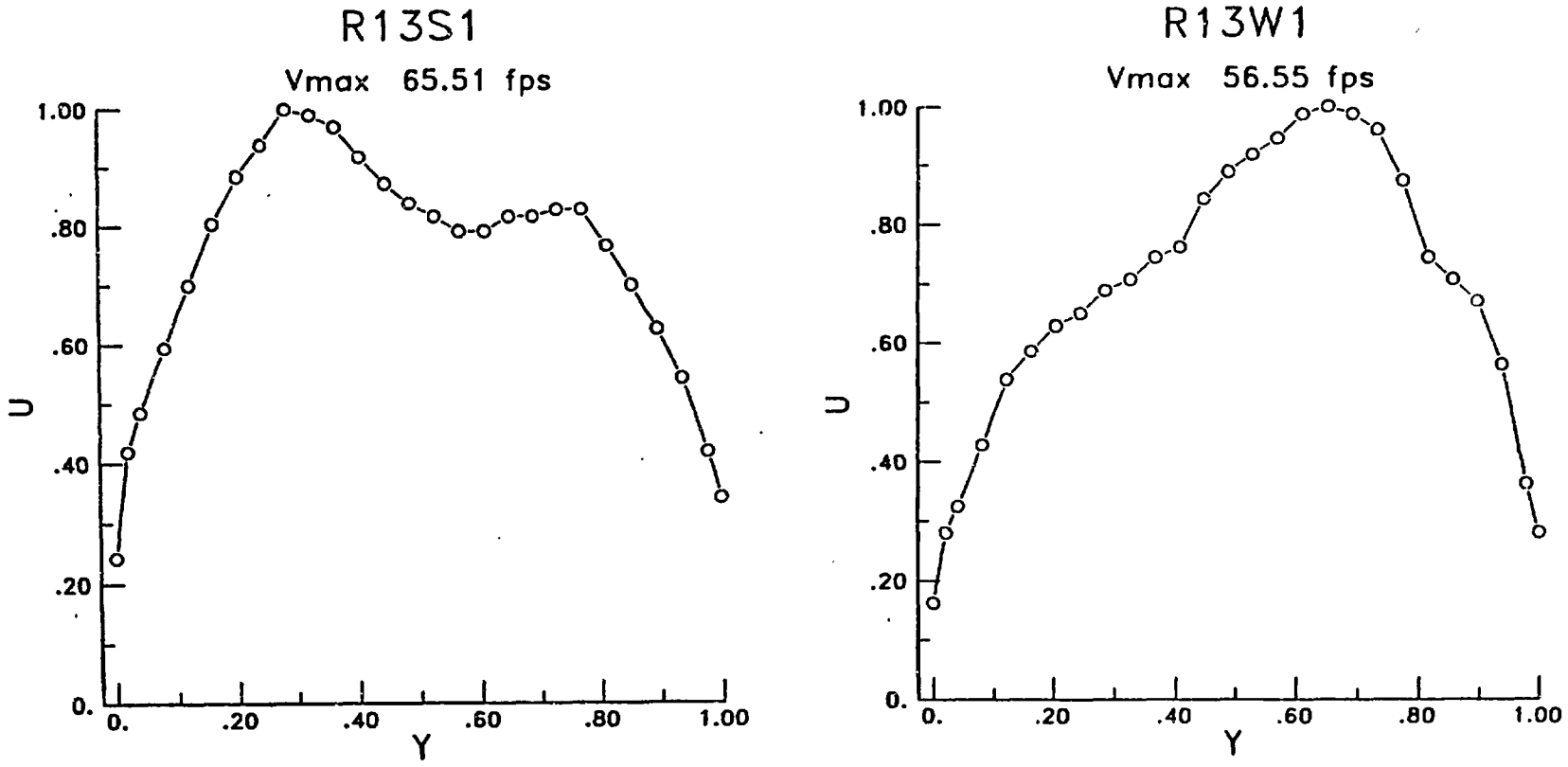

Figure 43 . Velocity distribution at location 13

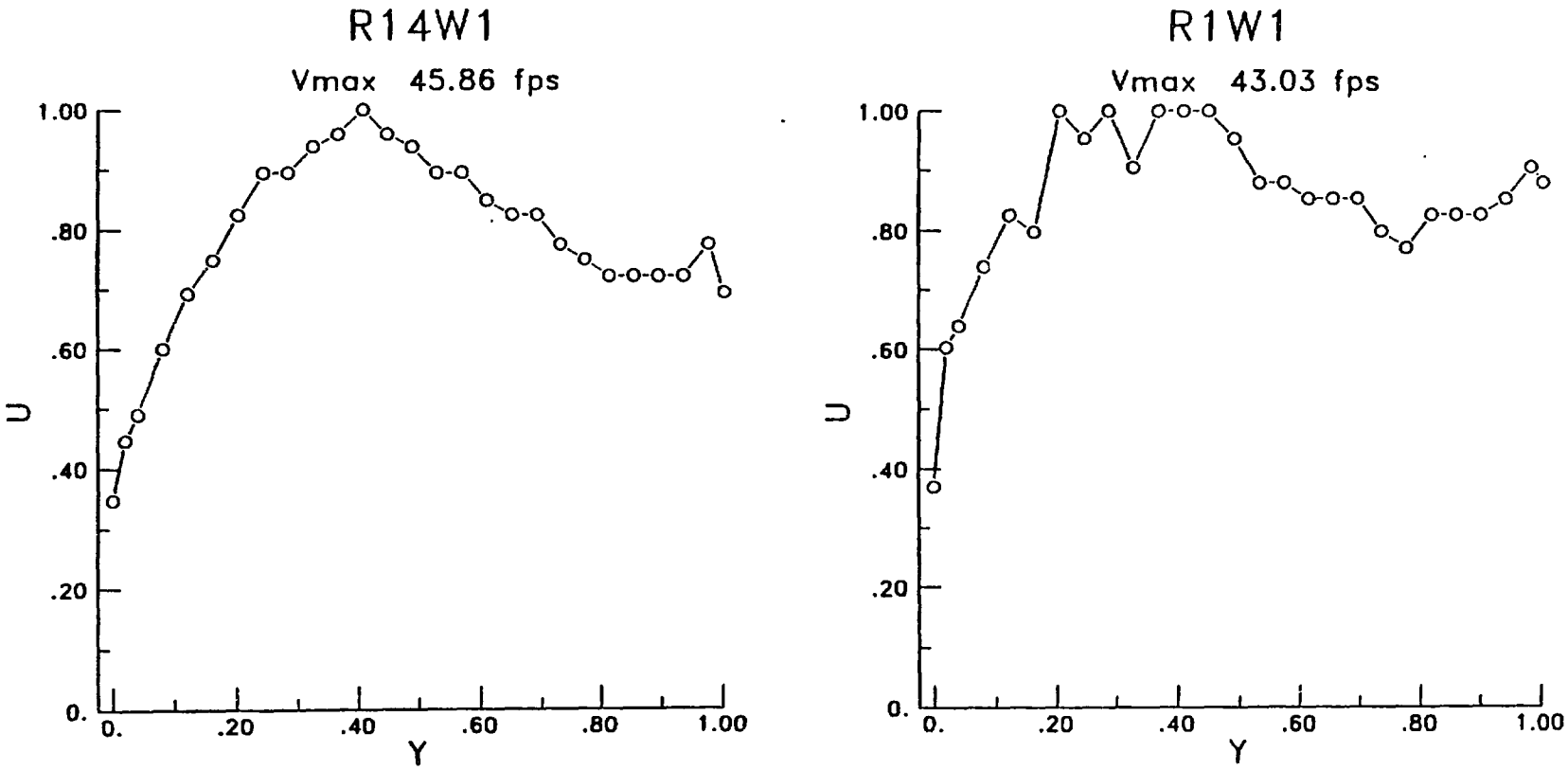

Figure 44 . Velocity distribution at locations 14 and 1

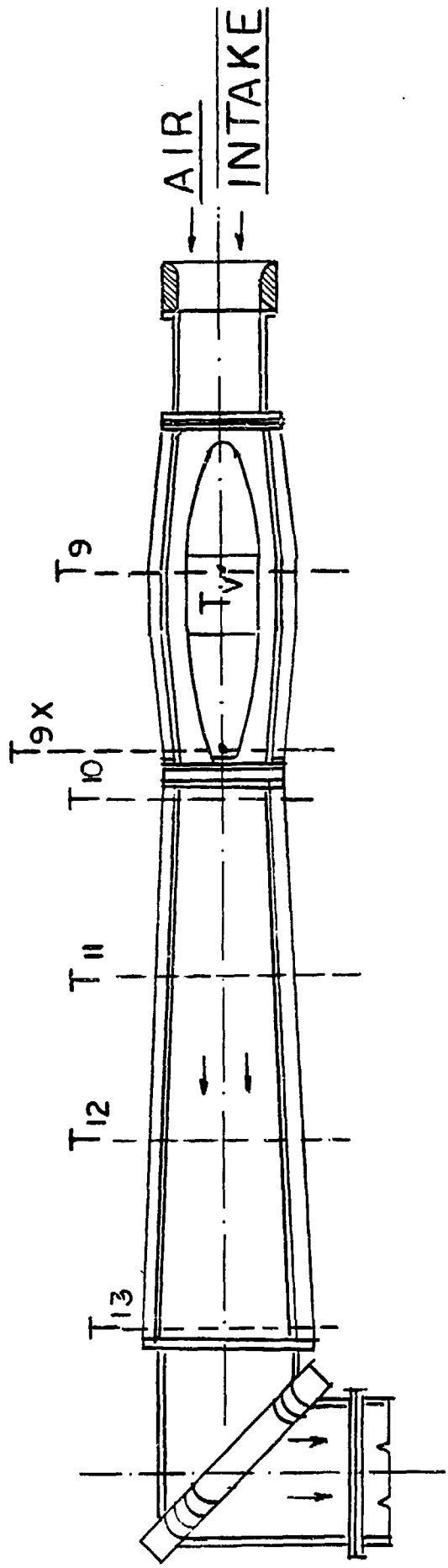

Figure 45. Plan view (detail) of the modified second open circuit

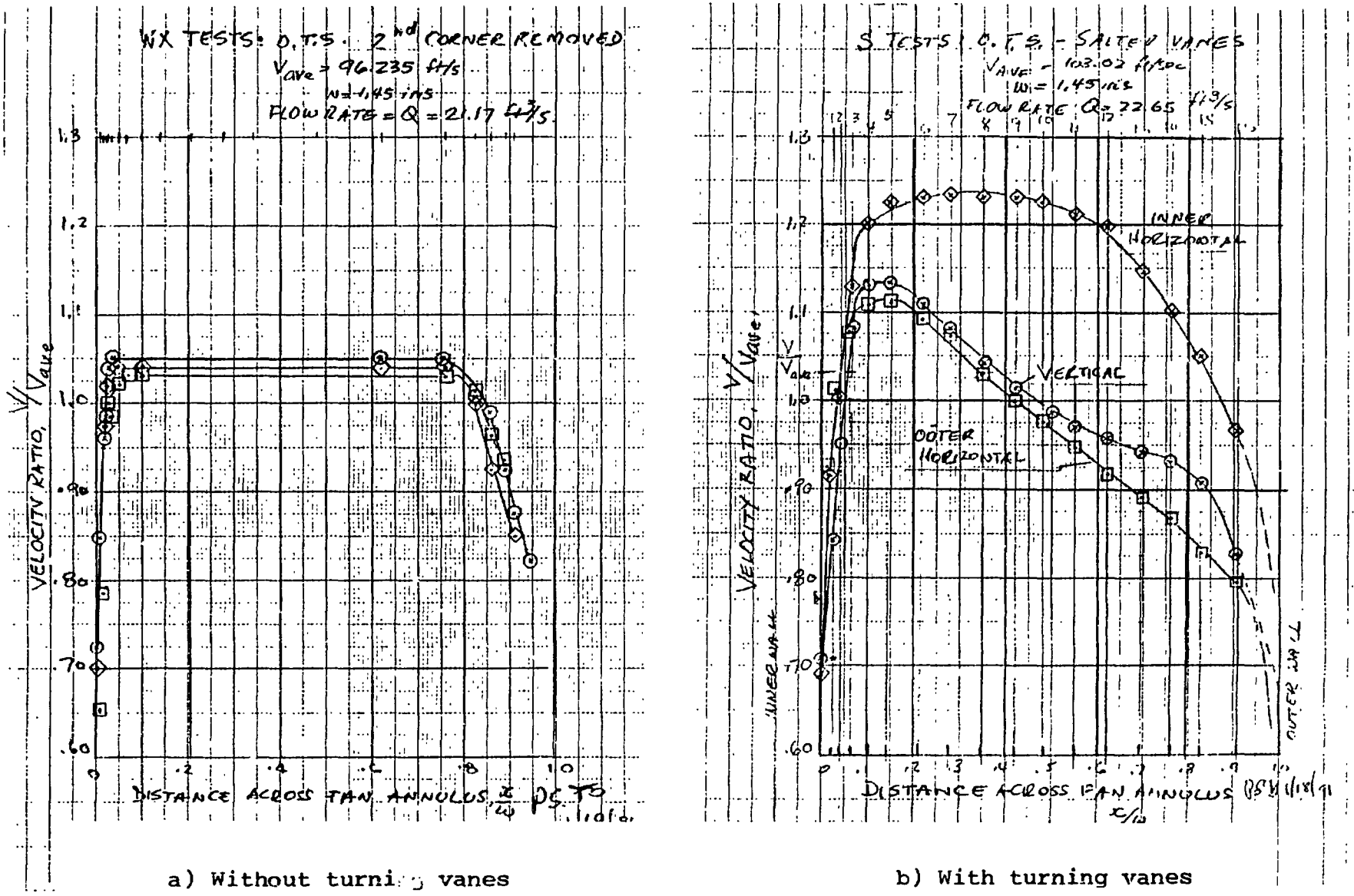

a) Without turning vanes

b) With turning vanes

Figure 46. Flow distribution at the fan section without and with turning vanes

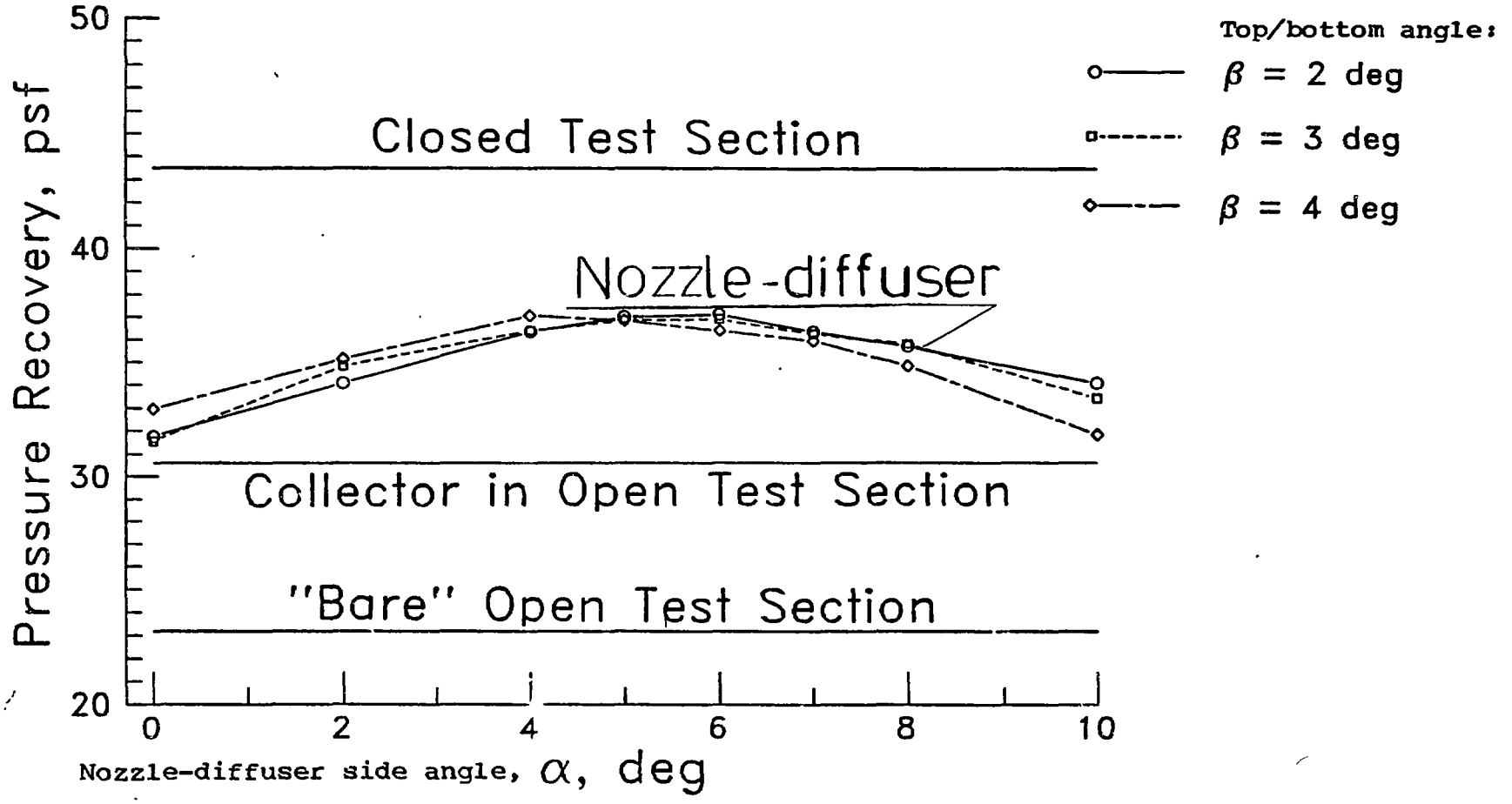

Figure 47 . Pressure recovery in the first diffuser for various test configurations

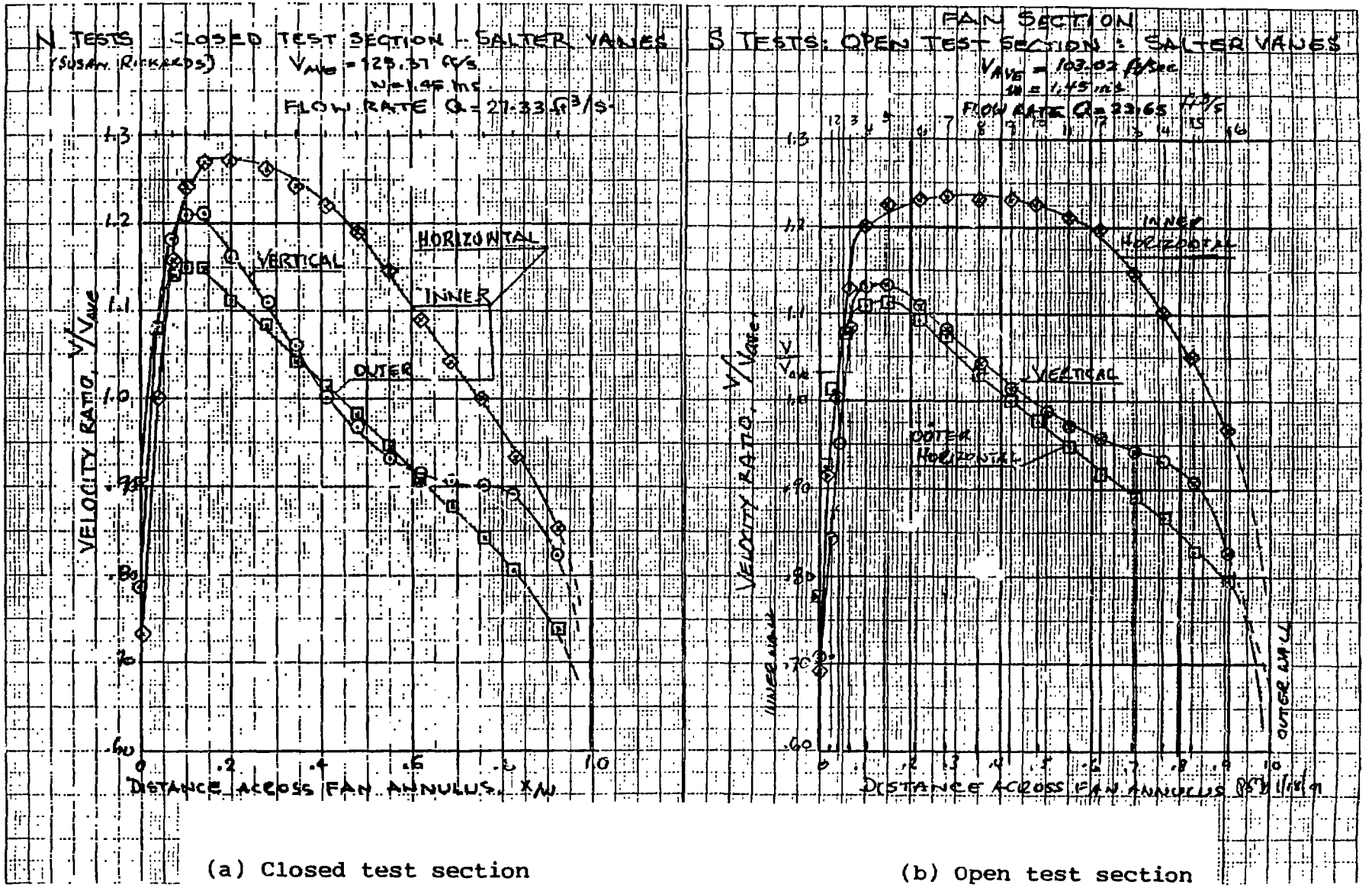

(a) Closed test section

(b) Open test section

Figure 48. Flow distribution at the fan section employing Salter turning vanes

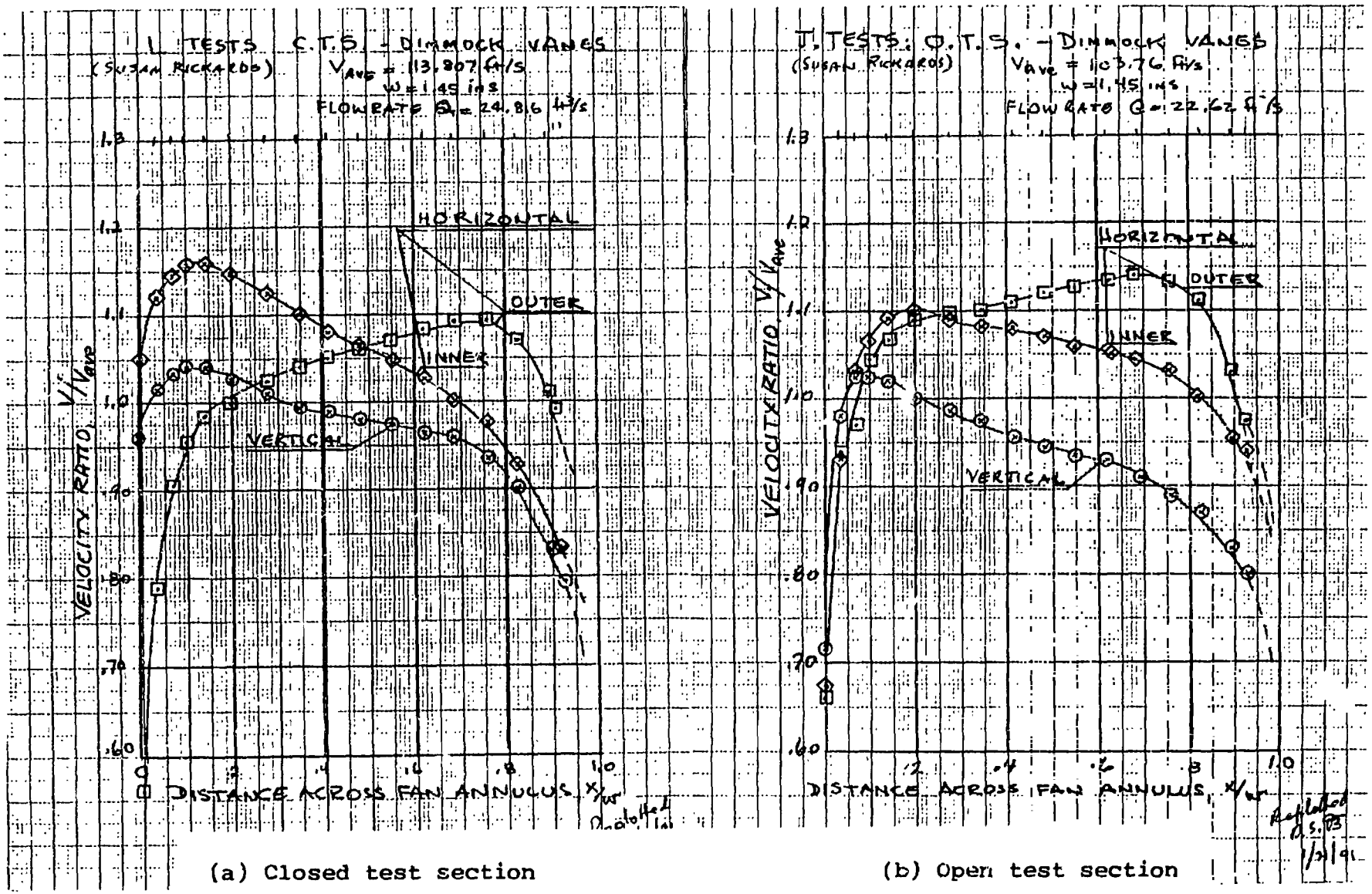

(a) Closed test section

(b) Open test section

Figure 49. Flow distribution at the fan section employing Dimmock turning vanes

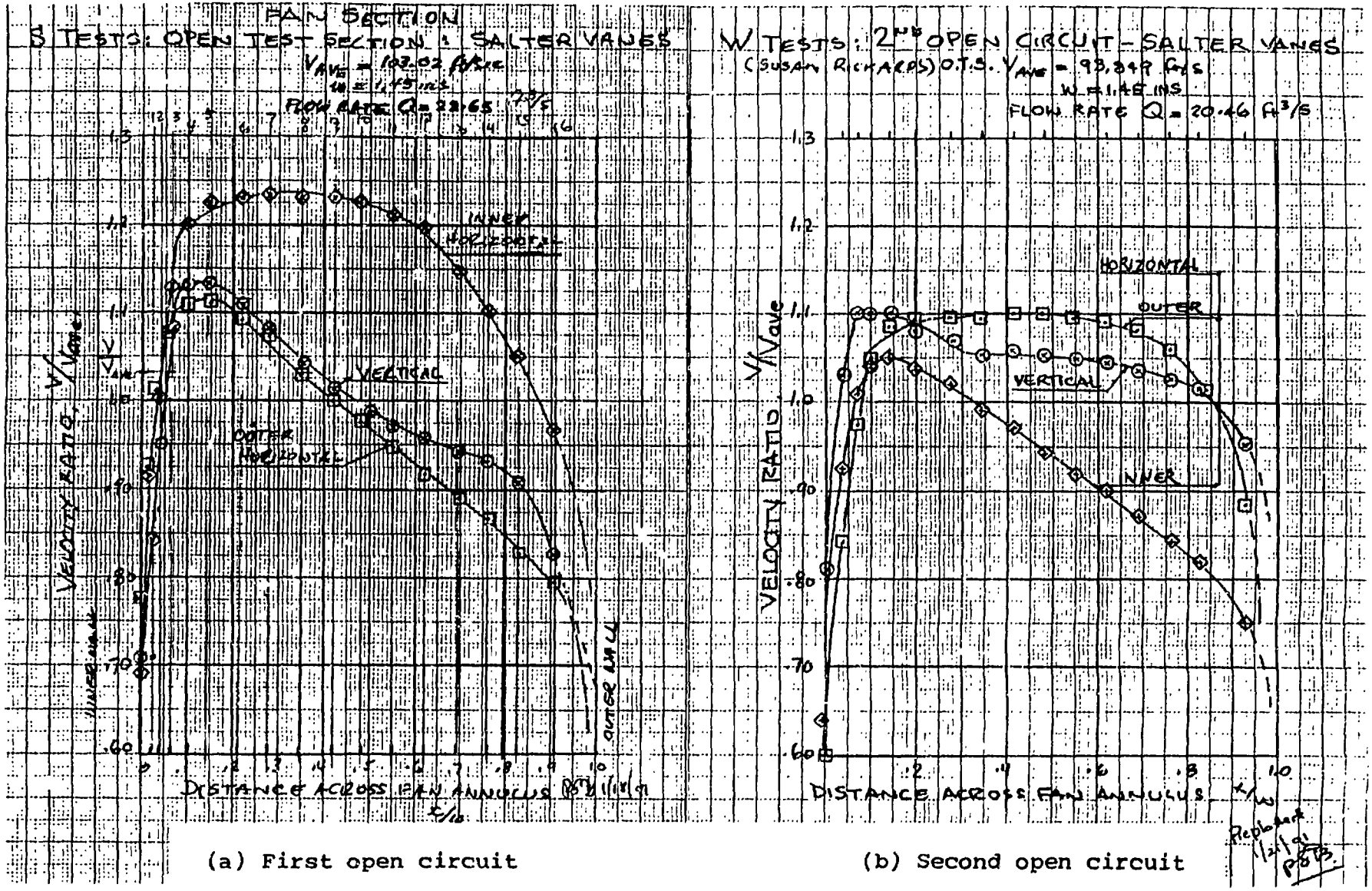

(a) First open circuit

(b) Second open circuit

Figure 50. Comparison of flow distribution at the fan section between 1st and 2nd open circuit.

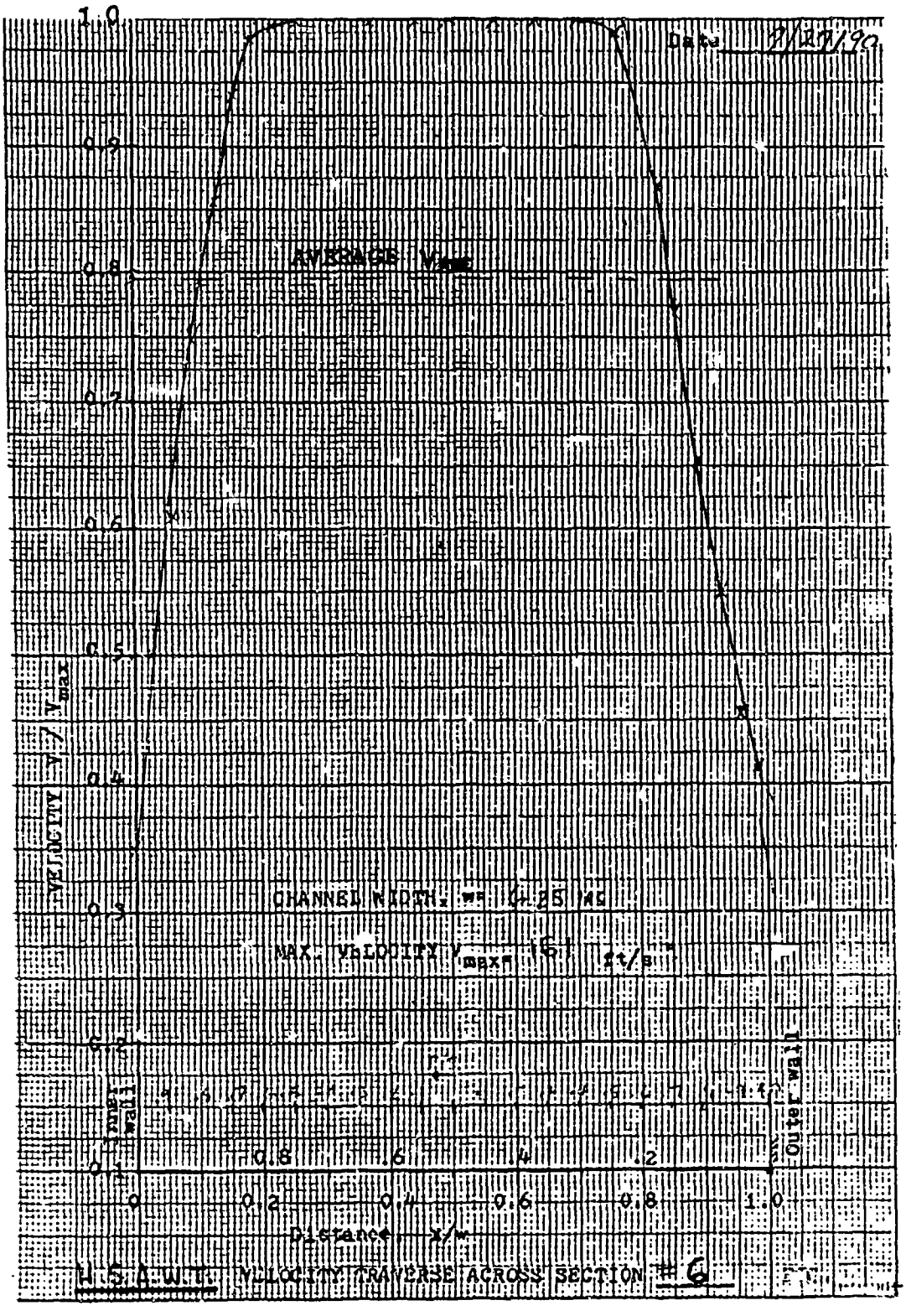

Figure 51. Flow distribution upstream of first corner Salter vanes

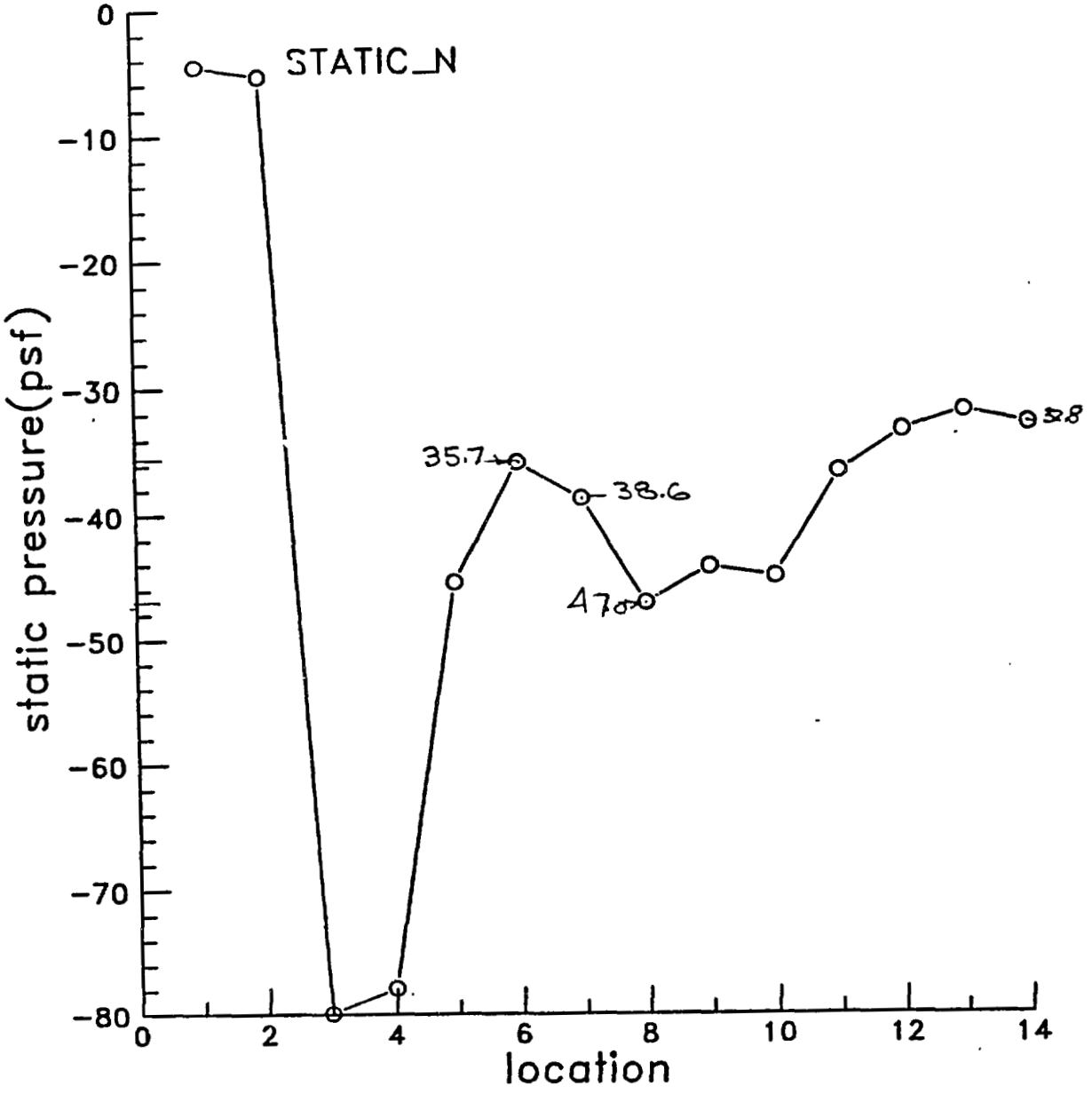

Figure 52. Variation of static pressure around the tunnel circuit. Closed test section-Salter vanes

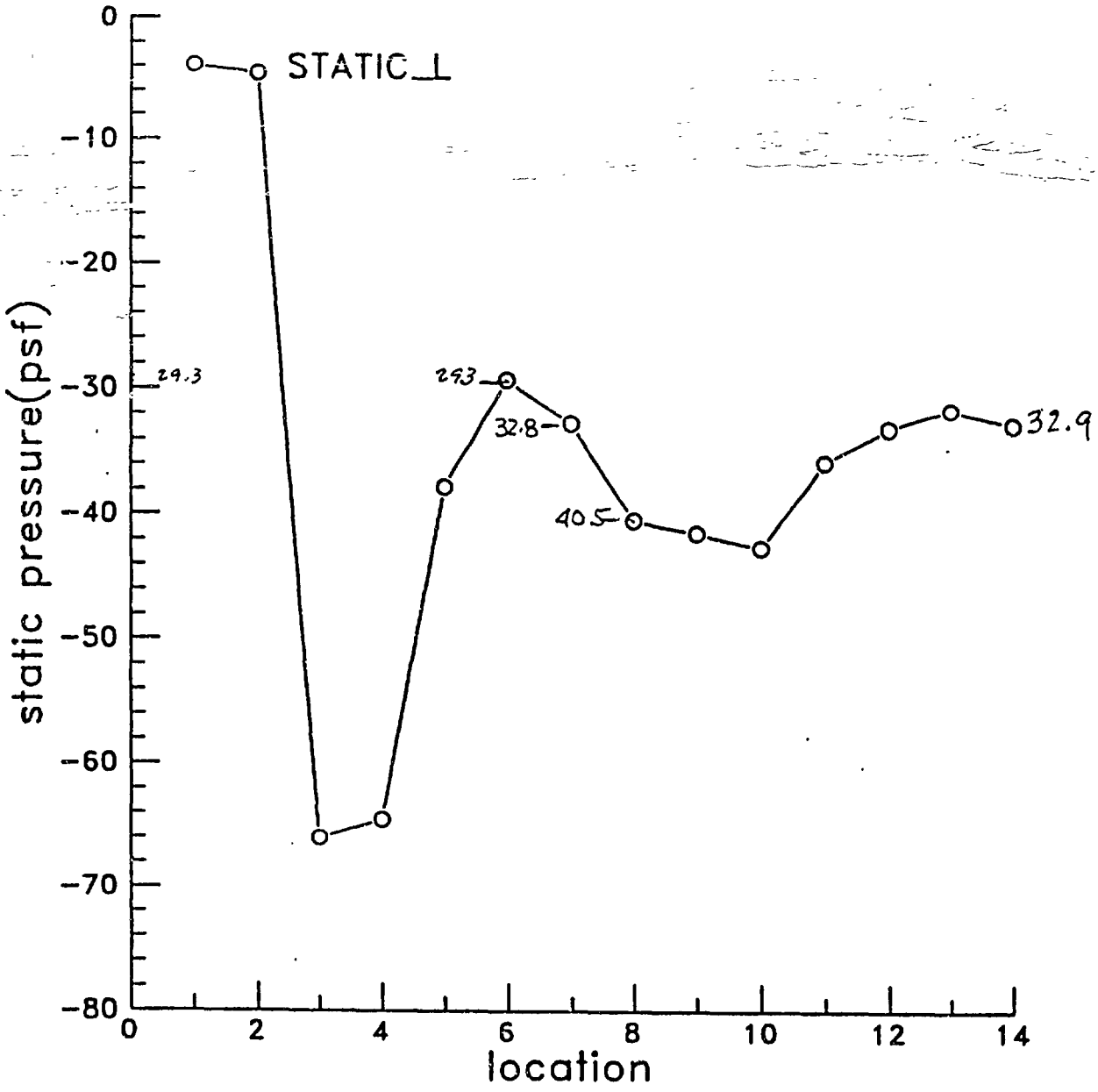

Figure 53. Variation of static pressure around the tunnel circuit. Closed test section-Dimmock vanes